# Ultrasound assisted synthesis of micro- and nano-crystals

**by**

**Cansu Yıldırım**

**A Thesis Submitted to the**
**Graduate School of Engineering**
**in Partial Fulfillment of the Requirements for**
**the Degree of**

**Master of Science**
**in**
**Materials Science and Engineering**

**Koç University**

**September 2012**

Graduate School of Sciences and Engineering

This is to certify that I have examined this copy of a master's thesis by

Cansu Yıldırım

and have found that it is complete and satisfactory in all respects,
and that any and all revisions required by the final
examining committee have been made.

Committee Members:

_____

Özgür Birer, Ph. D. (Advisor)

_____

Havva Funda Yağcı Acar, Ph. D.

_____

Nuri Solak, Ph. D.

Date: _____

## ABSTRACT

The application of ultrasound can facilitate reactions in milder conditions. In this thesis, two different inorganic materials with interesting properties were synthesized by the ultrasonic irradiation. The first chapter presents an introduction to the basic concepts of sonochemistry. The factors affecting the cavitational effect are discussed. The second chapter provides a fast and simple method for the synthesis of lanthanide doped ($Yb^{3+}$(20%)/$Er^{3+}$(2%) or $Yb^{3+}$(20%)/$Tm^{3+}$(2%)) upconverting $NaYF_4$ crystals by the application of ultrasonic waves. The optimized reaction conditions yields the synthesis of β-$NaYF_4$ microparticles and α-$NaYF_4$ nanoparticles at T< 80°C in aqueous phase. The crystal structure was determined by the X-ray diffraction and morphology was investigated with scanning electron microscopy. Upconverting crystals were excited with a continuous wave laser diode in the near infrared region.

In Chapter 3, a one step, simple route was developed for the aqueous phase synthesis of CdS quantum dots with ultrasound irradiation. As the precursor, bulk CdO with $Na_2S$ or elemental sulfur was utilized. 2-Mercaptopropionic Acid (2-MPA) or Poly(Acrylic Acid) PAA (5100g/mol) were used as the capping agent. The influence of the reaction conditions on the size and fluorescence was investigated. 2-MPA showed higher fluorescence intensity and narrower FWHM than PAA coated samples at any investigated temperature. Samples synthesized at T=70°C showed better crystallinity and higher quantum yield (38% with respect to Rhodamine B dye). The narrowest emission bandwidth and smallest size was obtained when elemental sulfur was utilized as the precursor.

## ÖZET

Sesüstü dalgaların kullanımı daha ılımlı koşullarda reaksiyonları sağlayabilir. Bu tezde, ilginç özelliklere sahip iki farklı anorganik malzeme sesüstü dalgalara mağruz bırakılarak üretilmiştir. İlk bölüm sonokimyanın temel kavramlarına bir giriş sağlamaktadır. Bu bölümde kavitasyon etkisini etkileyen etmenler tartışılmıştır. İkinci bölüm sesüstü dalgalarının kullanımı ile hızlı ve basit bir yöntemle lantanit katkılı yukarı dönüşüm yapan $NaYF_4$ kristallerinin ($Yb^{3+}$(20%)/$Er^{3+}$(2%) veya $Yb^{3+}$(20%)/$Tm^{3+}$(2%)) sentezini sunmaktadır. İyileştirilen reaksiyonlar koşullarıyla sulu ortamda, 80°C'nin altında, β-$NaYF_4$ mikroparçacıkları ve α-$NaYF_4$ nanoparçacıkları elde edilmiştir. Kristal yapılar X-ray kırınımı ile, morfoloji ise taramalı elektron mikroskobu ile belirlenmiştir. Yukarı dönüşüm yapan kristaller sürekli dalga lazer diyodu ile yakın kızılaltı bölgesinde uyarılmıştır.

3.Bölümde, tek adımda yapılan, sesaltı dalgaları ile sulu ortamda CdS kuvantum parçacıkları üretimi için basit bir yöntem üretilmiştir. Öncül madde olarak, yığın CdO ile $Na_2S$ veya yığın sülfür kullanılmıştır. Kaplama malzemesi olarak 2-Merkaptopropiyonik Asit (2-MPA) veya Poli(Akrilik Asit) PAA (5100g/mol) kullanılmıştır. Reaksiyon koşullarının boyut ve ışıma üzerindeki etkileri incelenmiştir. 2-MPA, incelenen sıcaklıklarda PAA kaplamaya göre daha yüksek ışıma şiddeti ve daha dar ışıma enliği göstermiştir. T=70°C'de sentezlenen numuneler daha iyi kristalinite ve daha yüksek kuvantum verim göstermiştir (38% Rodamin B boyaya göre). En dar ışıma genliği ve en küçük boyut, öncül madde olarak yığın sülfür kullanıldığında elde edilmiştir.

## ACKNOWLEDGMENTS

First of all, I would like to express my gratitude to my advisor Asst. Prof. Özgür Birer for his endless support and guidance throughout my journey. His enthusiasm to spread his knowledge has motivated me to learn more.

I would like to thank Assoc. Prof. Funda Yağcı Acar for providing me the opportunity to study quantum dots. I also appreciate Asst.Prof. Dr. Nuri Solak from İstanbul Technical University for being a member of my thesis committee.

I would like to acknowledge Asst. Prof. Özge Akbulut from Sabancı University for teaching the method for the purification of my lovely upconverting products.

Throughout my journey, I have learned so much and met interesting persona. There are few people worth mentioning.

My dear friend Recep Kaş has been a kind companion and a guide in the laboratory and he has been acknowledged many times. I'm sure that I helped him to change his stereotypes.

We share many special memories with İbrahim Hocaoğlu starting from our interviews. He have helped each other since then.

I really enjoyed working with Hüseyin Enis Karahan. His enthusiasm to learn and discover things, makes you become more productive. I hope we can possess many opportunities to work together again and fulfill our scientific hunger.

My first teaching assistant, Selçuk Acar deserves a proper addressing. I would like to thank Dr. Selçuk Acar for his help whenever it was needed. His sincere expressions has always made me laugh.

I express my thanks to Caner Nazlı and Neslihan Hancıoğlu for their accompaniment during our journey. We have learned so much from each other.

I would like to thank Asst. Prof. Uğur Ünal and his group members, especially Ceren Yılmaz and Refik Ergun. It's been a pleasure to work besides with these wonderful people. I appreciate Refik's patience and aspiration for any kind of discussion.

Maybe I would not have the strength to carry on without the support and guidance of my dear friends, Merve Göçmen and Duygu Biricik. They are the most precious friends I have gained at Koç University. I thank them for everything with all my heart. I will miss living with both of them.

These two years have been an interesting journey for me. I have grown-up a little more and learned to expect the unexpected.

I would like to dedicate this thesis to my mom, who has always supported me.

**TABLE OF CONTENTS**

**List of Tables…….....x**

**List of Figures……..xi**

**Nomenclature……....xvii**

**Chapter 1: Introduction……...1**

1.1 An overview of Sonochemistry……..……1

1.2 Factors affecting Cavitation…….……..3

1.2.1 Temperature…….……4

1.2.2 Dissolved Gases…….....……5

1.2.3 Solvent and the effect of surfactants…….……5

1.2.4 Acoustic Power…….……6

1.2.5 Types of Ultrasonic Systems…….6

1.3 Overview of the thesis……...……7

**Chapter 2: Sonochemical route to lanthanide doped $NaYF_4$ synthesis.....8**

2.1 Overview……8

2.2 Introduction..…….……9

2.2.1 Upconversion……...……9

2.2.1.1 Mechanism…….……10

2.2.1.2 Host and Dopant Materials…….....……11

2.2 Methods of $NaYF_4$ synthesis……12
2.3 Experimental……..……..13
2.4 Results and Discussion…….……16
2.4.1 Factors affecting $NaYF_4$ synthesis via ultrasound……..…….17
2.4.1.1 Temperature……...……19
2.4.1.2 Pulsation (Duty Cycle)……...……22
2.4.1.3 Dissolved Gases…….23
2.4.1.4 Power / Amplitude…….……25
2.4.2 Post Processes……..……26
2.4.2.1 Cleaning/ Purification ……...……26
2.4.2.2 Annealing ……..……29
2.4.3 Shape Control……...……29
2.4.4 Upconversion luminescence emission……..38
2.5 Conclusions…….……53

**Chapter 3: Ultrasound-assisted aqueous phase synthesis of CdS quantum dots.....54**

3.1 Introduction.……54
3.1.1 Quantum Dots…….55
3.1.2 Quantum confinement…….55
3.1.3 Crystal size determination with Brus equation……...……57
3.1.4 The Optical Properties……..……..58
3.1.5 Synthesis methods of CdS Quantum dots……...……..60
3.1.6 The aim of the research……...……62
3.2 Experimental……...…….63

3.3 Results and Discussion……..… 64
3.3.1 Effect of capping agent: PAA vs 2-MPA……...…….65
3.3.2 Effect of Temperature……..……68
3.3.2.1 Poly(Acrylic Acid) (PAA) as the surfactant……..…….68
3.3.2.2 2-Mercaptopropionic Acid, 2-MPA as the surfactant…….…….....70
3.3.3 Surfactant /Cd ratio……..……72
3.3.4 Effect of the Precursor…….……74
3.3.4.1 Cadmium Source: Cd Salt vs CdO…….……74
3.3.4.2 Sulfur source: $Na_2S$ vs Elemental Sulfur……76
3.3.4.3 2-MPA as the sulfur source…….……79
3. 4 Conclusions…….…….79

**Chapter 4: Conclusions……80**

**Appendix…….……82**
**References……..…….86**
**Vita……..92**

## LIST OF TABLES


Table 2.1 Properties of products as a function of temperature…….....……21

Table 2.2 Ionic radii of the lanthanides used in this thesis [50]…….……..22

Table 2.3 Properties of products without any surfactants……31

Table 2.4 Properties of the products with surfactants, for T=50°C, 3sec/3 sec pulse on/off, Amplitude: 50%.....34

Table 3.1 Electronic parameters for the indicated crystalline direct gap semiconductors, $E_g$ is the band gap, the effective masses are in units of the free electron mass and ε is the dielectric coefficient [67] …….……..58

Table 3.2 Properties of CdS QD as a function of capping agent……..……..67

Table 3.3 Properties of PAA-CdS QD as a function temperature……..…….70

Table 3.4 Properties of 2-MPA -CdS QD as a function temperature……..……72

Table 3.5 Properties of 2-MPA-CdS QD as a function of capping agent amount..…73

Table 3.6 Properties of 2-MPA-CdS QD as a function of Cd precursor…….76

Table 3.7 Properties of 2-MPA-CdS QD as a function of sulfur precursor……78

## LIST OF FIGURES


Figure 1.1 Frequency ranges of sound and ultrasound [1]…….…….2

Figure 1.2 The schematic representation of the cavitation cycle……3

Figure 2.1 Energy level diagrams showing typical upconversion processes for $Er^{3+}$, $Tm^{3+}$, and $Ho^{3+}$ lanthanide ions. The dashed-dotted, dotted, and full arrows represent excitation, multiphonon relaxation, and emission processes, respectively [36]…….....……12

Figure 2.2 XRD patterns of $YF_3$ (JCPDS card no: 74-0911), β- $NaYF_4$ (JCPDS card no: 16-0334) and α- $NaYF_4$ (JCPDS card no: 77-2042) crystals respectively. All doped with $Yb^{3+}$ / $Eu^{3+}$…….…..16

Figure 2.3 Effect of the sodium ion ratio ($Ln^{3+}$:$Na^{+}$) on the formed product (When reaction conditions are 20%$Yb^{3+}$/ 2% $Eu^{3+}$, T=25°C, 3sec/3sec pulse on/off, 50% amplitude)……17

Figure 2.4 Effect of $Ln^{3+}$:$F^{-}$ ratio at high sodium content (When reaction conditions are 20%$Yb^{3+}$/ 2% $Eu^{3+}$, T=25°C, 3sec/3sec pulse on/off, 50% amplitude)...…19

Figure 2.5 Effect of temperature on the formation of different crystals (Reaction conditions: $Ln^{3+}$:$Na^{+}$ =1:8, $Ln^{3+}$:$F^{-}$ = 1:3, 3sec/3sec pulse on/off, Amplitude= 50%, Dopant: $Eu^{3+}$ (2%))…….20

Figure 2.6 T=50°C leads to β-$NaYF_4$ when dopants are $Yb^{3+}$(20%) / $Eu^{3+}$(2%), $Yb^{3+}$(20%) / $Tm^{3+}$(2%) or $Yb^{3+}$ (20%) / $Er^{3+}$(2%)……21

Figure 2.7 Effect of pulsation to the crystal structure……23

Figure 2.8 Effect of purged gas on the synthesis of different crystals. (Reaction conditions: T=25°C, 3/3 sec pulse on/off for 2 hours, $Ln^{3+}$:$Na^{+}$ =1:12, $Ln^{3+}$:$F^{-}$ = 1:3, Amplitude= 50%, Dopant: $Eu^{3+}$(2%) )…….24

Figure 2.9 The effect of amplitude of the sound waves, for the reaction conditions of T=50° C, 3sec/3sec pulse on/off, $Ln^{3+}$:$Na^{+}$ =1:20, $Ln^{3+}$:$F^{-}$ = 1:3…….....25

Figure 2.10 Purification and the removal of the titanium impurities from the product. Glycerol is placed at the bottom and sample dispersed in water is at the top white phase. A) Before centrifugation, B) After centrifugation……..27

Figure 2.11 XRF of the sample before titanium impurities (indicated with orange lines) were removed by density gradient method……..28

Figure 2.12 XRF of the sample after titanium impurities (indicated with orange lines) were removed by density gradient method……..28

Figure 2.13 Effect of increasing sodium amount on the shape of β-$NaYF_4$ microcrystals. From A to C $Ln^{3+}$: $Na^+$ = 1:0, 1:12, 1:40. Scale bars are 300nm, 1 μm and 200 nm respectively. (Reaction conditions: T=50°C, 3/3 sec pulse on/off for 2 hours, $Ln^{3+}$:$F^-$ = 1:3, Amplitude= 50%, Dopants: $Yb^{3+}$(20%) /$Tm^{3+}$(2%))……30

Figure 2.14 Effect of the absence of $Yb^{3+}$ on the shape of β-$NaYF_4$ microcrystals. Scale bars is 100nm. (Reaction conditions: $Ln^{3+}$:$Na^+$ = 1:20, $Ln^{3+}$:$F^-$ = 1:3, T=50°C, 3/3 sec pulse on/off, Amplitude= 50%, Dopant: Only $Tm^{3+}$(2%))……31

Figure 2.15 Image of α-$NaYF_4$ nanocrystals. Scale bar is 100nm. Inset image shows the XRD pattern before and after annealing (Reaction conditions: T=30°C, 3/3 sec pulse on/off for 2 hours, $Ln^{3+}$:$F^-$ = 1:4, Amplitude= 50%, Dopants: $Yb^{3+}$(20%) /$Tm^{3+}$(2%))……32

Figure 2.16 Effect of sodium citrate on the shape of α- $NaYF_4$ nanocrystals. From A to F scale bars are 300nm, 1 μm, 100 nm, 200nm, 200nm and 100nm respectively. From A to F, $Ln^{3+}$: $Na^+$ = 1:0, 1:40, 1:40, 1:40, 1:30 and 1:60, Ln: Nacitrate = 1:2, 1:2, 1:13.24, 1:1, 1:10, 1:1. (Reaction conditions: T=50°C, 3/3 sec pulse on/off, $Ln^{3+}$: $F^-$ = 1:3, Amplitude= 50%, A to E dopants: $Yb^{3+}$(20%)/$Er^{3+}$(2%), $Yb^{3+}$(20%)/$Tm^{3+}$(2%),

$Yb^{3+}$(20%)/$Tm^{3+}$(2%), $Yb^{3+}$(20%)/$Tm^{3+}$(2%), $Yb^{3+}$(20%)/$Er^{3+}$(2%), $Yb^{3+}$(20%)/$Er^{3+}$(2%) )……..35

Figure 2.17 Effect of sodium acetate and citric acid on the shape of α- $NaYF_4$ nanocrystals First row corresponds to images before annealing and second row images are taken after annealing. Scale bars are 100nm, 100nm, 200nm, 300nm respectively. Third row shows the compared XRD patterns. For A, $Ln^{3+}$: $Na^+$ = 1:30, Ln: Nacitrate = 1:30. For B, $Ln^{3+}$: $Na^+$ = 1:50, Ln: Citric acid= 1:2. (Reaction conditions: T=50°C, 3/3 sec pulse on/off, $Ln^{3+}$: $F^-$ = 1:3, Amplitude= 50%, Dopants: $Yb^{3+}$(20%)/$Tm^{3+}$(2%) and $Yb^{3+}$(20%)/$Er^{3+}$(2%))……37

Figure 2.18 The energy level diagram of corresponding transitions of $Yb^{3+}$ /$Tm^{3+}$ co-doped crystals upon NIR excitation [49] where the full, dotted, and curly arrows represent emission, energy transfer, and multiphonon relaxation processes respectively.....40

Figure 2.19 The XRD patterns before and after annealing for the most UC efficient sample as seen in Figure 2.15 (α-$NaYF_4$: $Yb^{3+}$(20%) ,$Tm^{3+}$(2%) nanocrystals (Reaction conditions: T=30°C, 3/3 sec pulse on/off, $Ln^{3+}$:$F^-$ = 1:4)……..…….40

Figure 2.20 The excitation power dependence of the most UC efficient sample as seen in Figure 2.15 (α-$NaYF_4$: $Yb^{3+}$(20%) ,$Tm^{3+}$(2%) nanocrystals (Sample F2.15)……41

Figure 2.21 The excitation power dependence of the most UC efficient sample as seen in Figure 2.16 E (α-$NaYF_4$: $Yb^{3+}$(20%) , $Er^{3+}$(2%), nanocrystals (Reaction conditions: T=50°C, 3/3 sec pulse on/off, $Ln^{3+}$: $F^-$ = 1:3, $Ln^{3+}$: $Na^+$ = 1:30 , Ln: Nacitrate = 1:10).....43

Figure 2.22 The energy level diagram of corresponding transitions of $Yb^{3+}$ /$Er^{3+}$ co-doped crystals upon NIR excitation[50].....44

Figure 2.23 XRD diagram before and after annealing of the of α-$NaYF_4$: $Yb^{3+}$(20%) , $Er^{3+}$(2%), nanocrystals after annealing (SEM image in Figure 2.17 A2). (Reaction conditions: T=50°C, 3/3 sec pulse on/off, $Ln^{3+}$: $F^-$ = 1:3, $Ln^{3+}$: $Na^+$ = 1:10, Ln: NaAcetate = 1:10).....45

Figure 2.24 UC emission spectra of α-$NaYF_4$: $Yb^{3+}$(20%) ,$Tm^{3+}$(2%) nanocrystals (black) (Sample F2.15)and α- $NaYF_4$ + $YF_3$: $Yb^{3+}$(20%)/$Tm^{3+}$(2%) nanocrystals (red) (Sample F2.17 A1)synthesized with sodium acetate. (Reaction conditions: $Ln^{3+}$: $Na^+$ = 1:30, Ln: NaAcetate = 1:30, T=50°C, 3/3 sec pulse on/off, $Ln^{3+}$: $F^-$ = 1:3) Excitation power density is 2.7x$10^{-6}$ W/$cm^2$.....46

Figure 2.25 UC spectra of α-$NaYF_4$: $Yb^{3+}$(20%),$Tm^{3+}$(2%) nanocrystals (black line) and β-$NaYF_4$: $Yb^{3+}$(20%), $Tm^{3+}$(2%) microcrystals seen in Figure 2.13 A (red line) at the same excitation power density of 2.7E6 W/$cm^2$.....46

Figure 2.26 UC spectra of annealed β-$NaYF_4$ crystals doped with different concentrations of $Er^{3+}$ (Both crystals were excited with 2.77W/$cm^2$)……..48

Figure 2.27 XRD patterns and SEM images of β-$NaYF_4$ : $Yb^{3+}$(20%)/ $Er^{3+}$(2%) before and after annealing……....48

Figure 2.28 XRD patterns and SEM images of β-$NaYF_4$ : $Yb^{3+}$(20%) /$Er^{3+}$(0.2%) before and after annealing……49

Figure 2.29 UC emission spectra of α-$NaYF_4$: $Yb^{3+}$(20%) ,$Tm^{3+}$(2%) nanocrystals of Figure 2.16 C and D by excitation power density of 2.7E6 W/$cm^2$. The effect the amount of sodium citrate on the UC emission of α- $NaYF_4$ nanocrystals is observed. (Reaction conditions: T=50°C, 3/3 sec pulse on/off, $Ln^{3+}$: $Na^+$ = 1:40, $Ln^{3+}$: $F^-$ = 1:3, dopants: $Yb^{3+}$(20%)/$Tm^{3+}$(2%))...49

Figure 2.30 XRD patterns of the samples in Figure R before and after annealing. On the left $Ln^{3+}$: Nacitrate = 1:13.24, on the right $Ln^{3+}$: Nacitrate = 1:1……50

Figure 2.31 UC emission spectra of Sample F2.16E (blue), Sample F2.16F(red), Sample F2.17B2(black), sample synthesized in EtOH: $H_2O$ = 25:75 (v:v). (Reaction conditions: T=50°C, 3/3 sec pulse on/off, $Ln^{3+}$: $F^-$ = 1:3 for A to D with $Yb^{3+}$(20%)/$Er^{3+}$(2%) dopants ) Excitation power density of $2.7x10^6$ $W/cm^2$.....50

Figure 2.32 SEM image and XRD diagram of annealed β-$NaYF_4$ where reaction conditions were EtOH: $H_2O$ : 25:75 (v:v) , $Ln^{3+}$: $Na^+$ = 1:50, T=50°C, 3/3 sec pulse on/off, $Ln^{3+}$: $F^-$ = 1:3…….52

Figure 3.1 Schematic of semiconductor energies……...55

Figure 3.2 The dependence of the fluorescence on the size [66].....56

Figure 3.3 Normalized absoption spectra of the quantum dot…….……..59

Figure 3.4 Comparison of the emission and absorption spectra of QD (continuous line) and the organic dye (dotted line) (shaded area are the absorption spectra) [69].....60

Figure 3.5 Normalized absorbance spectra……...…….66

Figure 3.6 Absorption calibrated Fluorescence emission…….67

Figure 3.7 Normalized absorbance spectra of PAA-CdS……..69

Figure 3.8 Absorption calibrated fluorescence emission of PAA-CdS……....69

Figure 3.9 Normalized absorbance spectra of 2-MPA CdS…….…..71

Figure 3.10 Absorption calibrated fluorescence emission of 2-MPA-CdS…….……72

Figure 3.11 Normalized absorption spectra and absorption calibrated fluorescence emission of 2-MPA-CdS…….……..73

Figure 3.12 Normalized absorbance spectra of 2-MPA CdS of different precursors..…74

Figure 3.13 Absorption calibrated fluorescence emission of 2-MPA CdS of different precursors…….……75
Figure 3.14 Normalized absorbance spectra of 2-MPA CdS of different sulfur precursors…….……77
Figure 3.15 Absorption calibrated fluorescence emission of 2-MPA CdS of different sulfur precursors……78
Figure A.1 Representation of the absorption spectra……..83

## NOMENCLATURE

| | |
|---|---|
| CW | Continuous wave |
| EBR | Exciton Bohr Radius |
| EDTA | Ethylenediaminetetraacetic acid |
| $E_g$ | Gap Energy |
| ε | Dielectric Coefficient |
| ESA | Excited state absorption |
| EtOH | Ethanol |
| ETU | Energy transfer upconversion |
| eV | Electron Volt |
| CdS | Cadmium Sulfide |
| -COOH | Carboxylic Acid |
| FWHM | Full Width at Half Maximum |
| MAA | Mercaptoacetic acid |
| MPA | Mercaptopropionic acid |
| $m_e$* | Effective Mass of Electron |
| $m_h$* | Effective Mass of Hole |
| NaAc | Sodium Acetate |
| Nacitrate | Trisodium Citrate |
| $NaYF_4$ | Sodium Yttrium Fluoride |
| NIR | Near Infra-red |
| PAA | Poly(acrylic acid) |
| PL | Photo Luminescence |
| SEM | Scanning Electron Microscope |
| FE-SEM | Field Emission Scanning Electron Microscope |

| | |
|---|---|
| QD | Quantum Dot |
| QY | Quantum Yield |
| HS- | Thiol |
| T | Temperature |
| UC | Upconversion |
| UV | Ultra Violet |
| Vis | Visible |
| XRD | X-ray Diffraction |
| XRF | X-ray Fluorescence |

# Chapter 1

# INTRODUCTION

This thesis is focused on the development of unique synthesis methods by sonication. Two completely different inorganic materials with extraordinary properties are synthesized successfully via sonication. Both of these materials are the most intensively studied specimens in various fields with many applications which govern interesting features. In this chapter, the fundamentals of the sonochemistry are provided for the reader.

## 1.1 An overview of Sonochemistry

Sonication or the ultrasonic irradiation is the application of the ultrasonic waves to the reaction medium. In the field of sonochemistry, ultrasonic waves are applied to a liquid medium to study the effect of cavitation bubbles in a system. Although the concept of cavitation was first reported by Thornycroft and Barnaby in 1985 by the observation of an unexpected pitting and erosion on the propeller of their submarine, the scientific

publications has increased dramatically in the last twenty years. This is due to the scientific enhancement in the electronic and transducer technologies.

The high intensity, low frequency ultrasonic waves used in sonochemistry can be between 20 kHz to 1MHz depending on the application. For non-destructive evaluation and medical diagnosis, low intensity, high frequency ultrasonic waves are used. Unlike in sonochemistry, these waves do not change the state of the medium [1].

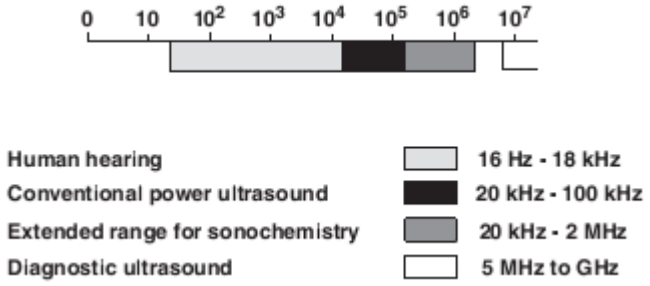


Figure 1.1 Frequency ranges of sound and ultrasound [1].

The impact of sonication originates from the acoustic cavitation. Simply, the cavitation is the formation, growth and implosive collapse of bubbles [2]. When ultrasound is applied to a system, the liquid molecules of the medium oscillate with the waves because like any other sound wave, ultrasound is transmitted by the compression and stretching of the molecular spacing of the medium. During the rarefaction or the negative pressure, if a "weak spot" is present in the liquid, in other words a nucleation point for the molecules to break apart from each other, a cavitation bubble is formed [1]. This bubble can be filled with gas or it can be a void depending on the liquid. Once the bubble is formed, its size changes with the sound pressure and the bubble grows in size by the successive cycles or irradiation. When the bubble reaches an unstable size, the intense collapse occurs. According to the mainly accepted "hot-spot theory", the collapse of the bubble causes

intense local heating (~5000 K) and pressures (~1000atm) with very fast cooling rates of $10^{10}$K/s [3, 4]. Therefore, the effect of cavitation can be seen as the local micro reactors. On the other hand, the electrical theory asserts that on the surface of the cavitation an electrical charge is created and the formation of large electrical field gradients can break the bonds upon collapse, therefore causing chemical changes [5].

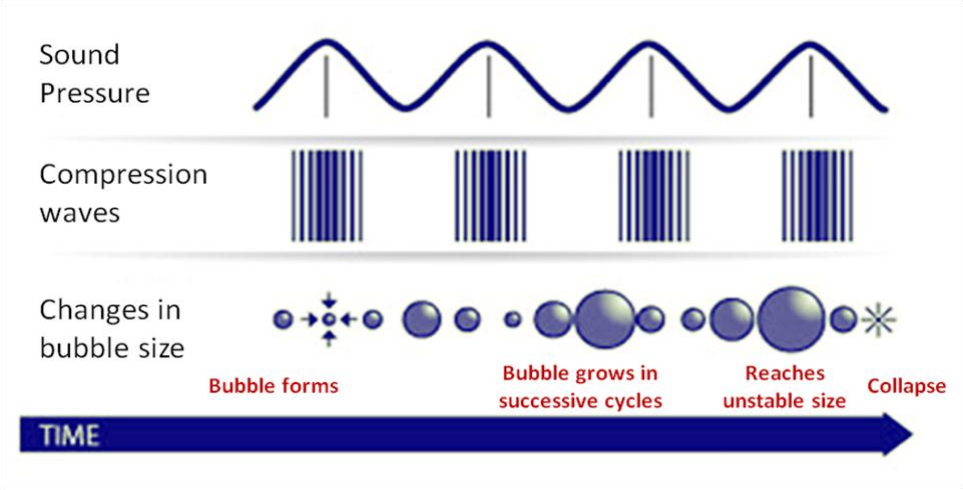


Figure 1.2 The schematic representation of the cavitation cycle

## 1.2 Factors affecting Cavitation

The occurrence of a sonochemical reaction is highly dependent on the cavitational impacts. The reaction is mostly favored when the cavitational effects are maximized. The application of ultrasound can change the reaction mechanisms and the conditions for a conventional method may not work in the case of ultrasound assisted reactions. Interestingly, the reaction conditions can be unusual for a sonochemical reaction.

This thesis is mainly focused on how the various reaction conditions were affecting the result of a reaction when ultrasound was applied. The most crucial and main factors affecting the cavitational impacts are explained in the next sections. Overall, this chapter will provide the reader the basic knowledge about how the cavitation bubbles are affected by the reaction conditions in general. Only the conditions which were studied in the chapters are included in this thesis. Further implementations in detail are presented in the forthcoming chapters.

### 1.2.1 Temperature

The relationship between the temperature and the cavitational effects is not always predictable for every reaction. In general, for a conventional reaction where ultrasound is not applied, high temperature favors a reaction to the products because the required energy to accomplish any chemical change is supplied by the heat. For the case of sonication, the relationship is not always linearly correlated. The completion of the cavitation cycle is the main factor that leads the reaction to the product. When the temperature is set high, the formation of a cavitation bubble will be enhanced. At high temperatures, when the bubble is formed, most probably the void will be filled with the vapor of the liquid medium or with the dissolved gases. As a result, the cavitational effect can be decreased by the prevention of the implosion. This phenomenon is called the cushioning effect. On the contrary, at low temperatures the implosion of the bubbles will be highly ensured. However, in that case, the formation of the bubble is harder since the cavitational threshold to form a bubble is increased. Thus, for a specific system, there is an optimum temperature for desired results. The effect of the temperature for the favorable results is further explained in detail in the synthesis methods in the forthcoming chapters.

### 1.2.2 Dissolved Gases

The presence of a dissolved gas is crucial for the formation of the bubbles. The dissolved gases in the liquid medium can act as the nucleation points to form cavitation bubbles. When the medium is degassed, probability of the formation of the bubble is decreased due to the increase in cavitational threshold. The type of gas is another factor which affects the cavitational processes. Highly soluble gases can redissolve before the implosion and gases with low solubility can cause the bubbles to merge with each other and float to the surface without any implosion. Also, gases with higher specific heat ratio ($\gamma=c_p / c_v$ ) provide enhanced cavitational effects by converting more energy upon cavitation [1].

### 1.2.3 Solvent and the effect of surfactants

In this thesis, all the reactions were carried out in the aqueous phase with a single exception of ethanol/water mixture which is presented in Chapter 2. A solvent with high vapor pressure, low viscosity and low surface tension will facilitate the formation of the cavitation. However, since the vapor pressure and the solubility are dependent on the temperature, the choice of solvent is also highly dependent on the temperature due to the factors which were introduced in the preceding sections.

Presence of the surfactant can also increase the cavitational impact by reducing the surface tension and facilitating the formation of the bubble. Due to larger partial pressure of the gas in the bubble, the gas tends to dissolve in the liquid medium. In the presence of surfactants, the bubble nuclei can be stabilized by retarding the diffusion of the gases through the bubble surface. Then, the acoustic cavitation can be initialized when these stabilized bubbles grow by coalescence and gas diffusion [6].

### 1.2.4 Acoustic Power

The acoustic intensity ($W/m^2$) is the directly related to the square amplitude of the acoustic wave [7]. When the amplitude of the wave is increased, the acoustic power is also increased. The acoustic power (W) is the intensity emitted by the surface. There is a minimum required acoustic power for the cavitational threshold in the formation of the bubbles. An increase in the intensity will enhance the sonochemical effects and increase the rate of the reaction by enhancing the bubble formation. However, after a critical power, increasing the intensity will deteriorate the rate of reaction. Therefore, as in the case of temperature, there is an optimum intensity of ultrasound waves for effective cavitational impacts.

### 1.2.5 Types of Ultrasonic Systems

The bath type and the ultrasonic horn are the two types of sonochemical reactors. Ultrasonic horns are the conventional devices for the sonochemical syntheses because the ultrasound is directly applied to the reaction medium without any barrier medium. The acoustic intensity of the horn systems is higher and more controlled than the ultrasonic baths. The temperature can be controlled in a sample container with a circulating chiller. The only drawback of the horn system is the metals detaching from the ultrasonic probes. This problem can be eliminated by using glass probes [8] or as it is presented in the next chapter, further purification can be applied.

In the case of ultrasonic baths, the sonication is applied indirectly where the acoustic intensity is transferred through the liquid inside the device and through the reaction container. The intensity is also lost due to the reflections from the walls of the device. The temperature control is highly difficult when ultrasonic baths are utilized[8]. Thus, ultrasonic baths are suggested for cleaning processes.

### 1.3 Overview of the thesis

This M.Sc. thesis provides alternative synthesis methods of two different inorganic materials by the sonochemical approach. Chapter 2 is based on the synthesis of micro- and nanocrystals of $NaYF_4$ as a host material for upconversion processes. The fundamental information of upconversion luminescence is introduced and the most common synthesis methods are reviewed. The optimum reaction conditions for pure phase crystals are investigated in detail. The study of the factors affecting the shape and morphology is presented. The upconversion luminescence spectra of these crystals are examined. In Chapter 3, by the utilization of ultrasonic waves, a unique synthesis method of CdS quantum dots is presented. At the beginning of the chapter, the relationship between the size and the fluorescence the quantum dots is briefly explained. The fluorescence emission properties of the synthesized quantum dots are examined under different reaction conditions. The thesis is concluded with a short summary of the performed studies in Chapter 4.

# Chapter 2

# SONOCHEMICAL ROUTE TO LANTHANIDE DOPED $NaYF_4$ SYNTHESIS

## 2.1 Overview

In this chapter, the concept of upconversion is introduced and one of the upconverting host material, $NaYF_4$, is presented by a different synthesis method. In literature, $NaYF_4$ is the most extensively studied host material for upconversion processes. In this research, for the synthesis of $NaYF_4$ crystals, the utilization of ultrasonic waves is studied in depth. In the results, initially, the investigation of the optimum reaction conditions yielding pure $NaYF_4$ crystals is explained in detail. Then, the factors affecting the shape of the $NaYF_4$ crystals are presented with the scanning electron microscope images. In the last section, the upconversion spectra of the annealed crystals are investigated.

## 2.2 Introduction

In the last decade, upconversion processes has gained interest in various fields. Easy and cheap synthesis methods and advancements solid state laser systems, have led the applications to expand to different fields such as solid state physics, materials science, photochemistry, and biology. Upconversion is a rather unusual phenomenon with great advantages.

### 2.2.1 Upconversion

Upconversion is a non-linear process where the high energy photons (e.g. visible) are emitted by suitable ions upon excitation with low energy radiation (e.g. infrared). This phenomenon was first discovered by Auzel, Ovsyankin and Feofilov in 1960's [9-11]. Today, with the development of cheap and high powered infrared diode lasers, upconversion is much of interest in various applications. Upconverting materials are produced for many applications, such as bio-imaging [12-19], lasers [20], display materials[21, 22], solar cells [23, 24]. Core-shell synthesis methods also draw interest to obtain inert coating for upconversion efficiency enhancement, active coating for functionalization[25-29] or for the biological applications[30], plasmonic enhancement [31-33], magnetic functionalization[34] are typical examples. There is high demand for upconverting materials in biological applications because upconversion process is highly advantageous for biological specimens. Unlike quantum dots or organic fluorophores which are excited with high energy UV photons, upconverting materials are excited with low energy NIR photons. This prevents the photodamage, autofluorescence and photobleaching. Also, for imaging applications, high penetration depth of NIR photons in the tissue is a benefit.

#### 2.2.1.1 Mechanism

Lanthanides are rare-earth elements (La, Ce, Pr, Nd, Pm, Sm, Eu, Gd, Tb, Dy, Ho, Er, Tm, Yb, Lu) with atomic numbers varying from 57 to 71 in the periodic table. Yttrium is also affiliated with the rare-earth elements. Lanthanides govern interesting spectroscopic properties because of their electronic energy levels. The 4f shell in the lanthanide ions is protected or shielded by the outer lying s and p shells thus the energy levels in the f shell is less affected by the external interactions and forces. The energy levels are slightly affected by the surrounding host environment. Although the 4f-4f electric-dipole transitions are parity forbidden for trivalent lanthanides, these transitions can be observed when the lanthanides are doped in a crystal where the parity rule is relaxed. These transitions are the main elements in UC processes.

Lanthanides are mainly found in trivalent states. Trivalent ytterbium, $Yb^{3+}$, has a single energy transition between $^2F_{7/2} \rightarrow {}^2F_{5/2}$ ($\Delta E = 10000 cm^{-1}$) where the difference between these states is in the 980 nm region. $Yb^{3+}$ has a large absorption cross-section in the near infrared region and the energy levels of $Yb^{3+}$ are resonant with the f-f transitions of other lanthanide ions. These properties make $Yb^{3+}$ a suitable sensitizer. As the sensitizer, when $Yb^{3+}$ is excited, the energy of the photon can be transferred to the nearby lanthanide ions. Due to forbidden nature of f-f transitions of lanthanide ions, the absorbed energy can have long lifetimes before relaxation. If another photon is absorbed due to the energy transfer from $Yb^{3+}$ to lanthanide ions, the total energy can be converted into a single photon by the lanthanide ion, which is called the activator. By successive multiphoton absorption, visible emission can be obtained by the accumulation of NIR photons. According to different ways of absorption, upconversion mechanisms govern different names. Excited state absorption (ESA) and energy transfer upconversion (ETU) are the main upconversion processes among many. ESA occurs when multiple pump photons are absorbed only by single ion. In

an ETU process, a sensitizer ion absorbs and transfers the photons to an activator ion to excite the ion from the ground state to a metastable energy level. A second or more successive energy transfer can results in emission by the activator lanthanide ion.

#### 2.2.1.2 Host and Dopant Materials

For the applications of upconversion emissions by the trivalent lanthanide ions, inorganic compounds of lanthanides are found to be ideal since the ionic size and chemical properties of these host materials are similar to lanthanides. Therefore, the most studied host materials are found as $Y_2O_3$, $NaYF_4$, $LiYF_4$, $LaF_3$, $YF_3$ [35-41].

Single inorganic crystals, metal oxides, glass materials, semiconductor materials can also be utilized as upconverting materials for good chemical, thermal, mechanical properties[42]. The crystal matching with lanthanide ions and low vibrational energy is required for the host materials for highly efficient upconverting materials. Any crystal mismatch in the host material would cause quenching due to crystal defects such as interstitial anions and cation vacancies to preserve charge neutrality. Also, low lattice phonon energies in the host material are required for minimized non-radiative losses. Otherwise, the absorbed photon energy would be lost as vibrational relaxation instead of photon emission. Chlorides, bromides, iodides can exhibit low phonon energies (300 $cm^{-1}$) however the hygroscopic properties can limit the applications. High chemical stability can be obtained by oxides but the high phonon energy is a drawback (500$cm^{-1}$). In overall, fluorides are found to be ideal host materials for upconverting materials due to low phonon energies(350 $cm^{-1}$) and high chemical stability [43]. As a result, lanthanide doped $NaYF_4$ particles are the most extensively studied host materials. Most studied phases of these crystals are the hexagonal (β) and cubic (α) phases of $NaYF_4$. Hexagonal phase is reported to be more chemically stable and an order of magnitude enhanced in upconversion

efficiency compared to cubic phase. This phenomenon is due to the increased symmetry in the crystal structure.

Thulium (Tm), Erbium(Er), Holmium (Ho) are the most studied visible emitting lanthanide ions. Upon ~980nm excitation blue, red and near infrared (NIR) emission by Tm, red and green emission by Er, blue emission by Ho ions can be observed. In highly efficient upconverting materials, ultra-violet emission can also be observed.

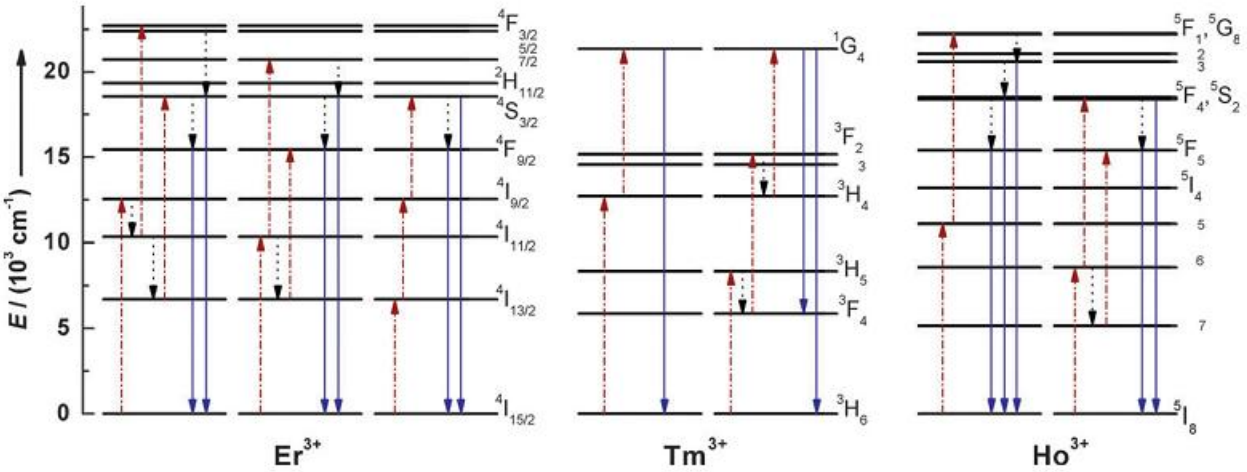


Figure 2.1 Energy level diagrams showing typical upconversion processes for $Er^{3+}$, $Tm^{3+}$, and $Ho^{3+}$ lanthanide ions. The dashed-dotted, dotted, and full arrows represent excitation, multiphonon relaxation, and emission processes, respectively [43].

### 2.2.2 Methods of $NaYF_4$ synthesis

$NaYF_4$ has two main crystal phases as α- $NaYF_4$ and β- $NaYF_4$. The synthesis of high purity β- $NaYF_4$ can require difficult synthesis conditions, such as long reaction times (24 hours [44]) , high temperatures (180°C [45]) , high pressures and high annealing temperatures (500°C [46]) . These conditions are required to overcome the energy barrier for the phase transition from cubic to hexagonal structure. Various synthesis methods are

developed for different size and morphologies of two phases of $NaYF_4$ crystals. By hydrothermal methods at very high reaction temperatures and reaction durations, single crystal $NaYF_4$ nanoparticles can be obtained [46]. However, these particles can be non-dispersible in water and non- biocompatible. Surfactants can be used to achieve biocompatible, soluble and functional particles. Co-precipitation is another mainly used method which is fast, easy and cheap. However, complex routines and requirement for the post-heat treatment are important remarks. The size and morphology are two important factors affecting the upconversion luminescence efficiency and different applications require different structures. For nanoparticle synthesis, usually surfactants are utilized in organic solvents.

Alternatively, in this chapter, a fast, easy, relatively cheap method is presented for both β-$NaYF_4$ and α-$NaYF_4$ by the application of ultrasonic waves. In all the reactions, the medium was the aqueous phase and the reaction temperature was below 80°C. The effect of the amount of precursors and the presence of surfactant or chelating agents on the size and morphology is presented in the results. The spectra of the annealed upconverting materials are presented in the results and discussion part.

## 2.3 Experimental

All chemicals were analytical grade and all of the chemicals and solvents were used as received without further purification. Deionized water (18.2 $M\Omega cm^{-1}$) was used throughout. $Y_2O_3$ and $Er_2O_3$ were purchased from Sigma Aldrich. $Eu_2O_3$, $Yb_2O_3$, $Tm_2O_3$, NaF were purchased from Alfa Aesar. $HNO_3$ (65%), NaOH, $NaNO_3$, Tri-sodium Citrate dihydrate ($HOC(COONa)(CH_2COONa)_2 \cdot 2H_2O$, sodium acetate ($CH_3COONa$) were purchased from Merck. Glycerin (Glycerol, $HOCH_2CH(OH)CH_2OH$) was purchased from Suvar Kimya.

Stock solution of lanthanide precursors was prepared as follows:

The required amount of $Y_2O_3$ and desired amount of the dopants ($Eu_2O_3$, $Yb_2O_3$, $Er_2O_3$, or $Tm_2O_3$) were added to ~40 ml water and concentrated nitric acid was added dropwise. In order to speed up the dissolution, the mixture was kept at ultrasound bath for several hours (at T=50°C) and it was left overnight for complete dissolution. The next day, if the mixture was completely dissolved, the solution was completed to the required volume with water. For stock the solutions [$Y^{3+}$] and [$H^+$] was fixed at 0.09M and 1M respectively.

For the synthesis, desired amount of stock solution is taken and required amount of $NaNO_3$ and surfactant were added. 2.5M NaOH or 10% $HNO_3$ was used to adjust the initial pH of this solution to 3. Meanwhile, required amount of NaF was dissolved in 8 ml water in ultrasound bath (T=50°C) in 30 minutes and the pH was adjusted to 11 with 2.5M NaOH solution. The main solution was transferred in the custom glass sonication vessel with a water jacket and purged with Argon gas before and during the sonication. The temperature of the solution was adjusted with a circulating chiller. For the sonication, ultrasonic probe (Bandelin HD 3200 model, 20 kHz) with 13 mm $TiAl_6V_4$ alloy tip (VS70T horn) was used. NaF solution was added to the main solution dropwise with a syringe pump during the reaction. For CW ultrasonic irradiation, reaction duration was 1 hour. In order to transfer the same amount of energy, for 3sec/3sec pulse on/off cases reaction duration was 2 hours. At the end of the reactions, the products were collected by centrifuging. The precipitate was washed with deionized water several times and dried at 90 °C for 24 hours in the oven to obtain white powders.

The crystal structure of the product was determined with the powder X-ray diffraction (XRD) measurements using a HUBER-G670 diffractometer utilizing a Germanium monochromator and Cu Kα radiation (λ = 1.5406 Å) or a Bruker D2 PHASER table-top diffractometer with the Cu Kα radiation (λ=1.54 Å) source which was operated at 30 kV

and 10 mA. For Bruker, the 2θ scan data were collected at 0.02 intervals over the range 10–80° and at a scan speed of 1 second per interval.

The scanning electron microscopy (SEM) studies were carried out in a Zeiss Ultra Plus FE-SEM or in a Zeiss Evo 40 SEM furnished with a W electron source. The crystals were cast on aluminum stubs from alcohol suspensions and were not coated for analysis if it was not necessary.

For the upconversion measurements, 5 mg of the product was annealed at 300 °C for 4 hours in air. The duration to reach 300°C is set to be 2 hours and the furnace is left to cool by itself. Annealed samples were dispersed in 2 ml deionized water in ultrasound bath for 30 minutes. The upconversion emission spectra were measured in quartz cuvettes of 1 cm path-length. The samples were excited by a 965nm continuous wave (CW) diode laser through a 10x microscope objective. A SPEX 1681B monochromator with femtowatt photodiode (Thorlabs) was used to detect the emission. The signal from the photodiode was digitized with a PIC based A/D converter and a Labview code was used to record the spectrum. All spectra were corrected for the sensitivity of the detector and transmittance of the 850nm shortpass filter (Edmund Optics). The sensitivity of the monochromator was not included in the corrections due to lack of data. In all the experiments the excitation laser was focused with a 10x microscope lens with a numerical aperture of 0.22. All the measurements were performed at room temperature while stirring the samples.

## 2.4 Results and Discussion

In this thesis, for the first time, a relatively fast and simple method for $NaYF_4$ synthesis via sonication is developed. The reaction conditions for both β- $NaYF_4$ and α-$NaYF_4$ are optimized for ultrasound assisted aqueous phase reactions below T<100°C. In the reactions, $YF_3$, β- $NaYF_4$ or α-$NaYF_4$ are possible crystals as the products (Figure 2.2) and $Yb^{3+}$(20%) / $Eu^{3+}$(2%), $Yb^{3+}$(20%) / $Tm^{3+}$(2%), $Yb^{3+}$ (20%) / $Er^{3+}$(2%) co-doped or $Eu^{3+}$(2%), $Tm^{3+}$(2%) single doped crystals are synthesized. For the reactions, the yield is found as ~90%.

In this part, firstly, the reaction conditions leading to pure phase products will be presented and then, for the shape control, the effect of surfactants on the crystal shape will be presented.

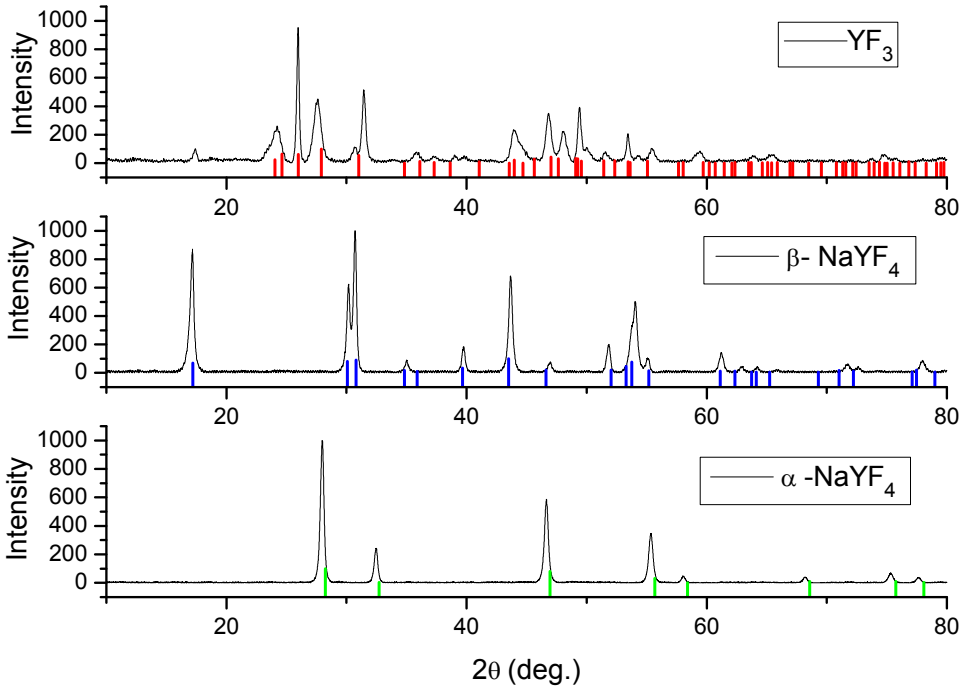


Figure 2.2 XRD patterns of $YF_3$ (JCPDS card no: 74-0911), β- $NaYF_4$ (JCPDS card no: 16-0334) and α-$NaYF_4$ (JCPDS card no: 77-2042) crystals respectively. All doped with $Yb^{3+}$ / $Eu^{3+}$.

### 2.4.1 Factors affecting $NaYF_4$ synthesis via ultrasound

In certain conditions, sonication can promote $NaYF_4$ formation. Different reaction conditions, such as precursor amounts, pulsation, temperature, dissolved gases, intensity of ultrasound, surfactants can change the product as well as the shape of the crystals.

The main factor leading to $NaYF_4$ is the amount of precursors. The precursor ratios as $Ln^{3+}$:$Na^{+}$, $Ln^{3+}$:$F^{-}$ can be altered to synthesize desired phase of pure $NaYF_4$. Since the precursors consist of $Y^{3+}$ and the dopant lanthanides, the total moles of reactant is abbreviated as $Ln^{3+}$ where $[Ln^{3+}] \neq [Y^{3+}]$.

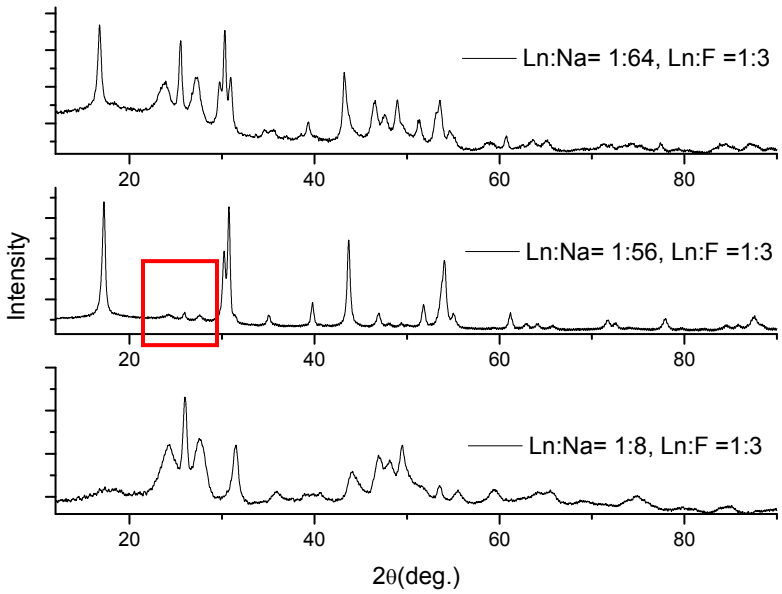


Figure 2.3 Effect of the sodium ion ratio ($Ln^{3+}$:$Na^{+}$) on the formed product (When reaction conditions are 20%$Yb^{3+}$/ 2% $Eu^{3+}$, T=25°C, 3sec/3sec pulse on/off, 50% amplitude)

For single doped systems such as 2% $Eu^{3+}$ or 2% $Tm^{3+}$, at T=25°C, Ln:Na = 1:8 is sufficient to obtain pure β-$NaYF_4$ (XRD not shown here). However, when higher dopant amount is present such as in the case of $NaYF_4$ co-doped with $Yb^{3+}$(20%)/ $Eu^{3+}$(2%), $Yb^{3+}$(20%) / $Tm^{3+}$(2%) or $Yb^{3+}$ (20%) / $Er^{3+}$(2%), sodium amount should be higher than Ln:Na = 1:8. As seen in Figure 2.3, increased sodium amount enhances the β-$NaYF_4$ formation, but after some point very high concentration of sodium is not effective for the β-$NaYF_4$ synthesis. Nevertheless, as emphasized with the red box, the minimum $YF_3$ impurity was observed when $Ln^{3+}$:$Na^+$ =1:56 and there is not a $Ln^{3+}$:$Na^+$ ratio that would produce pure β-$NaYF_4$ (Not all tried $Ln^{3+}$:$Na^+$ ratios are shown). The high sodium concentration may have led to inefficient cavitation due to increased viscosity and decreased vapor pressure. Therefore, in order to increase cavitational effect at the same conditions increasing the temperature to 50°C yields pure β-$NaYF_4$ which is discussed further in the next section.

For the effect of Ln:F ratio, only Ln:F =1:3 and Ln:F =1:4 was investigated. For safety reasons, excess NaF usage was avoided since the $F^-$ can react with the glass reaction container and HF gas formation is highly dangerous. When stoichiometric amount of $F^-$ is used, at high sodium content, the reaction tends to go to α-$NaYF_4$. Similar to the sodium amount, NaF content can also affect the morphology and size of the synthesized crystals. In this thesis, since the NaF usage was kept within limits, only the effect on the crystal phase was observed.

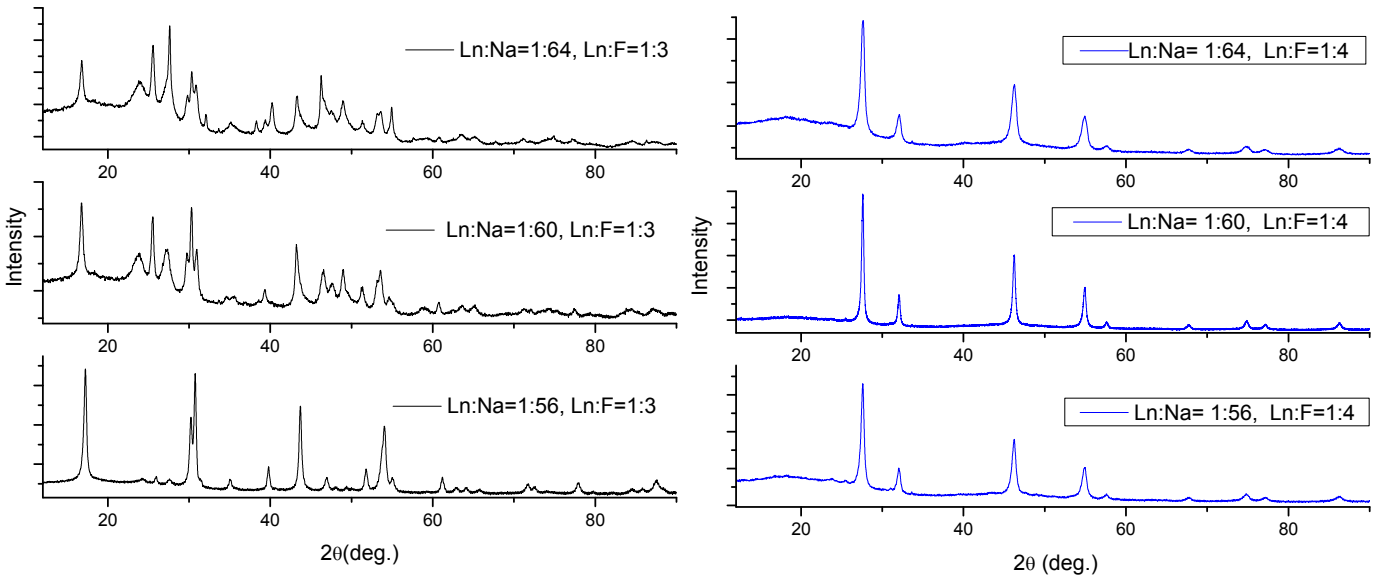


Figure 2.4 Effect of $Ln^{3+}$:$F^-$ ratio at high sodium content (When reaction conditions are 20%$Yb^{3+}$/ 2% $Eu^{3+}$, T=25°C, 3sec/3sec pulse on/off, 50% amplitude)

Overall, when Ln:F = 1:3, intermediate Ln:Na ratio leads to β-$NaYF_4$ phase, otherwise the product will be mixed with $YF_3$ crystals. If Ln:F =1:4, high Ln:Na ratio leads to α-$NaYF_4$. In some cases, if the sodium content is not high enough, when Ln:F =1:4, mixed α- and β-$NaYF_4$ can be observed. Scanning microscopy images are presented in forthcoming sections.

#### 2.4.1.1 Temperature

By the conventional methods, high temperature can facilitate the formation of high quality, highly upconversion efficient $NaYF_4$ crystals. However, in ultrasound assisted syntheses, increased temperature can lead to a decrease in the cavitational effect. As the temperature of the reaction medium is increased, although the bubble formation is faciliated by decreasing the cavitation threshold, the collapse of the bubbles can be prevented by the gases filling the cavitation bubble [47]. When the bubble is formed, it can be filled with the

vapor of the reaction medium or with the dissolved gases. According to what filled the bubble, there would be several types of bubbles present, such as empty cavity, the vapor filled cavity, the gas filled cavity and combination of vapor and glass filled cavities [48]. Therefore, if the bubble contents are mostly gas, the most sonochemical effects would be observed when temperature is lowered. At low temperatures, also the successive collapse of the bubbles is assured. On the other hand, further lowering the temperature would prohibit the formation of the bubbles. This is either due to the increase in the surface tension or viscosity of the liquid. Also, the liquid's vapor pressure decreases with the decreasing temperature. In overall, it is suggested that, sonochemical effects are maximized when a solvent of low vapor pressure is used or the temperature is lowered as possible [49].

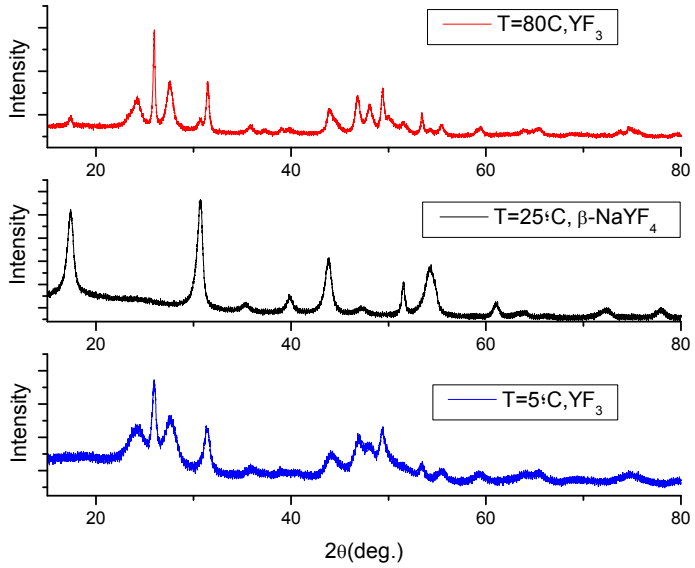


Figure 2.5 Effect of temperature on the formation of different crystals (Reaction conditions: $Ln^{3+}$:$Na^{+}$ =1:8, $Ln^{3+}$:$F^{-}$ = 1:3, 3sec/3sec pulse on/off, Amplitude= 50%, Dopant: $Eu^{3+}$ (2%))

Table 2.1 Properties of products as a function of temperature

| Sample | XRD | T(°C) | Pulse(on/off) | Amplitude | $Ln^{3+}:F^-$ | $Ln^{3+}:Na^+$ |
|---|---|---|---|---|---|---|
| **T1** | $YF_3$: $Eu^{3+}$ (2%) | 5 | 3sec/3sec | 50% | 1:3 | 1:8 |
| **T2** | β-$NaYF_4$: $Eu^{3+}$ (2%) | 25 | 3sec/3sec | 50% | 1:3 | 1:8 |
| **T3** | $YF_3$+ β-$NaYF_4$: $Eu^{3+}$ (2%) | 80 | 3sec/3sec | 50% | 1:3 | 1:8 |

As suggested in literature, too low (T=5°C) or too high (T=80°C) temperatures lead to synthesis of $YF_3$ crystals. When single dopant such as $Eu^{3+}$ (2%) or $Tm^{3+}$ (2%) is present, for the formation of pure β-$NaYF_4$, T=25°C is found to be sufficient (Figure 2.5). However, if the system is co-doped with such as $Yb^{3+}$(20%) / $Eu^{3+}$(2%), $Yb^{3+}$(20%) / $Tm^{3+}$(2%) or $Yb^{3+}$ (20%) / $Er^{3+}$(2%), as it is explained in the preceding part, at T=25°C, further increasing the sodium content does not yield pure $NaYF_4$ due to increased ionic strength of the reaction medium. Therefore, in order to obtain pure phase $NaYF_4$ crystals, at high sodium content, temperature should be 50°C to enhance sonochemical effect (Figure 2.6).

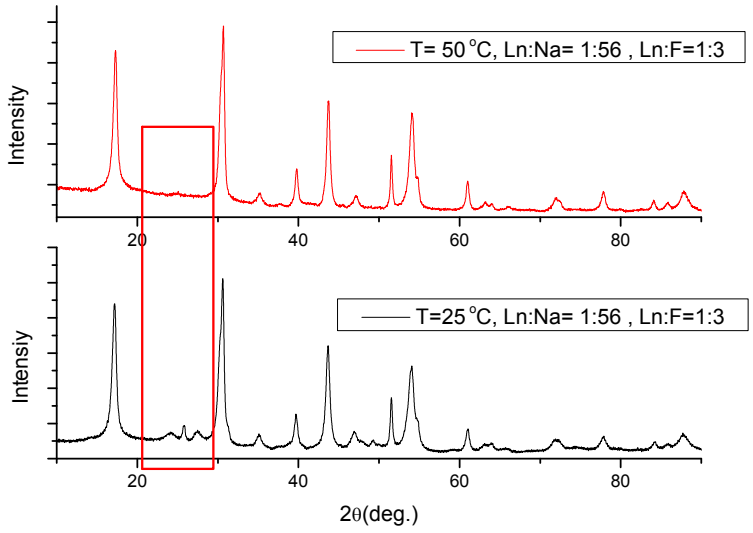


Figure 2.6 T=50°C leads to β-$NaYF_4$ when dopants are $Yb^{3+}$(20%) / $Eu^{3+}$(2%), $Yb^{3+}$(20%) / $Tm^{3+}$(2%) or $Yb^{3+}$ (20%) / $Er^{3+}$(2%)

The similar ionic radius of the lanthanide ions makes it possible to confine them in the host lattice by the replacement of the host ions. When the ytterbium dopant amount is 20%, the conditions which lead to pure $NaYF_4$ is not the same when only 2% dopant is present. More sodium is required and temperature is elevated from 25 to 50°C. Ytterbium ionic radius is the smallest among the lanthanides that are used in this study (Table 2.2). Thus, crystal formation in the presence of ytterbium requires altered reaction conditions.

Table 2.2 Ionic radii of the lanthanides used in this thesis [50]

| **Ion** | **Ionic radius** |
|---|---|
| $Y^{3+}$ | 90.0 pm |
| $Eu^{3+}$ | 94.7 pm |
| $Er^{3+}$ | 89.0 pm |
| $Tm^{3+}$ | 88.0 pm |
| $Yb^{3+}$ | 86.8 pm |

In overall, at fixed temperature (T=50°C), $Ln^{3+}$: $Na^{+}$ and $Ln^{3+}$: $F^{-}$ amounts are the most important phase determining factors. These conditions can be altered to tune the crystal type. However, as any chemical reaction, the outcome of the reaction is not always very strict on close reaction conditions. Same phase, without any impurity, can be obtained for similar reaction conditions. The suggested reaction conditions reported so far are based on the most possible outcomes.

#### 2.4.1.2 Pulsation (Duty Cycle)

Duty cycle is defined as the ratio of the duration of the active state of sonication to the period of the application. In other words, duty cycle will be the time spent on the ON state to the total time spent (Pulse On+Off). In the reactions, when continuous wave (CW) ultrasound is applied, $NaYF_4$ synthesis was unpredictable. For the pulsed cases, when pulse was applied for 8 minute/ 2 minute pulse on/off (duty cycle=0.80), pure $NaYF_4$ synthesis

was also unpredictable because $NaYF_4$ was not successfully formed for every single run (Bottom of Figure 2.7). The best and consistent condition was determined as 3sec/3sec pulse on/off. The application of the pulsation, enhances the successful collapse of the cavitation bubbles and facilitating the formation of pure phase $NaYF_4$. This is rather unusual, when the conventional cavitation lifetime is considered. An average lifetime of a cavitation bubble is on the order of microseconds. Even when the duty cycle is remained the same and the duration of the pulse is changed, such as 5sec/5sec pulse on/off and 1sec/1sec pulse on/off, $YF_3$ and β-$NaYF_4$ mixed with $YF_3$ crystals was obtained respectively.

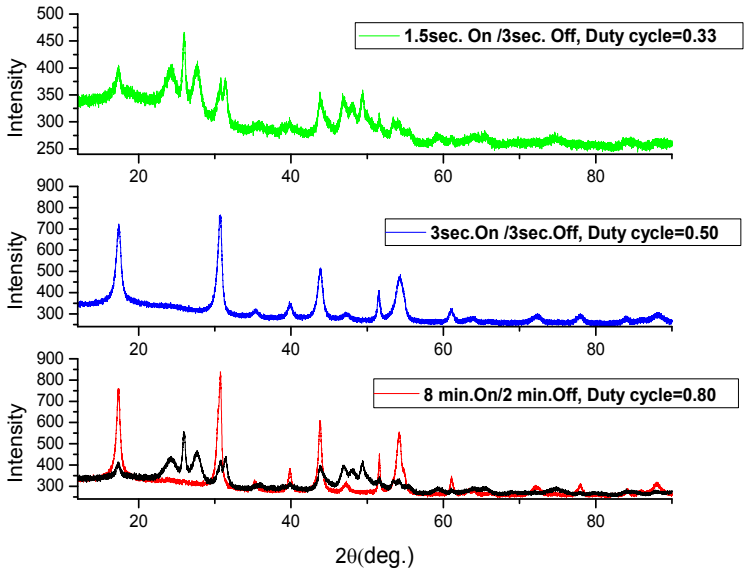


Figure 2.7 Effect of pulsation to the crystal structure

### 2.4.1.3 Dissolved Gases

The sonication is only effective when the cavitation occurs. The presence of dissolved gases can promote the formation of cavitation bubbles by creating nucleation centers. Therefore, when the liquids were degassed, the values of the applied acoustic pressure

necessary to create cavitation bubbles were increased, i.e. cavitation threshold was increased [7, 47-49]. The type of the gas is also important because larger specific heat ratio ($\gamma=c_p / c_v$ ) of the gas, creates greater cavitational effect. Monatomic gases such as argon ($\gamma=1.66$) and helium can convert more energy compared to diatomic gases such as nitrogen ($\gamma=1.40$) and oxygen (for air $\gamma=1.40$) and $CO_2$ is found to be the most unsuitable gas [7, 47, 49].

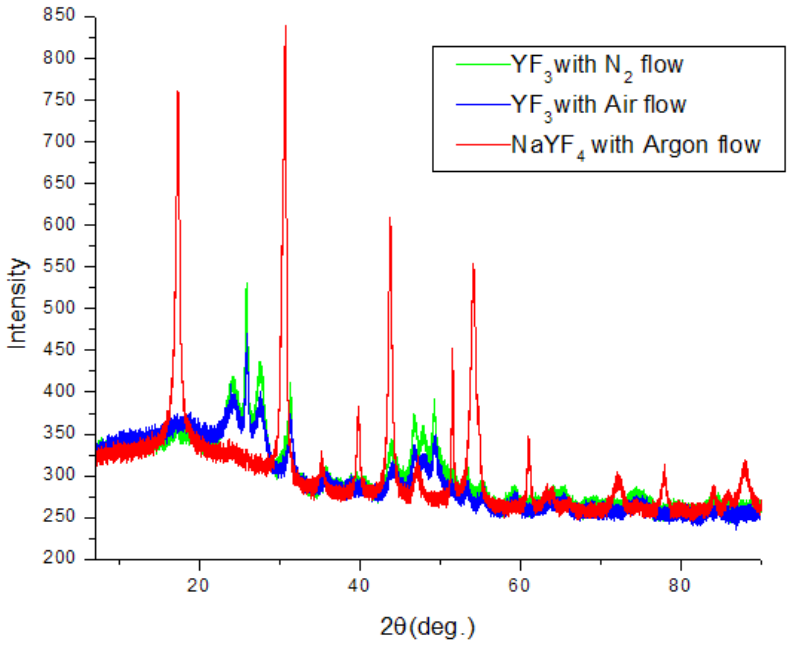


Figure 2.8 Effect of purged gas on the synthesis of different crystals. (Reaction conditions: T=25°C, 3/3 sec pulse on/off for 2 hours, $Ln^{3+}$:$Na^{+}$ =1:12, $Ln^{3+}$:$F^{-}$ = 1:3, Amplitude= 50%, Dopant: $Eu^{3+}$(2%) )

For the same reaction conditions, the type of purged gas through the reaction liquid affects the type of the product. In Figure 2.8, it is seen that greater cavitational effect which was created by Argon, lead to formation of pure $NaYF_4$. Therefore, in all the reactions Argon gas was chosen to purge to system.

#### 2.4.1.4 Power / Amplitude

By changing the amplitude of the ultrasound that is applied, the intensity of ultrasound or the irradiation power can be altered. There is a threshold for the formation of $NaYF_4$ crystals. As the irradiation power is increased, the pressure amplitude of the applied sound increases. This will increase the number of cavitations and the intensity of the collapse. However, after a certain point, increasing the acoustic intensity creates less effect because as the number of the formed bubbles increases, these bubbles merge with each other and rather than collapsing, they float to the surface of the liquid and become useless at the process. Therefore, there is an optimum intensity of ultrasound for the specific reaction medium which efficiently creates the cavitation process. At the same reaction conditions (T=50° C, 3sec/3sec pulse on/off, $Ln^{3+}$:$Na^+$ =1:20, $Ln^{3+}$:$F^-$ = 1:3), for the pure $NaYF_4$ synthesis, the optimum intensity is found as 50%.

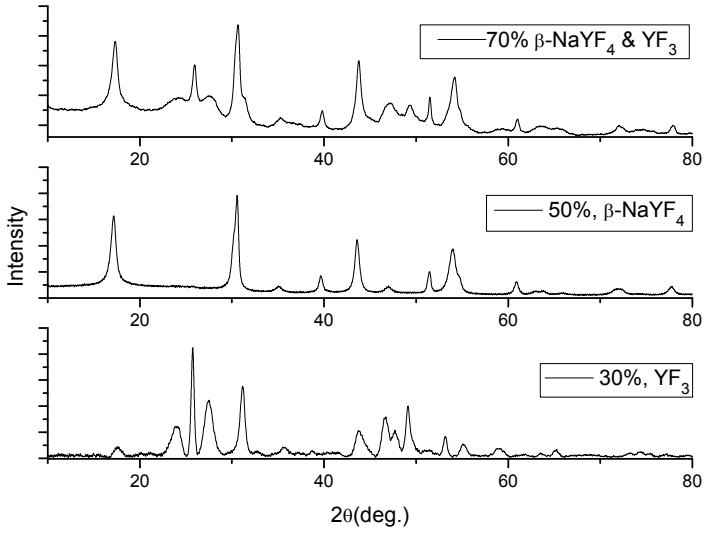


Figure 2.9 The effect of amplitude of the sound waves, for the reaction conditions of T=50° C, 3sec/3sec pulse on/off, $Ln^{3+}$:$Na^+$ =1:20, $Ln^{3+}$:$F^-$ = 1:3.

### 2.4.2 Post Processes

#### 2.4.2.1 Cleaning/ Purification

Due to intense bombardment by shock waves from cavitation implosions, the radiating face of the horn can be eroded during the reaction. According to the solution's conditions such as temperature, viscosity or concentration, the erosion can be fast or slow. Eroded face should be smoothed before the sonication with polishing or with fine emery paper if necessary because the rate of erosion is faster for rough surfaces and the product will be further contaminated with titanium erosion from the tip. The erosion of titanium is visible to the eye and the product and these titanium impurities can be separated from the product by using density gradient method.

Density gradient method allows you to separate particles with different densities by centrifugation. The motivation of using density gradient method was to separate different phases or crystals or create monodispersity. However, the density of the two phases of $NaYF_4$ crystals is very close to each other which makes them inseparable for the attempted mediums (For α-$NaYF_4$ d=4.21 g/cm$^3$ and β-$NaYF_4$ d=4.23 g/cm$^3$, $YF_3$ d= 4.01g/cm$^3$). On the other hand, Ti impurities (Ti d=4.5 g/cm$^3$) from the ultrasonic horn can be removed from the products by creating a density gradient between glycerin (d= 1.258g/cm$^3$) and water. For this process, it is found out glycerol was the best medium of choice in terms of ease of use and separation ability among 30% dextran solution (d=1.1g/cm$^3$), 65% sucrose solution (d=1.316 g/cm$^3$) or honey (d=1.36g/cm$^3$).

For this process, 28 mg product was dispersed in 8ml water in ultrasound bath for 30 minutes. Larger titanium impurities were collected at the bottom of the vial and discarded. In a 15 ml centrifuge tube, 2 ml glycerol was placed at the bottom and 1.5-2 ml of the product which was dispersed in water was placed on top of the glycerol (Figure 2.10 A).

After centrifugation at 1500 rpm for 1.5 minutes, titanium particles travel to the bottom of the centrifuge tube and cleaner suspension was collected from the top layer and washed with deionized water. The same glycerol layer was used for multiple times until glycerol starts to mix with water phase.

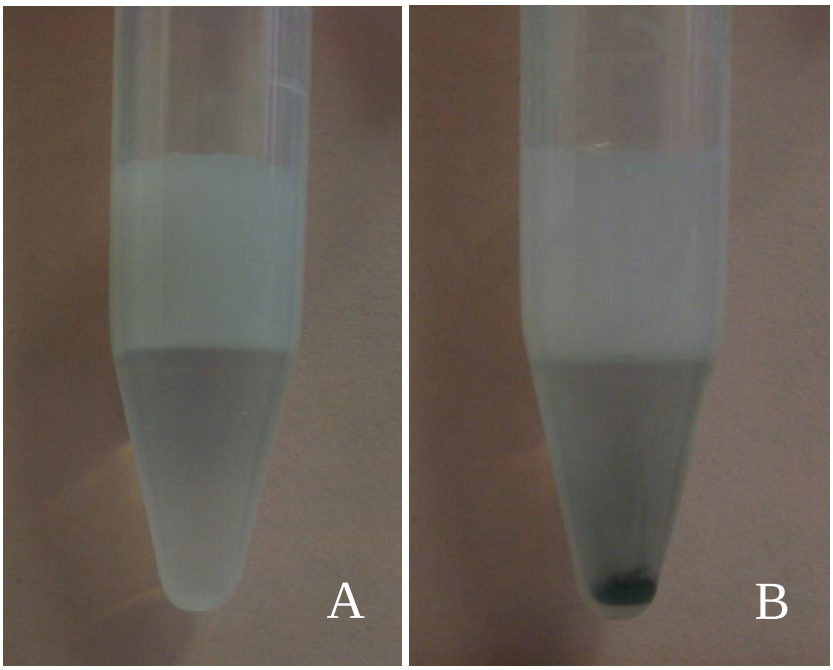


Figure 2.10 Purification and the removal of the titanium impurities from the product. Glycerol is placed at the bottom and sample dispersed in water is at the top white phase. A) Before centrifugation, B) After centrifugation

According to X-ray fluorescence (XRF) of the samples before and after this purification process, the ~1% Ti impurity by weight can be almost completely eliminated from the samples (Figure 2.11 and Figure 2.12).

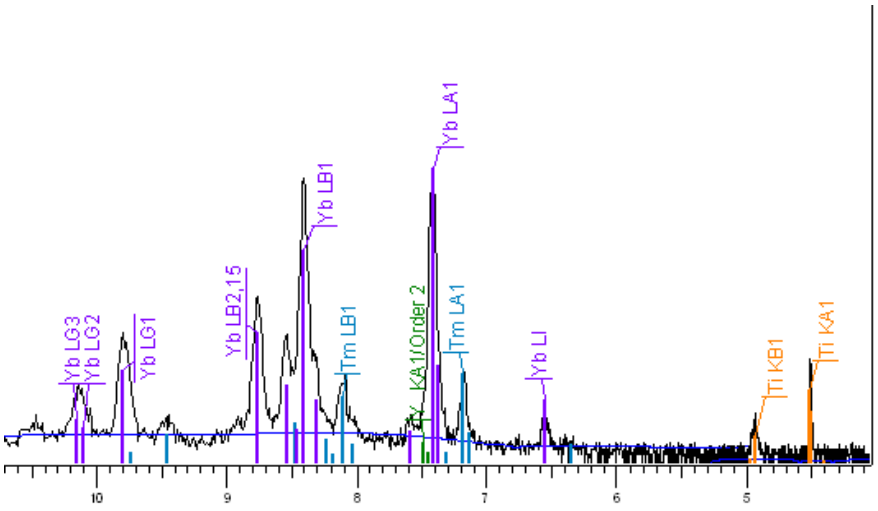


Figure 2.11 XRF of the sample before titanium impurities (indicated with orange lines) were removed by density gradient method

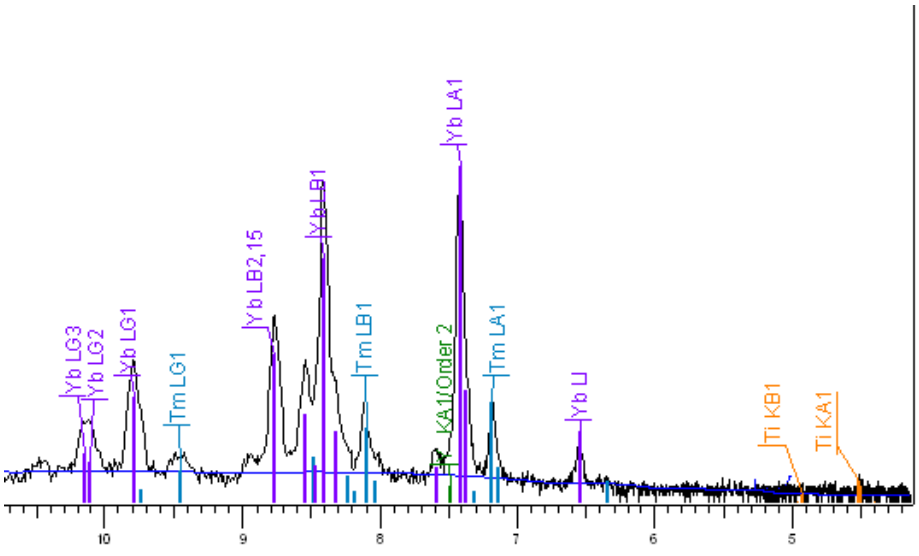


Figure 2.12 XRF of the sample after titanium impurities (indicated with orange lines) were removed by density gradient method

The titanium impurities due to the erosion of the sonication horn can be discarded by density gradient method. However, the effect of the cleaning process on the upconversion efficiency is not included in this thesis.

#### 2.4.2.2 Annealing

Upconversion luminescence can be affected by the crystals defects. According to the synthesis method, heat treatment such as annealing may be necessary in order to decrease crystal defects and enhance upconversion luminescence. For this purpose, pure single phase products were annealed at 300°C for 4 hours. XRD patterns and SEM images are recorded before and after annealing. The effect of annealing is further discussed in upconversion luminescence.

### 2.4.3 Shape control

Until this section, presented $NaYF_4$ syntheses were carried out when the surfactant molecules were not present. In order to achieve shape control, different surfactant materials or chelating agents were investigated. It is important to remember that, when ultrasound is applied to a system, the system may not behave as it is expected in conventional methods, since the ultrasonic waves change the whole reaction mechanism. Therefore, a method which is successful in conventional processes may not have an effect on the systems where sonication is applied. Usage of surfactants can enhance the cavitational activity by decreasing the surface tension of the liquid. At smaller surface tensions, the energy required to form cavitation bubbles can be lower.

Just like surfactants or chelating agents, the precursor amounts also have an effect on the size and morphology of the crystals. In the preceding sections, it was shown that sodium amount was effective to achieve different phases of $NaYF_4$ crystals. According to scanning microscopy images (SEM), the increasing sodium amount is also effective on the shape of

the β-$NaYF_4$ microcrystals. When the sodium concentration is low, needle-like micrometer sized crystals are formed (Figure 2.13 A). As the sodium concentration gets higher, the edges of these microcrystals get sharper and rice shaped microparticles are formed (Figure 2.13 C). Presence of different dopants can also affect the size and morphology of $NaYF_4$ crystals [51, 52]. However, according to Figure 2.14, the absence of 20% Yb ions does not have a dramatic effect on the morphology of β-$NaYF_4$ microcrystals.

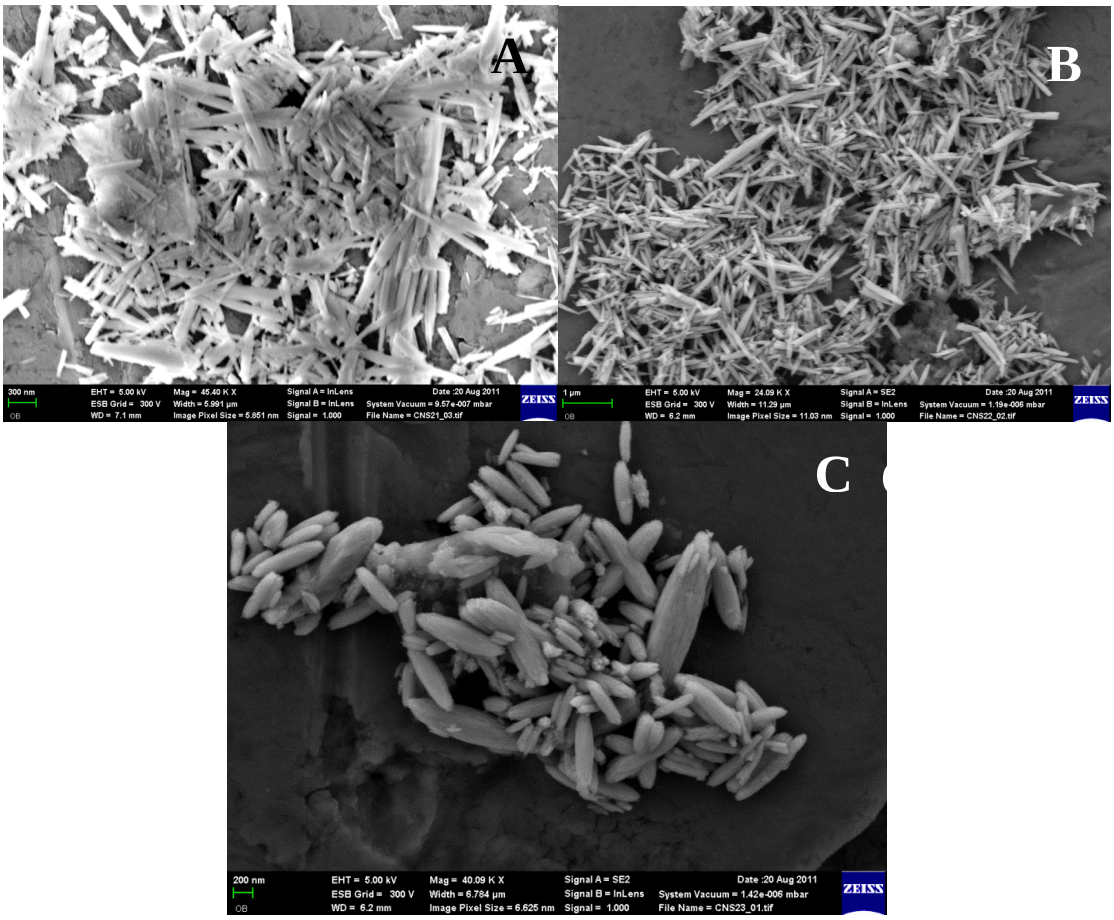


Figure 2.13 Effect of increasing sodium amount on the shape of β-$NaYF_4$ microcrystals. From A to C $Ln^{3+}$: $Na^+$ = 1:0, 1:12, 1:40. Scale bars are 300nm, 1 µm and 200 nm respectively. (Reaction conditions: T=50°C, 3/3 sec pulse on/off for 2 hours, $Ln^{3+}$:$F^-$ = 1:3, Amplitude= 50%, Dopants: $Yb^{3+}$(20%) /$Tm^{3+}$(2%))

Table 2.3 Properties of products without any surfactants

| Sample | XRD | T(°C) | Pulse(on/off) | Amplitude | $Ln^{3+}:F^-$ | $Ln^{3+}:Na^+$ |
|---|---|---|---|---|---|---|
| **F2.13A** | β-$NaYF_4$: $Yb^{3+}$(20%), $Tm^{3+}$(2%) | 50 | 3sec/3sec | 50% | 1:3 | 1:0 |
| **F2.13B** | β-$NaYF_4$: $Yb^{3+}$(20%), $Tm^{3+}$(2%) | 50 | 3sec/3sec | 50% | 1:3 | 1:12 |
| **F2.13C** | β-$NaYF_4$: $Yb^{3+}$(20%), $Tm^{3+}$(2%) | 50 | 3sec/3sec | 50% | 1:3 | 1:40 |
| **F2.14** | β-$NaYF_4$: $Tm^{3+}$(2%) | 50 | 3sec/3sec | 50% | 1:3 | 1:20 |
| **F2.15** | α-$NaYF_4$:$Yb^{3+}$(20%), $Tm^{3+}$(2%) | 30 | 3sec/3sec | 50% | 1:4 | 1:0 |

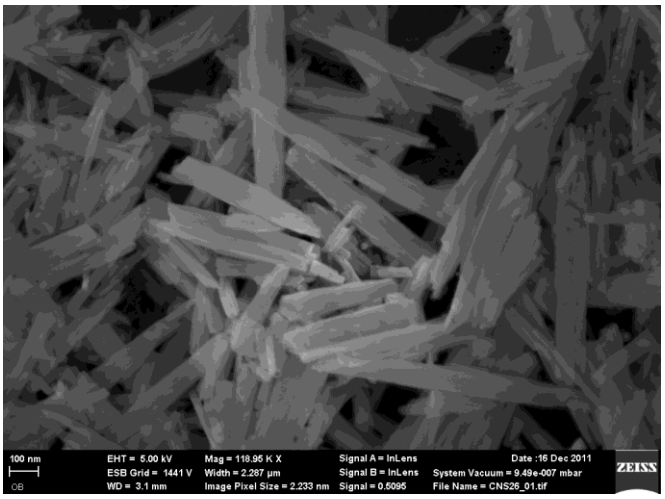


Figure 2.14 Effect of the absence of $Yb^{3+}$ on the shape of β-$NaYF_4$ microcrystals. Scale bars is 100nm. (Reaction conditions: $Ln^{3+}:Na^+$ = 1:20, $Ln^{3+}:F^-$ = 1:3, T=50°C, 3/3 sec pulse on/off, Amplitude= 50%, Dopant: Only $Tm^{3+}$(2%))

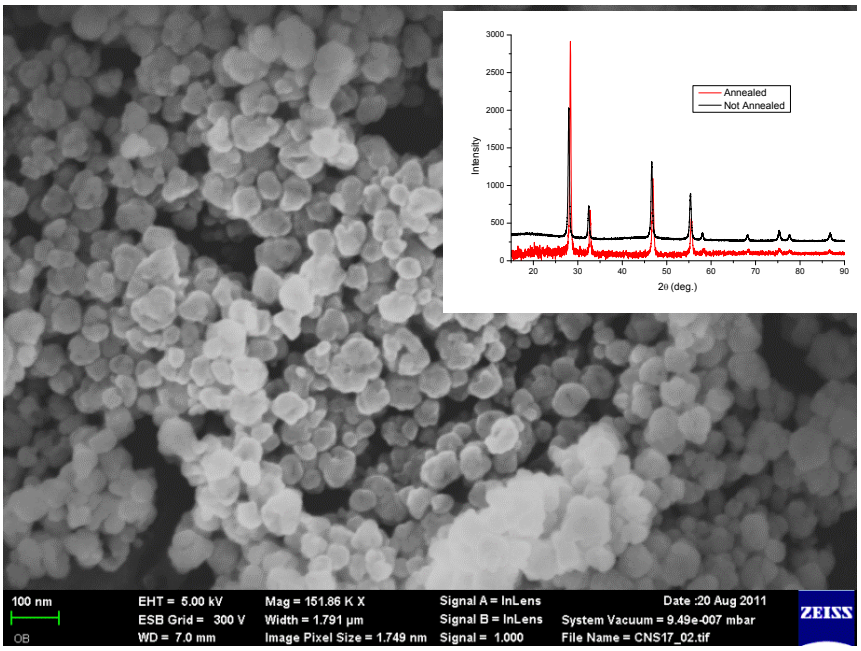


Figure 2.15 Image of α-$NaYF_4$ nanocrystals. Scale bar is 100nm. Inset image shows the XRD pattern before and after annealing (Reaction conditions: T=30°C, 3/3 sec pulse on/off for 2 hours, $Ln^{3+}$:$F^-$ = 1:4, Amplitude= 50%, Dopants: $Yb^{3+}$(20%) /$Tm^{3+}$(2%))

According to Figure 2.15, two synthesized phases of $NaYF_4$ crystals are dramatically different in size and morphology. β-$NaYF_4$ crystals are much bigger than the α-$NaYF_4$ nanocrystals. Basically, when there is not any surfactant or chelating agent present, the reaction conditions for β-$NaYF_4$ creates microcrystals and the conditions for α-$NaYF_4$ leads to spherical nanocrystals. This phenomenon can be due to the nature of the crystal phase and/or due to the high concentrations of ions present. For α-$NaYF_4$ case, it is important to remember that there are much more ions of $Na^+$, $F^-$, $NO_3^-$ present in the reaction medium which can limit the growth of the crystals. Therefore α-$NaYF_4$ is obtained in smaller sizes.

For the shape and morphology control, trisodium citrate (abbreviated as Nacitrate) and Ethylenediaminetetraacetic acid (EDTA) are the mostly studied chelating agents [32, 44, 53-55]. Binding of cations in the reaction medium with Nacitrate or EDTA creates a cation chelated complex. The competition between the $F^-$ anion and the chelators lead to transformation of the Ln-complex to the $NaYF_4$ lattice [53]. To determine the effect of the chelating agents in the presence of ultrasonic irradiation, reactions with Nacitrate and EDTA were carried out. Unfortunately, reactions with EDTA did not yield any form of crystal. This unexpected result can be due to the strong binding between the EDTA and the cations. However, the cavitational collapses were expected to break these bonds throughout the reaction. Therefore, the reason may be that, at pH=3, the equilibrium with the EDTA and cation could have shifted the reaction and EDTA complex was not established.

On the other hand, unexpectedly, utilization of Nacitrate as the chelating agent led to formation of α-$NaYF_4$ nanocrystals where the reaction conditions were the established for the β-$NaYF_4$ formation. In Figure 2.16, the effect of different Nacitrate amounts and Na amounts can be observed. In the reactions with Nacitrate, size of the nanoparticles were between 50-100 nm, however, small particles have formed aggregations of bigger chunks. In Figure 2.16 C and E, Nacitrate was used as the sodium source and $NaNO_3$ was not added to the system. According to the results, when Ln: Nacitrate ratio was above unity, no significant change in the size was observed and high Nacitrate content led to aggregations of smaller particles to each other. Only in the case of D, individual spheres can be easily observed.

Table 2.4 Properties of the products with surfactants, for T=50°C, 3sec/3 sec pulse on/off, Amplitude: 50%

| Sample | XRD | $Ln^{3+}:F^-$ | $Ln^{3+}:Na^+$** | $Ln^{3+}$:Ligand |
|---|---|---|---|---|
| **F2.16A** | α- $NaYF_4$: $Yb^{3+}$(20%), $Er^{3+}$(2%) | 1:3 | 1:0 | $Ln^{3+}$:Nacitrate = 1:2 |
| **F2.16B** | α -$NaYF_4$: $Yb^{3+}$(20%), $Tm^{3+}$(2%) | 1:3 | 1:40 | $Ln^{3+}$:Nacitrate = 1:2 |
| **F2.16C** | α -$NaYF_4$: $Yb^{3+}$(20%), $Tm^{3+}$(2%) | 1:3 | 1:40 | $Ln^{3+}$:Nacitrate = 1:13.24* |
| **F2.16D** | α -$NaYF_4$: $Yb^{3+}$(20%), $Tm^{3+}$(2%) | 1:3 | 1:40 | $Ln^{3+}$:Nacitrate = 1:1 |
| **F2.16E** | α-$NaYF_4$: $Yb^{3+}$(20%), $Er^{3+}$(2%) | 1:3 | 1:30 | $Ln^{3+}$:Nacitrate = 1:10* |
| **F2.16F** | α-$NaYF_4$: $Yb^{3+}$(20%), $Er^{3+}$(2%) | 1:3 | 1:60 | $Ln^{3+}$:Nacitrate = 1:1 |
| **F2.17A1** | α- $NaYF_4$: $Yb^{3+}$(20%), $Tm^{3+}$(2%) | 1:3 | 1:50 | $Ln^{3+}$:NaAc =1:50 * |
| **F2.17B1** | α -$NaYF_4$: $Yb^{3+}$(20%), $Er^{3+}$(2%) | 1:3 | 1:50 | $Ln^{3+}$:Citric Acid =1:2 |
| **S1** | $YF_3$: $Yb^{3+}$(20%), $Er^{3+}$(2%) | 1:3 | 1:50 | $Ln^{3+}$:MAA =1:2 |
| **S2** | $YF_3$ + β-$NaYF_4$ $Yb^{3+}$(20%), $Er^{3+}$(2%) | 1:3 | 1:50 | $Ln^{3+}$:3-MPA =1:2 |

***Ligand as the sodium source, $NaNO_3$ was not added.**

**** When ligands with $Na^+$ cation were used, $Ln^{3+}:Na^+ \neq Ln^{3+}:NaNO_3$. $Ln^{3+}:Na^+$ calculated from the total number of moles of $Na^+$ present.**

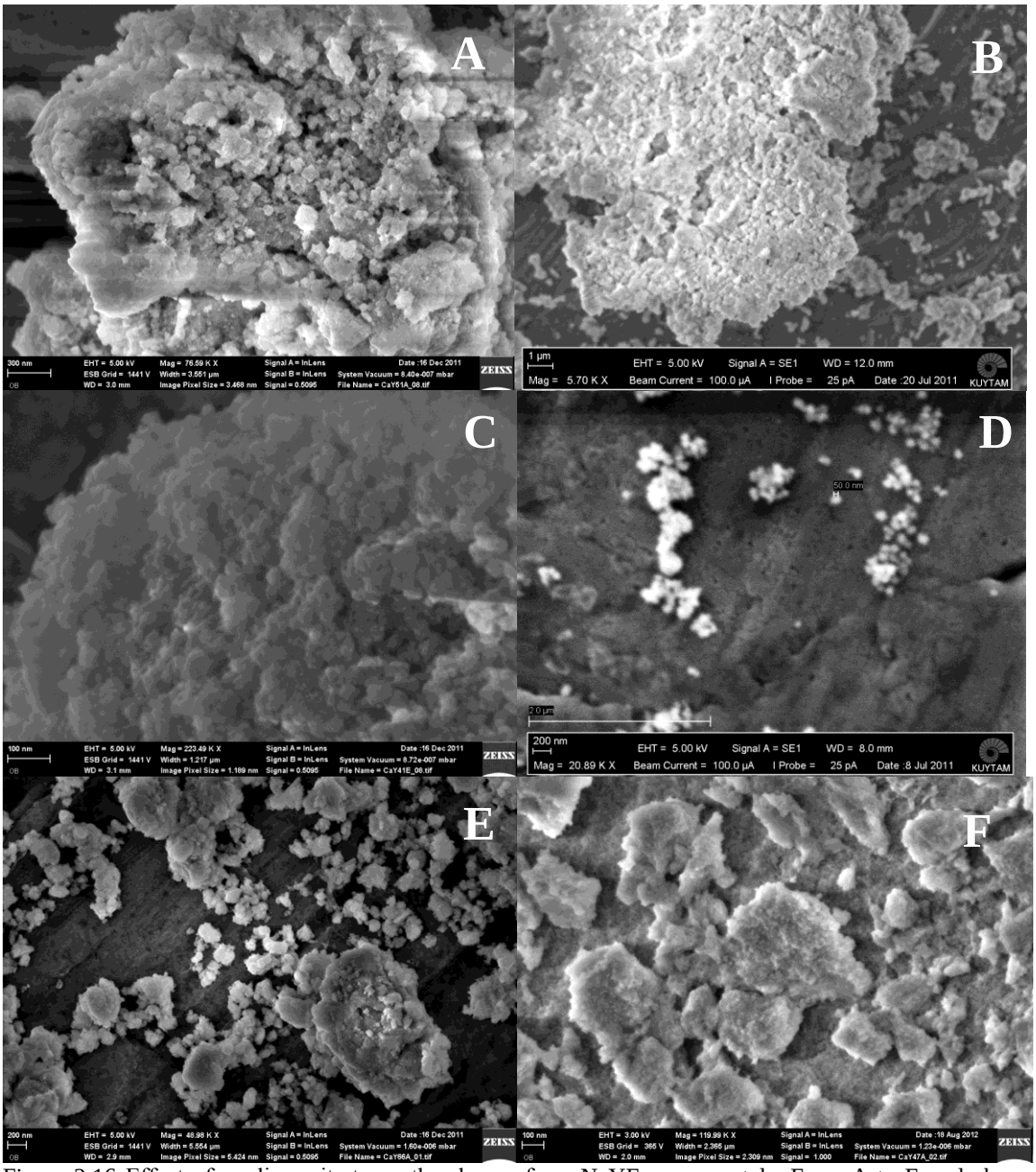


Figure 2.16 Effect of sodium citrate on the shape of α- $NaYF_4$ nanocrystals. From A to F scale bars are 300nm, 1 μm, 100 nm, 200nm, 200nm and 100nm respectively. From A to F, $Ln^{3+}$: $Na^{+}$ = 1:0, 1:40, 1:40, 1:40, 1:30 and 1:60, Ln: Nacitrate = 1:2, 1:2, 1:13.24, 1:1, 1:10, 1:1. (Reaction conditions: T=50°C, 3/3 sec

pulse on/off, $Ln^{3+}$: $F^-$ = 1:3, Amplitude= 50%, A to E dopants: $Yb^{3+}$(20%)/$Er^{3+}$(2%), $Yb^{3+}$(20%)/$Tm^{3+}$(2%), $Yb^{3+}$(20%)/$Tm^{3+}$(2%), $Yb^{3+}$(20%)/$Tm^{3+}$(2%), $Yb^{3+}$(20%)/$Er^{3+}$(2%), $Yb^{3+}$(20%)/$Er^{3+}$(2%) )

Figure 2.17, shows the case where sodium acetate (NaAc) and citric acid was used to control the shape of the crystals. Similar to the case of Nacitrate, utilization of NaAc or citric acid also led to the formation of α-$NaYF_4$ nanocrystals where the reaction conditions were established for the β-$NaYF_4$ formation. In the case of NaAc (Figure 2.17 A1), interestingly, sphere nanoparticles of ~200 nm were observed. These spheres were seemed to be formed by even smaller particles or the particles have high surface roughness. Unlike the case in Nacitrate, particles synthesized with NaAc were not aggregated or stuck to each other. For the case of Citric acid (Figure 2.17 B1), particles smaller than 100nm were observed and similar to Nacitrate cases, particles were stuck to each other. Therefore, citrate ion as the chelating agent not only leads to formation of α- $NaYF_4$ which is smaller in size compared to the case when chelating agent was not utilized, but also cause aggregated particles. For both cases, annealing changed the crystal pattern. For NaAc, $YF_3$ crystals were formed (Figure 2.17 A3). These crystals are also apparent in the SEM images (Figure 2.17 A2). For citric acid, some of the α- $NaYF_4$ crystals were transformed to β-$NaYF_4$ phase upon annealing.

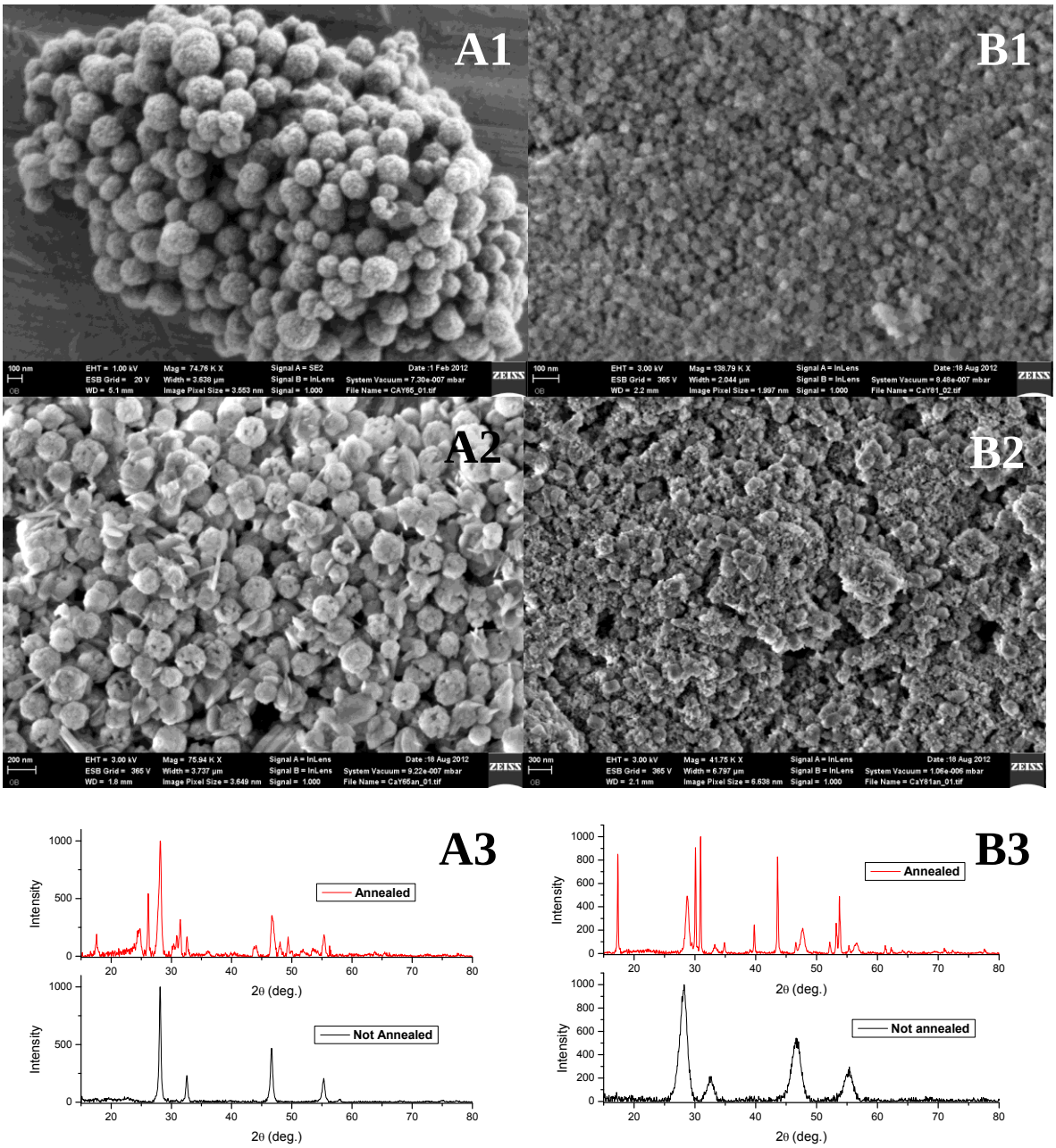


Figure 2.17 Effect of sodium acetate and citric acid on the shape of α- $NaYF_4$ nanocrystals First row corresponds to images before annealing and second row images are taken after annealing. Scale bars are 100nm, 100nm, 200nm, 300nm respectively. Third row shows the compared XRD patterns. For A, $Ln^{3+}$: $Na^{+}$

= 1:50, Ln: NaAc = 1:50. For B, $Ln^{3+}$: $Na^+$ = 1:50, Ln: Citric acid= 1:2. (Reaction conditions: T=50°C, 3sec /3sec pulse on/off, $Ln^{3+}$: $F^-$ = 1:3, Amplitude= 50%, Dopants:$Yb^{3+}$(20%)/$Tm^{3+}$(2%) and $Yb^{3+}$(20%)/$Er^{3+}$(2%))

Similarly, Mercaptoacetic acid(MAA) and 3-Mercaptopropionic acid (3-MPA) molecules were investigated as surfactants. These molecules also contain carboxylic acids that can interact with cations and they are widely used as surfactants in the quantum dot stabilization. However, reactions with MAA and 3-MPA caused formation of $YF_3$ crystals and were not studied further.

### 2.4.4 Upconversion luminescence emission

In this section, due to low efficiency of the non-annealed samples, the upconversion spectra of only annealed samples are shown. The samples which were not annealed do not show UC emission until the excitation power density is as high as $4.2x10^6$ W/cm$^2$. On the contrary, almost all the annealed samples begin to show upconversion luminescence when excited by laser power density of $0.27x10^6$ W/cm$^2$. The maximum excitation power density was kept at $4.2x10^6$ W/cm$^2$ for annealed samples. Before annealing, only the most efficient samples showed UC emission upon minimum excitation density of $2.7x10^6$ W/cm$^2$ (data not shown). Therefore, the relatively low efficiency of upconversion luminescence requires intense excitation sources and sensitive systems of detection. Upon excitation in the NIR at room-temperature, the powders can yield visible emissions to the naked eye.

In some of the samples, annealing had caused a transformation in the phase. Phase transformation is possible or expected upon annealing since the stability of the alpha and beta phases are not the same. Only for the crystals synthesized with NaAc, upon annealing, the host material was changed from $NaYF_4$ to $YF_3$ crystals. However, a change in the host matrix is not expected because 300°C is very low for decomposition. Therefore, it can be suggested that $YF_3$ impurities may have been already present in the samples, if $YF_3$ crystals

were observed upon annealing. $YF_3$ matrix should have been detected in the XRD patterns, however, the signal can be repressed by the main host material or the impurity can be too low to be detected in the XRD. Also, enhanced signal can be due to the increased crystallinity after annealing.

For the most efficient upconversion emitter nanocrystals which were doped with 20% $Yb^{3+}$ and 2% $Tm^{3+}$, intense blue, red and NIR emissions were recorded with maxima at 454 nm (blue) ( $^1D_2 \rightarrow {}^3F_4$ transition), 475 nm(blue) ( $^1G_4 \rightarrow {}^3H_6$ transition), 650 nm (red) ($^3F_2$, $^3F_3 \rightarrow {}^3H_6$ transition), 798 nm (NIR) ($^3H_4 \rightarrow {}^3H_6$ transition) respectively [56]. A considerably weaker emission at 515nm appears for the excitations at high power density. The corresponding transitions are depicted in Figure 2.18 and the luminescence spectra are shown in Figure 2.19 A. Upconversion luminescence occurs when 2 or 3 successive photons are absorbed by $Yb^{3+}$ ions and transferred to $Tm^{3+}$ ions for visible emission. For this sample, according to XRD patterns, crystal or phase transition did not occur (Figure 2.19). For an unsaturated upconversion process, the integrated UC luminescence intensity is proportional to $P^n$ where P is the laser power density and n is the number of absorbed photons required in populating the upper emitting state. When log(Integrated Intensity) vs log(P) is plotted, the slope of the linear fit gives the average number of absorbed photons, n. Due to deviation from the linear region, high power densities are not included in the linear fit. This deviation can be due to saturation by increased thermal effects. For high energy blue emissions, n is calculated as 1.98 and 2.28 for 475nm and 454 nm respectively, suggesting that 2 photon or mixed 2 and 3 photons are required for the multiphoton upconversion process for these transitions. For red emission, n is calculated as 1.62 where 2 photons are required for the emission.

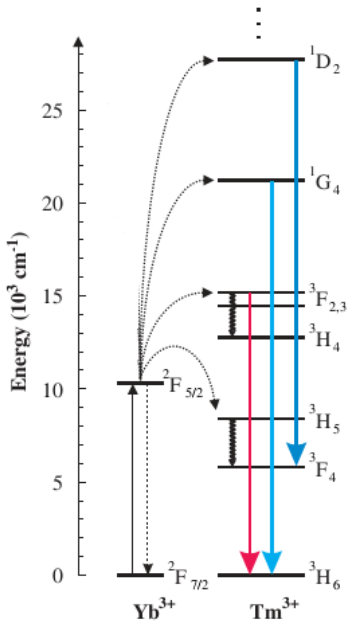


Figure 2.18 The energy level diagram of corresponding transitions of $Yb^{3+}$ /$Tm^{3+}$ co-doped crystals upon NIR excitation [56] where the full, dotted, and curly arrows represent emission, energy transfer, and multiphonon relaxation processes respectively.

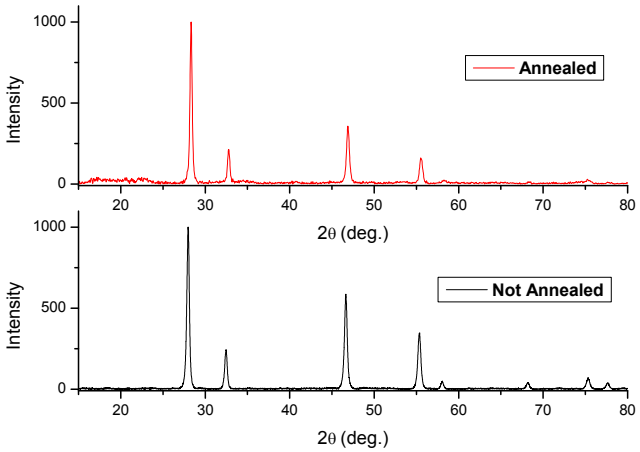


Figure 2.19 The XRD patterns before and after annealing for the most UC efficient sample as seen in Figure 2.15 (α-$NaYF_4$: $Yb^{3+}$(20%) ,$Tm^{3+}$(2%) nanocrystals (Sample F2.15), Reaction conditions: T=30°C, 3/3 sec pulse on/off, $Ln^{3+}$:$F^-$ = 1:4).

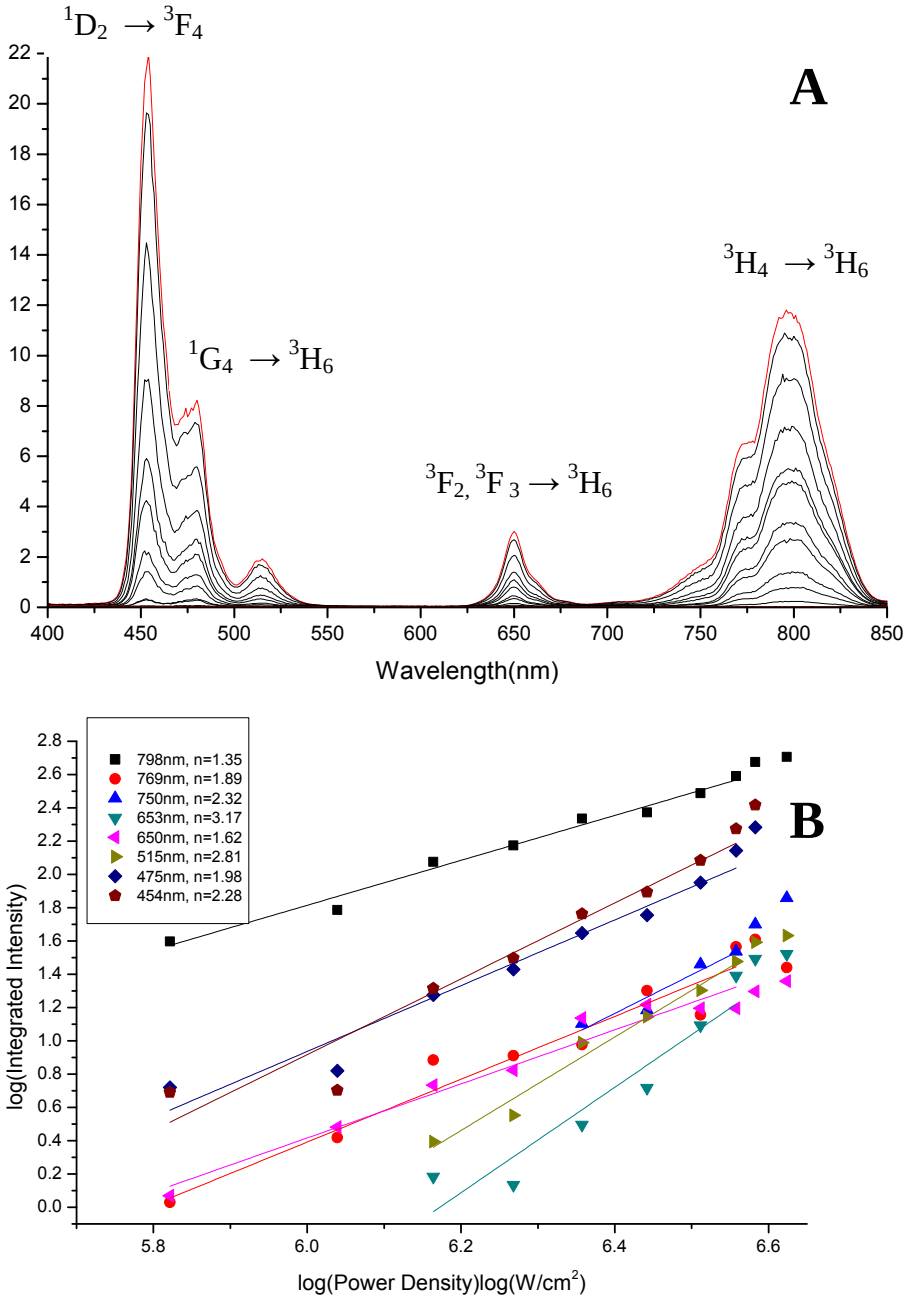


Figure 2.20 The excitation power dependence of the most UC efficient sample as seen in Figure 2.15 (α-$NaYF_4$: $Yb^{3+}$(20%) ,$Tm^{3+}$(2%) nanocrystals (Sample F2.15)

For the most UC luminescence efficient α-$NaYF_4$:$Yb^{3+}$(20%)/$Er^{3+}$(2%) nanocrystals (Figure 2.21), the green emissions between 500 and 575nm are assigned as the transitions from the $^4S_{3/2} \rightarrow {}^4I_{15/2}$ and $^2H_{11/2} \rightarrow {}^4I_{15/2}$ energy levels for the peaks with 542nm and 524nm maxima. The intense red emission at 654nm is assigned as the $^4F_{9/2} \rightarrow {}^4I_{15/2}$. The weaks emission at 409 nm corresponds to the $^2H_{9/2} \rightarrow {}^4I_{15/2}$ transition [57, 58]. The red line in Figure 2.21 A, corresponds to the excitation with the maximum and minimum power density. It is seen that, after some point the system becomes saturated and increasing the excitation energy does not increase the UC emission intensity. The corresponding number of photons for the are presented in Figure 2.21 B for the unsaturated transitions. Approximately upon 2 photon absorption the green and red emissions are observed. For the transition at 654nm, 2 photon process occurs as the following: First the Er ion is excited to $^4I_{11/2}$ by a ground state absorption. By non-radiative relaxation $Er^{3+}$ ion can relax and populate the $^4I_{13/2}$ level. By another successive transfer of photon, ion can populate the $^4F_{9/2}$ level, resulting in a red emission from this level to the ground state. When n is smaller than 1, the quenching effect occurs due to thermal effects as it is seen for the transition at 409nm [57].

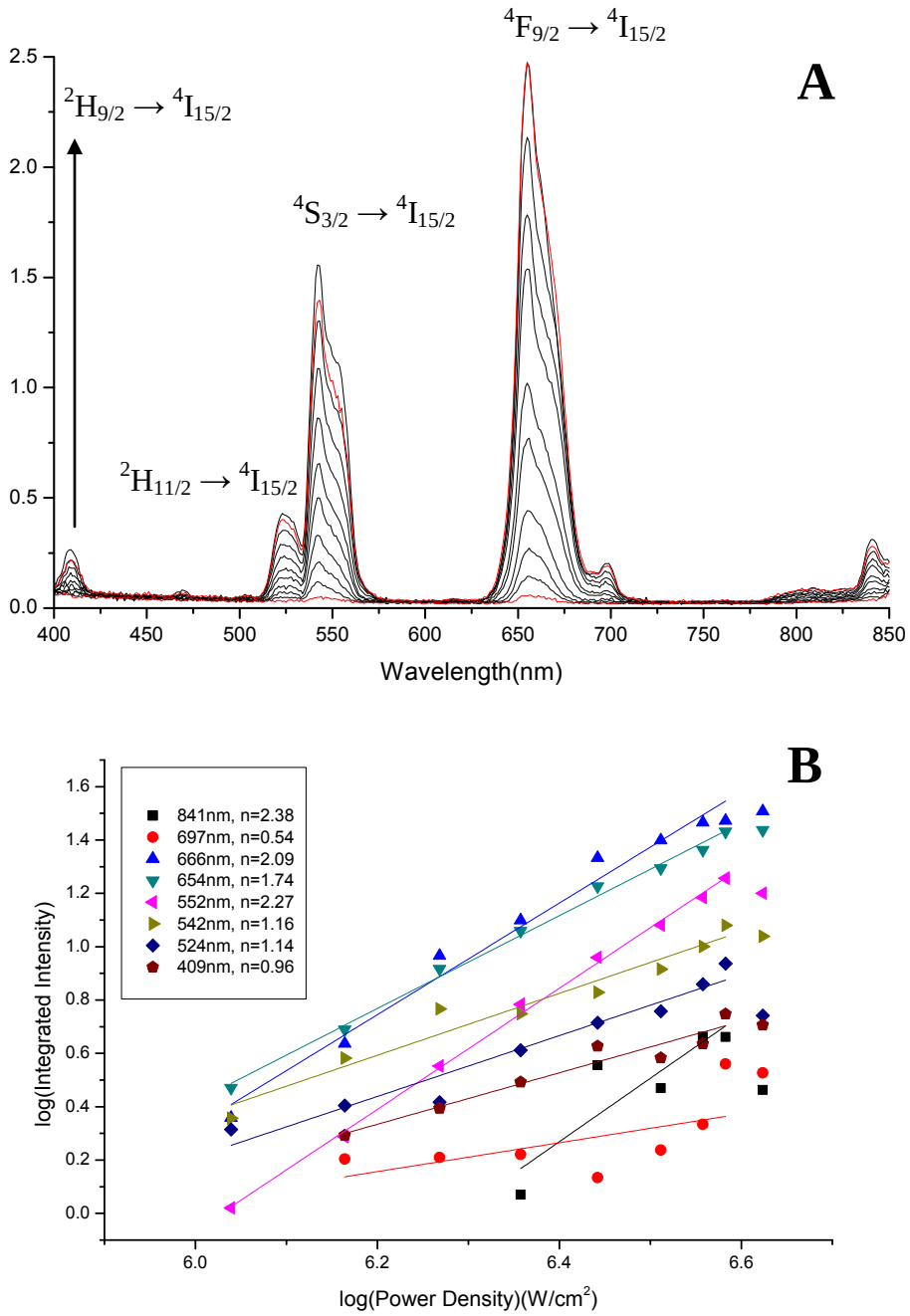


Figure 2.21 The excitation power dependence of the most UC efficient sample as seen in Figure 2.16 E (α-$NaYF_4$: $Yb^{3+}$(20%) , $Er^{3+}$(2%), nanocrystals (Sample F2.16E)

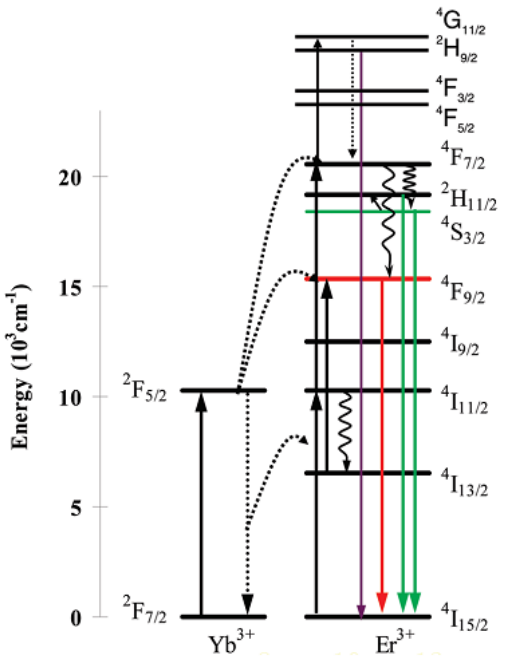


Figure 2.22 The energy level diagram of corresponding transitions of $Yb^{3+}$ /$Er^{3+}$ co-doped crystals upon NIR excitation[57] .

For the nanocrystals in Figure 2.21 A, according to XRD diagrams, annealing had caused a transition from the α to β phase where no apparent form of different crystal was observed in the SEM images (See Figure 2.23). The UC emission of the crystals can be both from the small sized alpha phase or the newly formed beta phase.

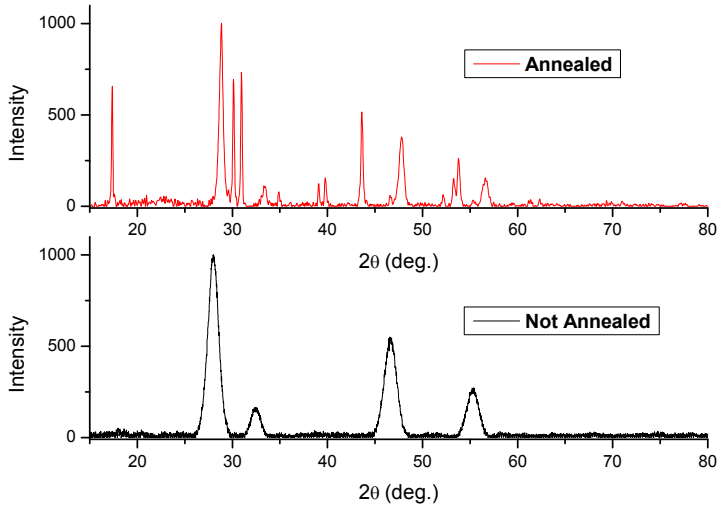


Figure 2.23 XRD diagram before and after annealing of the of α-$NaYF_4$: $Yb^{3+}$(20%) , $Er^{3+}$(2%), nanocrystals after annealing. ((Annealed Sample F2.16E) Reaction conditions: T=50°C, 3/3 sec pulse on/off, $Ln^{3+}$: $F^-$ = 1:3, $Ln^{3+}$: $Na^+$ = 1:30, Ln: NaCitrate = 1:10).

The emission spectra of the most efficient UC emitting samples are compared in Figure 2.24 for $2.7x10^{-6}$ $W/cm^2$ excitation power density. Black line corresponds to α-$NaYF_4$: $Yb^{3+}$(20%) ,$Tm^{3+}$(2%) nanocrystals (Sample F2.15) and red line corresponds to the sample with NaAc synthesis(Sample F2.17 A1) . As it was shown in Figure 2.17 before, upon annealing, the sample synthesized with NaAc, showed $YF_3$ crystals in the XRD. Therefore, the high UC emission can also be emitted by the $YF_3$ crystals. Therefore, the effect of NaAc on the luminescence properties is vague for this sample.

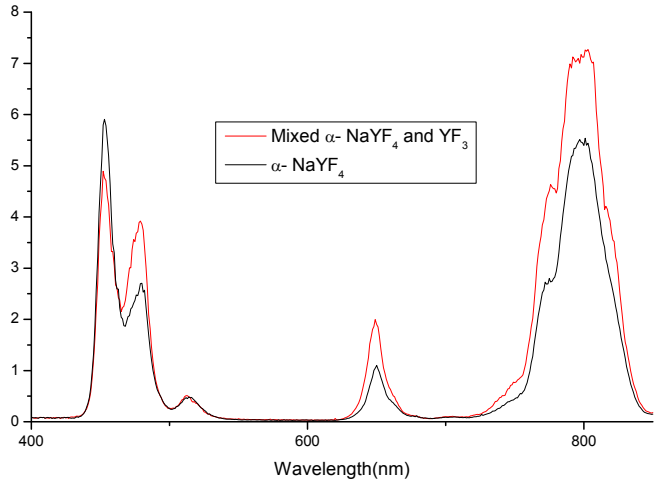


Figure 2.24 UC emission spectra of α-$NaYF_4$: $Yb^{3+}$(20%) ,$Tm^{3+}$(2%) nanocrystals (black) (Sample F2.15)and α- $NaYF_4$ + $YF_3$: $Yb^{3+}$(20%)/$Tm^{3+}$(2%) nanocrystals (red) (Sample F2.17 A1)synthesized with sodium acetate. (Reaction conditions: $Ln^{3+}$: $Na^+$ = 1:30, Ln: NaAcetate = 1:30, T=50°C, 3/3 sec pulse on/off, $Ln^{3+}$: $F^-$ = 1:3) Excitation power density is $2.7x10^6$ W/$cm^2$.

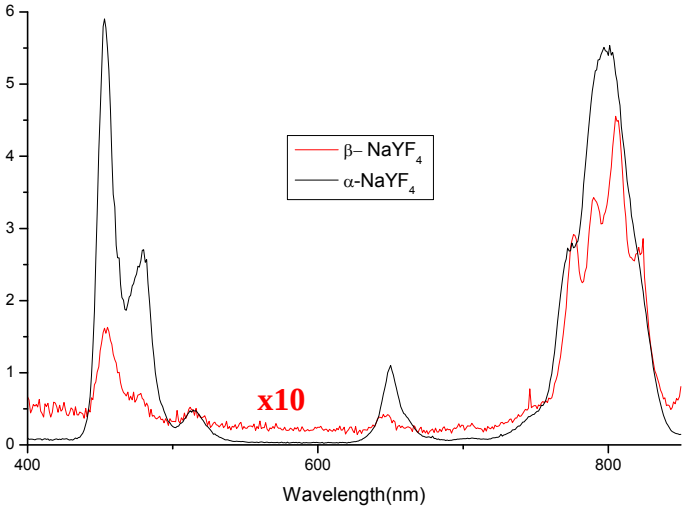


Figure 2.25 UC spectra of α-$NaYF_4$: $Yb^{3+}$(20%),$Tm^{3+}$(2%) nanocrystals (black line) and β-$NaYF_4$: $Yb^{3+}$(20%), $Tm^{3+}$(2%) microcrystals seen in Figure 2.13 A (red line) at the same excitation power density of $2.7x10^6$ W/$cm^2$.

Although β-$NaYF_4$ crystals are more UC efficient than α-$NaYF_4$ crystals, the UC efficiency for α-$NaYF_4$ crystals are found to be much higher according to reported UC spectra (Figure 2.25). As the crystal size of upconverting materials gets bigger, UC emission intensity is expected to increase, if they are formed by single crystals. Even though the β-$NaYF_4$ crystals are much larger than the α-phase, still α-$NaYF_4$ crystals are found to be more UC efficient. There can be several factors affecting the UC process in β-$NaYF_4$ crystals. Ultrasonic irradiation may have created high crystal defects or trap states which quenches the radiative emission. The distribution of emitting centers in the host matrix is also effective on the UC efficiency. If the emitting ions are found to be closer to the surface, the dangling bonds can cause non-radiative emissions. Also, the incoming light may be scattered because of the large size of crystals. Polymer coatings can be effective to enhance UC emission by eliminating the non-radiative losses by the surface dangling bonds and by decreasing the internal reflectance losses due to refractive index mismatch [59]. However, the UC efficiency was not enhanced when the β-$NaYF_4$ crystals were coated with polymers such as polyvinylpyrrolidone (PVP) or poly(ethylene glycol)-poly(propylene glycol)-poly(ethylene glycol) (Pluronic F127) block co-polymer (data not shown here). Therefore, low UC intensity can be due to high crystal defects. In the case of α-$NaYF_4$, smaller size of crystals with less crystal defects may have formed. As a result, for the upconverting particles synthesized via sonication, UC efficiency is found to be not affected by the size of the crystals, but by the irregularities in the host matrix. That concludes why the synthesized crystals were not UC efficient when they were not annealed.

Figure 2.26 shows the difference in the UC emission when β-$NaYF_4$ crystals were doped with different concentrations of $Er^{3+}$. The peak intensities were linearly correlated with the concentrations. This comparison shows that low UC emission efficiency was not due to the concentration quenching of the lanthanide ions. Concentration quenching depends not only on the concentration but also on the distribution of the lanthanide ions. Assuming that rare-

earth ions are homogeneously distributed in the crystal matrix, concentration quenching can occur if the lanthanide ions are too close each other. As a consequence, the absorbed energy is lost non-radiatively. According to Figures 2.27 and 2.28, different concentration of $Er^{3+}$ ions does not have an effect on the size or morphology. Also, after annealing β-$NaYF_4$ crystals are not transformed into any other matrix and size or morphology is not affected by annealing.

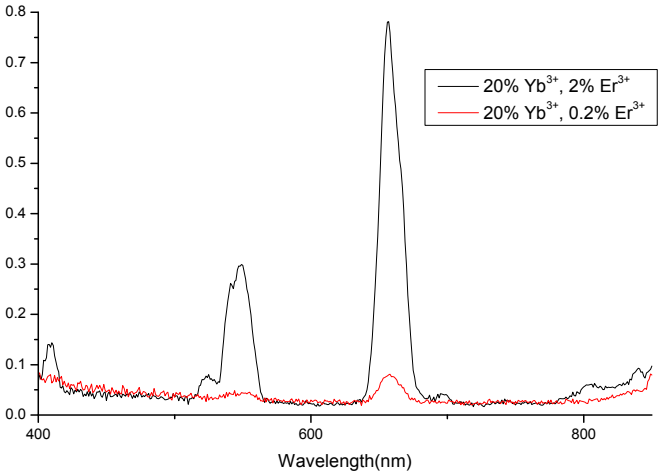


Figure 2.26 UC spectra of annealed β-$NaYF_4$ crystals doped with different concentrations of $Er^{3+}$ (Both crystals were excited with 2.7 x$10^6$ W/$cm^2$)

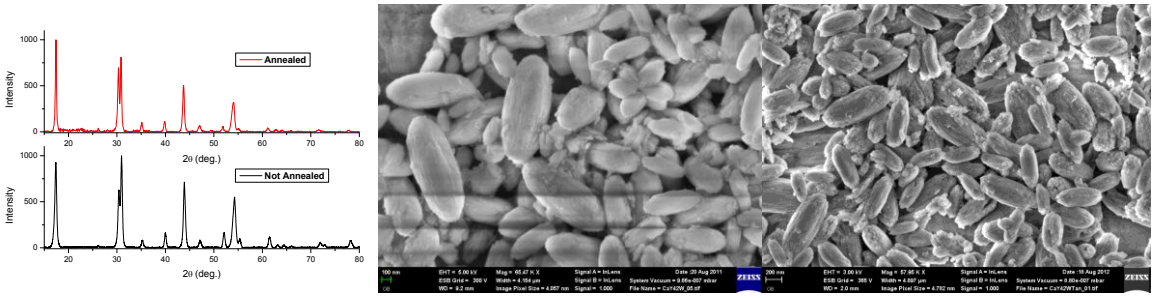


Figure 2.27 XRD patterns and SEM images of β-$NaYF_4$ : $Yb^{3+}$(20%)/ $Er^{3+}$(2%) before and after annealing

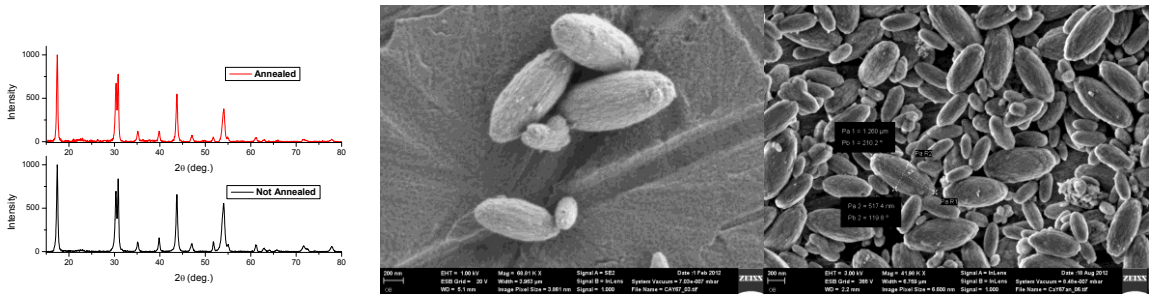


Figure 2.28 XRD patterns and SEM images of β-$NaYF_4$ : $Yb^{3+}$(20%) /$Er^{3+}$(0.2%) before and after annealing

Figure 2.29 depicts the effect of the amount of sodium citrate on the UC emission. When Nacitrate was used as the sodium source ($Ln^{3+}$: Nacitrate = 1:13.24, blue line in the spectra), UC emission was found to be larger. According to XRD patterns recorded after annealing for the case of $Ln^{3+}$: Nacitrate = 1:13.24 (Figure 2.30, left), beta phase was observed. For $Ln^{3+}$: Nacitrate = 1:1 (Figure 2.30, right), XRD showed pure phase of α-$NaYF_4$. Therefore, it is hard to say whether the high UC emission is due to eliminated dangling bonds by the Nacitrate coating or due to occurrence of high luminescence efficient beta phase.

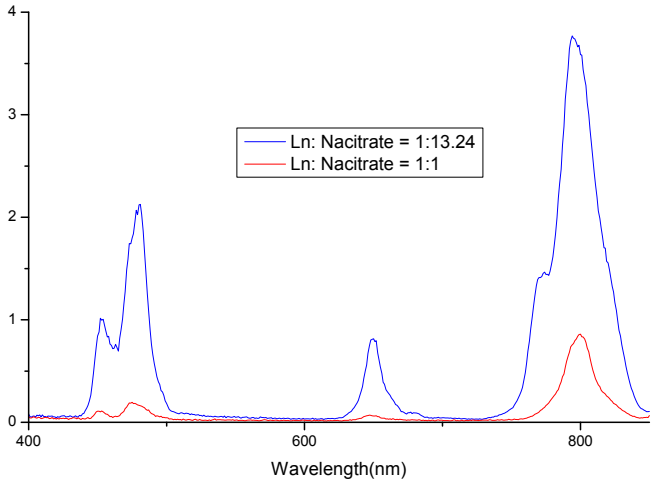


Figure 2.29 UC emission spectra of α-$NaYF_4$: $Yb^{3+}$(20%) ,$Tm^{3+}$(2%) nanocrystals of Figure 2.16 C and D by excitation power density of 2.7 x$10^6$ W/$cm^2$. The effect the amount of sodium citrate on the UC emission of

α- $NaYF_4$ nanocrystals is observed. (Reaction conditions: T=50°C, 3/3 sec pulse on/off, $Ln^{3+}$: $Na^{+}$ = 1:40, $Ln^{3+}$: $F^{-}$ = 1:3, dopants: $Yb^{3+}$(20%)/$Tm^{3+}$(2%))

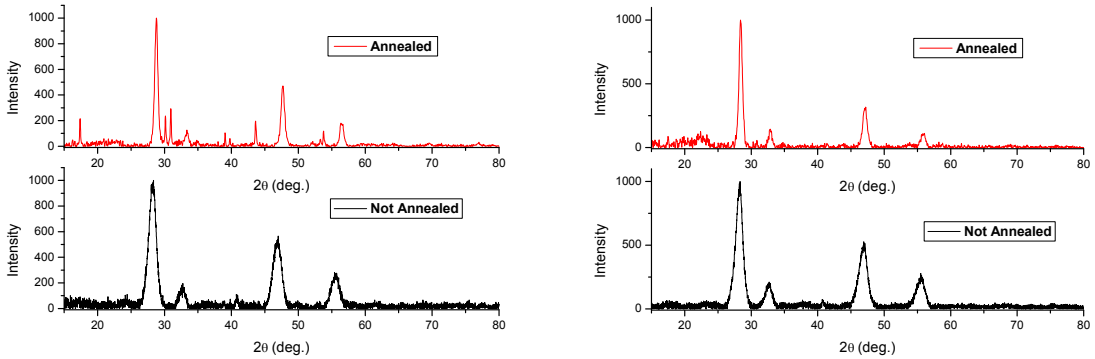


Figure 2.30 XRD patterns of the samples in Figure 2.29 before and after annealing. On the left $Ln^{3+}$: Nacitrate = 1:13.24, on the right $Ln^{3+}$: Nacitrate = 1:1.

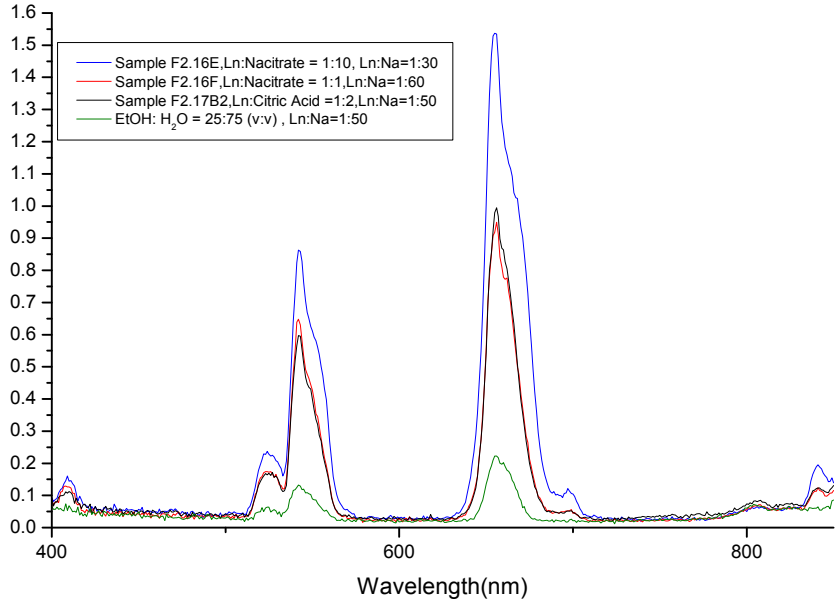


Figure 2.31 UC emission spectra of Sample F2.16E (blue), Sample F2.16F(red), Sample F2.17B2(black), sample synthesized in EtOH: $H_2O$ = 25:75 (v:v). (Reaction conditions: T=50°C, 3/3 sec pulse on/off, $Ln^{3+}$: $F^{-}$ = 1:3 for A to D with $Yb^{3+}$(20%)/$Er^{3+}$(2%) dopants ) Excitation power density of $2.7x10^6$ W/$cm^2$.

All reactions reported until here, were carried out in 100% aqueous phase. Only the sample with green line in Figure 2.31 was performed in the presence of ethanol (EtOH) where EtOH: $H_2O$ = 25:75 (v:v). In literature, ethanol/water mixtures are studied for shape and morphology control of inorganic particles. Zhang et al. showed how the various amounts of ethanol/ water ratios can affect the shape of $Cu_2O$ microparticles [60]. The due to strange interaction between water and ethanol, reaction in mixed media can be totally different when synthesis is carried out in the pure ethanol or water medium. Ethanol/ water mixture can enhance the cavitational effect by decreasing the surface tension. Smaller surface tension can enhance the cavitation activity by providing easier formation of cavitational bubbles. In the presence of ethanol, pure β-$NaYF_4$ particles were synthesized and even after annealing, the size of the crystals were smaller than the usual microparticles of pure β-$NaYF_4$ synthesized in only water (SEM image in Figure 2.32, top).

It is important to remind that, samples in Figure 2.31, were α-$NaYF_4$ before annealing. After annealing, XRD of samples turned partially into β-$NaYF_4$. On the other hand, sample synthesized in ethanol/water mixture was observed as pure β-$NaYF_4$ before and after the annealing process (Figure 2.32, bottom). However, even after annealing, the UC emission intensity (Figure 2.31, green line) was still the lowest for pure β-$NaYF_4$ crystals which were obtained smaller in size. Therefore, it suggests that the crystal defects created upon ultrasonic irradiation are excessive.

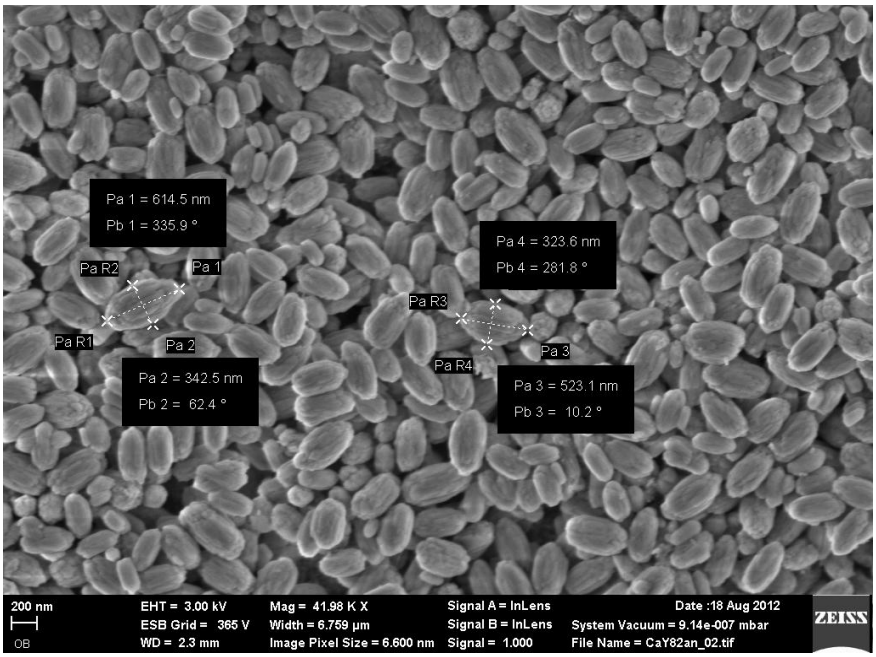


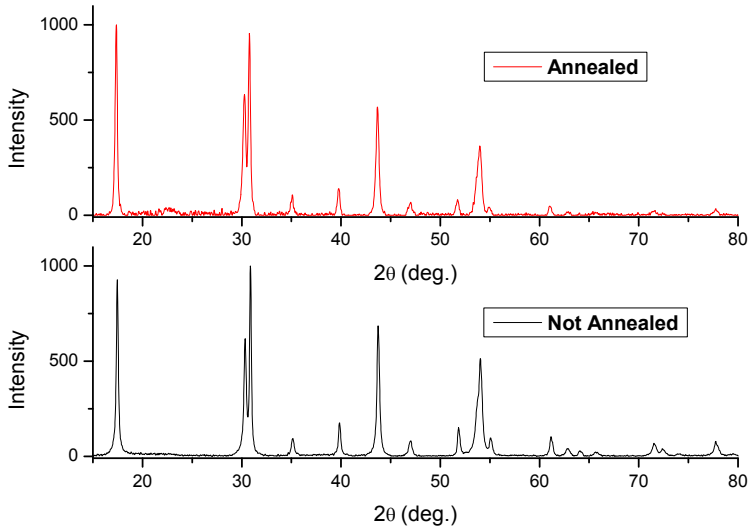


Figure 2.32 SEM image and XRD diagram of annealed β-$NaYF_4$ where reaction conditions were EtOH: $H_2O$ : 25:75 (v:v) , $Ln^{3+}$: $Na^{+}$ = 1:50, T=50°C, 3/3 sec pulse on/off, $Ln^{3+}$: $F^{-}$ = 1:3.

## 2.5 Conclusions

A fast and simple method for the synthesis of lanthanide doped upconverting $NaYF_4$ crystals were developed under sonication. Ultrasonic irradiation and the cavitational effects provided the conditions for the synthesis of β-$NaYF_4$ microparticles and α-$NaYF_4$ nanoparticles at T< 80°C in aqueous phase. In order to be able to observe upconversion luminescence at room temperature, annealing process of the crystals at 300°C for 4 hours was found to be necessary. Upon annealing, some α-$NaYF_4$ nanoparticles were transformed into more symmetrical and stable β-$NaYF_4$ phase or in some samples $YF_3$ impurity was observed. The shape or size control was carried out with many chemicals such as, tri-sodium citrate, EDTA, sodium acetate, citric acid, ethanol/water mixture, and so on. The effect of the amount of surfactants or reactants on the type of crystal, shape and morphology is reported. Upconversion spectra of the $Yb^{3+}$(20%) , $Er^{3+}$(2%) or $Yb^{3+}$(20%) , $Tm^{3+}$(2%) co-doped , α- and β- $NaYF_4$ were investigated. Upconversion luminescence which can be observed by the naked eye was observed for the annealed samples. Higher laser excitation power density compared to the conventional methods was required to observe upconversion luminescence. Low upconversion efficiency in the particles which were synthesized via sonication can be due to the remaining crystal defects after annealing. Application of intense ultrasonic waves facilitated the synthesis of $NaYF_4$ particles at relatively low temperatures, but high crystal defects which cause non-radiative relaxation upon photon excitation existed in the formed particles.

# Chapter 3

# ULTRASOUND-ASSISTED AQUEOUS PHASE SYNTHESIS OF CdS QUANTUM DOTS

## 3.1 Introduction

Quantum dots (QDs) are among the most extensively studied nanoparticles which govern unique properties due to their size. These nanoparticles are well-known for their size dependent fluorescence properties which are not observed in their bulk forms. These properties have led to diverse application opportunities in different fields such as optics, nanobiotechnology, photovoltaics and electronics. In addition to their commercial availability, quantum dots are utilized in solar cells, light emitting diodes (LEDs), electronics, sensors, lasers[61], medical imaging[62], biological labeling [63, 64].

In this chapter, a new, unusual and simple method for aqueous phase CdS quantum dot synthesis with ultrasound irradiation will be explained in detail. Following sections will introduce the main concepts of quantum dots, traditional synthesis methods and an alternative aqueous phase synthesis of CdS QDs. The fluorescence characteristics are the main feature which determines the quality of the quantum dots. The reaction conditions affecting the fluorescence properties of the quantum dots will be presented.

### 3.1.1 Quantum Dots

Quantum dots are basically semiconductor nanoparticles with size dependent fluorescence properties. Mostly studied semiconductor quantum dots are usually composed of II-VI (CdS, CdTe, CdSe), III-V (GaAs, InP) or IV-VI (PbS, SnTe) group elements. Among these crystals, Group II-VI semiconductors emit in the visible region.

### 3.1.2 Quantum confinement

Quantum dots exhibit significantly unique optical properties which are not available in the bulk form. The size dependence of the band gap energy is the most famous property of the quantum dots. The band gap energy is the sufficient amount of energy that is required for a transition to occur in a semiconductor nanoparticle. When this energy is provided, an electron from the valence band is excited to the conduction band by creating a hole in the valence band. This electron and the hole as a pair is called the exciton (Figure 3.1).

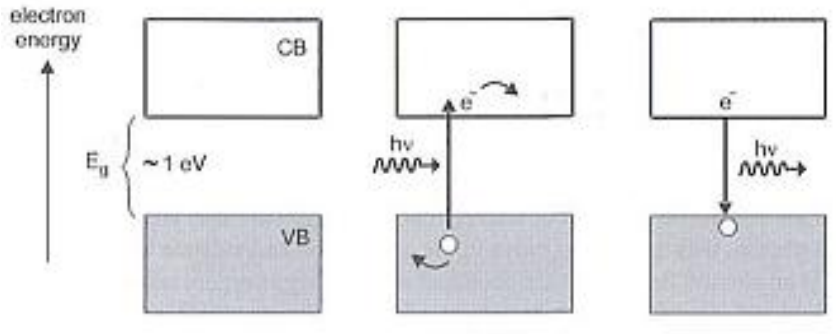


Figure 3.1 Schematic of semiconductor energies[65]

Bulk semiconductor crystals have a certain band gap energy which is independent of the crystal size. On the other hand, the band gap energy is highly dependent on the size of the semiconductor nanoparticles (QDs). This property occurs when the crystal size is comparable to Exciton Bohr Radius (EBR) which is the distance between the electron and the hole. When the size of the crystal is small enough, the quantum size effects as

quantized energy levels can be observed whereas the bulk the energy levels are continuous. This *quantum confinement* can be explained by the particle-in-a-box model phenomenon. In this quantum model, the energy levels are an inverse function of the length of the box.

$$E_n = \frac{h^2 n^2}{8md^2} \qquad \text{Eq 3.1}$$

In the case of quantum dots, the excited electron cannot escape the crystal (as well as the hole) and it behaves as a particle in a confined space which is the crystal itself. This electron can return to the valence band by emitting a photon with the energy equal to the band gap energy. This is the reason why the wavelength (color) of the emitted photon depends on the crystal size.

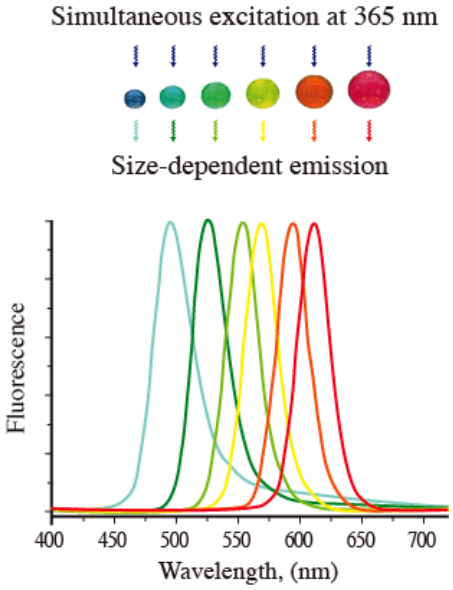


Figure 3.2 The dependence of the fluorescence on the size [66]

### 3.1.3 Crystal size determination with Brus equation

When semiconductor crystals are sufficiently small, they no longer exhibit the bulk energy level scheme or the electronic spectra, even though they have the bulk-like crystal structure, bond length and the same unit cell as the bulk.

In 1984, L.E Brus explained the correlation between the size of the small semiconductor crystals and the band gap energy by the electron-hole interactions [67].

The bandgap energy of a semiconductor is defined as the energy required to create an electron ($e^-$) and a hole ($h^+$) at rest with respect to the crystal lattice. It is stated that, as the crystallite approaches small sizes, the electron and hole interactions with the crystallite surfaces will dominate in the electronic properties and the energy level scheme will depend on the size, shape and the crystal itself. Therefore, quantum size effects are apparent when the crystallite is small enough not to have bulk-like electronic wave functions.

Brus asserts that [68], when the electron and the hole interact with each other via a shielded Coulomb interaction and the model can be written as:

$$\hat{H} = \frac{-\hbar^2}{2m_e}\nabla_e^2 \frac{-\hbar^2}{2m_h}\nabla_h^2 - \frac{e^2}{\epsilon|r_e - r_h|} + \text{polarization terms} \qquad \text{Eq. 3.2}$$

Therefore the lowest eigenvalue or the first excited electronic state is analytically approximated as:

$$E^* \cong E_g + \frac{\hbar^2\pi^2}{2R^2}\left(\frac{1}{m_e} + \frac{1}{m_h}\right) - 1.8\frac{e^2}{\epsilon R} + \text{smaller terms} \qquad \text{Eq.3.3}$$

In Eq.3.2, $m_e$ is the effective mass of the electron and $m_h$ is the effective mass of the hole. $\varepsilon$ is the dielectric constant of the crystallite, $E_g$ is the band gap energy of the bulk and R is the crystallite radius for spherical nanocrystals.

As a result, according to equation 3.3, the energy of the observed band gap of the quantum dots depends on the size of the crystal. The energy increases with decreasing size and vice versa.

The size calculation from the absorption edge by using the Brus equation is further explained in Appendix.

Table 3.1 Electronic parameters for the indicated crystalline direct gap semiconductors, $E_g$ is the band gap, the effective masses are in units of the free electron mass and ε is the dielectric coefficient [67]

| | **$E_g$ (0 K) (eV)** | **$m_e$*** | **$m_h$*** | **ε** |
|---|---|---|---|---|
| **InSb** | 0.24 | 0.015 | 0.39 | 15.6 |
| **GaAs** | 1.52 | 0.07 | 0.68 | 10.9 |
| **CdS** | 2.58 | 0.19 | 0.8 | 5.7 |
| **ZnO** | 3.44 | 0.24 | 0.45 | 3.7 |

### 3.1.4 The Optical Properties

Optical properties of the synthesized quantum dots can be investigated by their absorption and fluorescence spectra. In terms of absorption and emission characteristics quantum dots have various advantages over traditional commercial dyes such as organic fluorophores.

For quantum dots, several features can be observed in the fluorescence spectra. The emission wavelength is an indicator of the size of the QDs. As the size gets smaller, the band gap energy increases, therefore the wavelength of the emitted light shifts to smaller wavelength. Therefore, size tunability, variation of the emitted colors by changing the size is possible.

Occurrence of broad bands in absorption spectra of QDs is a result of the combination of the transitions from different exciton energy levels. In the absorption spectra of QDs, the wavelength where the sample starts to absorb light is called the absorption edge and this

wavelength is used to calculate the size via Brus equation. A peak in the absorption spectra is called the absorption onset, indicating the highest distribution of average particle size. As the emission wavelength, this feature is also dependent on the size of the nanocrystals. As the size gets smaller, the absorption onset shifts to smaller wavelengths.

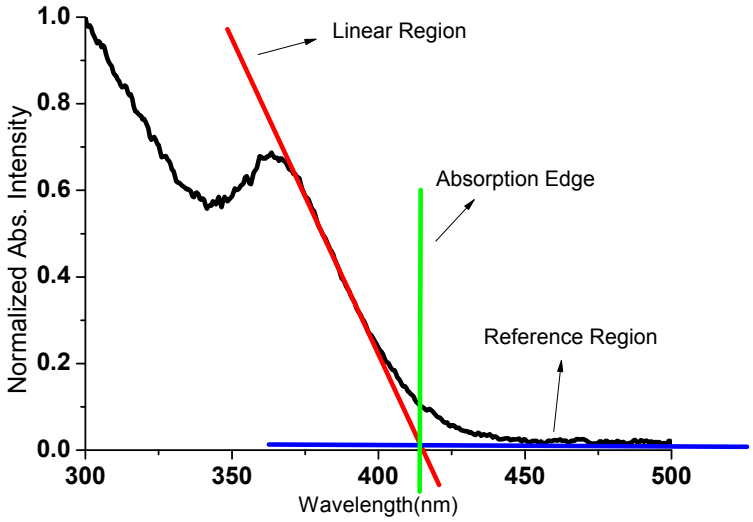


Figure 3.3 Normalized absoption spectra of the quantum dot

Unlike organic fluorophores, simultaneous excitation of various sizes with a single excitation wavelength is possible provided that the excitation energy is sufficient. In general, organic fluorophores have narrow band absorption and wide band of emission which limits the application opportunities. Conversely, quantum dots govern wide band of absorption however they can have narrow emission bands. Therefore, for various applications, narrow spectral bandwidth is desired to be able to excite various colors of dots at the same time. For quantum dots, the full width at half maximum (FWHM) of the emission peak gets narrower as the size distribution gets monodispersed.

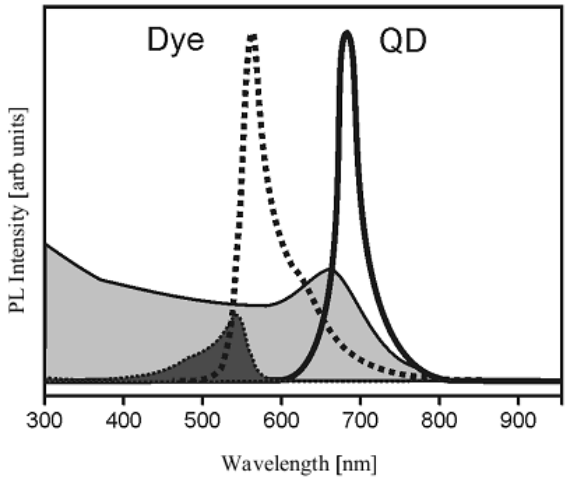


Figure 3.4 Comparison of the emission and absorption spectra of QD (continuous line) and the organic dye (dotted line) (shaded area are the absorption spectra)[69]

Long term photostability, longer fluorescence lifetime, functionality are some other advantageous features that quantum dots can attain compared to organic fluorophores. This features make them suitable for tagging, bioimaging, biolabeling applications.

### 3.1.5 Synthesis methods of CdS Quantum dots

Due to the big interests and efforts to produce high-quality quantum dots, there are many possible synthetic methods for the synthesis of semiconductor nanoparticles. These methods can be collected in main groups such as colloidal methods, lithography, epitaxial growth or solid state methods. In this thesis, only colloidal synthesis methods of CdS quantum dots will be reviewed and the emphasis will be given to the type of precursors.

The quality of quantum dots is determined by several factors. As stated before, they should have narrow size distribution as well as colloidal stability and high quantum yield.

Size control and monodispersity can be achieved by using capping agents. The capping agents can be small molecules or polymers. They can be used separately or at the same time to ensure surface coverage. During synthesis, these molecules can prevent crystal growth by adsorption or attachment to the crystal surface or molecules with thiol groups (HS-) can provide slow release of sulfur for the case of CdS quantum dots. In the long term, capping agents provide colloidal stability by preventing aggregation and precipitation of the crystals. Also, functionality is available when capping agents are utilized.

When an electron is excited to higher energy levels, the system can relax by giving out photon or by losing this extra energy in non-radiative pathways i.e. by vibrational relaxation. High quantum yield indicates that the non-radiative relaxations are partly eliminated. Quantum yield of quantum dots are highly affected by the structural defects, surface defects, atomic vacancies, dangling bonds on the surface of the crystals and relaxations by the adsorbents. Highly crystalline dots would have less crystal related defects and capping agents would reduce the negative effects caused by the surface defects and dangling bonds.

For the syntheses, different cadmium precursors can be used such as cadmium salts ($Cd(NO_3)_2$, $CdCl_2$, $Cd(SO_4)_2$, $Cd(CH_3COO)_2$) , organocadmium compounds (i.e. dimethyl cadmium, $Cd(CH_3)_2$) or cadmium oxide (CdO) [70-72]. However, for the reactions, the cadmium precursor is dissolved in an appropriate solvent.

The colloidal synthesis methods of the CdS quantum dots can be categorized as organic and aqueous phase syntheses. In organic phases, highly crystalline and best quality quantum dots can be established by utilization of high temperatures. Cadmium precursors, even CdO, are soluble in organic phases at high temperatures, where $T>100$ °C [73]. Narrow emission profiles and high quantum yields are obtained with organic phase syntheses. However, transfer of organically synthesized quantum dots to the aqueous phase by ligand-exchange causes a decrease in the fluorescence intensity or increase in the

particle size due to less colloidal stability and surface passivization due to strong polarity of water. In this manner, organic phase synthesis suffers from practical functionality. Therefore, for many applications, desired greener, direct and simpler methods can be obtained with aqueous phase syntheses. In aqueous phase, CdS quantum dots can be produced from soluble cadmium salts [70-72]. But in aqueous media, low quantum yield and polydispersity (wide emission bandwidth) is an important issue. In order to control size and increase fluorescence intensity, the effects of different capping agents, pH, temperature, length of the capping agents etc. are heavily being investigated. The size control can be restrained by the nucleation rate of the nanoparticles. Nucleation rate is linked to the interaction between the precursor and the surfactant. Slow release of the precursor can lead to smaller particles or controlled size.

### 3.1.6 The aim of the research

For many applications of quantum dots; easy, fast, reproducible, water soluble, inexpensive synthesis methods are desired. Aqueous phase synthesis can fulfill these requests and offer relatively greener one-pot synthesis with relatively less toxic and easily handled precursors. The main aim of this research is the synthesis of CdS quantum dots from bulk CdO in aqueous phase under ultrasound (T<100 °C). The application of ultrasonic waves and occurance of cavitation can promote the slow release of cadmium during the reaction even though cadmium oxide is insoluble in water ($K_{sp}$~ $10^{-27}$). On the other hand, a fast and simple method is offered by the application of ultrasound at relatively low temperatures.

The effect of sonication for the synthesis of CdS quantum dots was investigated by Ghows and Entezari [74]. In their work, formation of CdS nanoparticles without surfactant by the combination of micro-emulsion method and ultrasound was presented. As the cadmium source different cadmium salts, such as $Cd(NO_3)_2$, $CdCl_2$, $Cd(SO_4)_2$, $Cd(CH_3COO)_2$ were

used. As the sulfur source $CS_2$ was introduced as the oil phase. CdS synthesis without additives and calcination was achieved with ultrasound.

In this chapter, for the synthesis of CdS quantum dots under ultrasound, the effects of the type of precursors (as Cd or S source), temperature, capping agent will be investigated.

### 3.2 Experimental

All chemicals were analytical grade or of the highest purity available and used without further purification. Cadmium oxide (CdO) was purchased from Alfa Aesar, Sodium sulfide trihydrate ($Na_2S.3H_2O$), 2-mercaptopropionic acid ($CH_3CH(SH)COOH$, 2-MPA), cadmium acetate dihydrate ($Cd(CH_3COO)_2.2H_2O$), Rhodamine B was purchased from Merck, Poly(Acrylic Acid) Sodium Salt, Average $M_W$ ~5100 g/mol by GPC (PAA) was purchased from Sigma-Aldrich and elemental sulfur ($S_8$) was purchased from Tekkim.

In a typical experiment, 32 mg (0.25 mmol) cadmium oxide was dispersed in 52 ml deionized water (18.2 MΩ $cm^{-1}$) in an ultrasound bath for 30 minutes. With the addition of 44μL 2- MPA or 35.8mg PAA, the mixture was placed for another 5 minutes in the ultrasound bath. The pH of the mixture was adjusted to 7-8 with 2.5M NaOH or acetic acid solution. In the meanwhile, the sulfur source (13.2 mg $Na_2S$ or 3.2 mg $S_8$) was put into 8 ml deionized water and purged with Argon gas. All reactions took place in a custom glass sonication cell fitted with a water jacket for temperature control. For the reactions, an ultrasonic probe (Bandelin HD 3200 model, 20 kHz, 200 W) with 13 mm $TiAl_6V_4$ alloy tip (VS70T) was used. The average intensity was on the order of 50 W/$cm^2$. The temperature of the solution was adjusted to 25, 55 or 70 °C with a circulating chiller. The solution mixture was placed in the sonication vessel and purged with Argon gas to remove dissolved oxygen before and during the reaction. After 2 minutes of sonication, the sulfur

source is added dropwise to the solution mixture. The solution was sonicated for 30 minutes for reactions with $Na_2S$ prescursor or 60 minutes for $S_8$ precursor.

Absorption spectra were recorded with a Shimadzu UV-Vis-NIR spectrophotometer model 3101 PC in the 200-500 nm range immediately after the sonication of the solution. Absorption of samples at the excitation wavelength of 355 nm was kept under 15 % and three dilutions were recorded for the quantum yield calculation. The reported particle size was determined from the absorption onset wavelength of the samples using the Brus equation.

A Horiba Jobin-Yvon Fluoromax-3 spectrometer was used for fluorescence experiments. Samples were excited at 355 nm and the emission between 370 and 750 nm were collected through a 370nm high pass filter (KV370) at room temperature immediately after recording the absorption spectra of the solution. Photoluminescence (PL) spectra were calibrated with respect to the absorption value at the excitation wavelength. Quantum yields (QY) of the samples were calculated using the area under the emission curves of the samples with respect to Rhodamine B dye dissolved in water as a reference.

### 3.3 Results and Discussion

When ultrasound is applied to a reaction, the mechanism can totally change. Therefore, for a reaction carried out with ultrasound, basically, it can be said that the conditions are unique and can be completely different than the reactions that are not performed under ultrasound. In this part, some of the investigated conditions are presented. The sizes of the synthesized quantum dots reported in the subsequent tables are determined by Brus Equation (See Appendix).

All of the samples appear yellow under 365nm UV excitation if otherwise is not mentioned.

### 3.3.1 Effect of capping agent: PAA vs 2-MPA

Capping agents are molecules that can prevent crystal growth by adsorption or attachment to the crystal surface of the nanocrystals. Surface passivization is required to control size and eliminate surface related non-radiative relaxations such as dangling bonds. Therefore, utilization of capping agents can provide size control, enhancement of the quantum yield and further surface functionalization.

In this section, as the capping agent, the effect of the Poly (Acrylic Acid) sodium salt (PAA) will be compared to 2-Mercaptoproponic acid (2-MPA) at the same temperature of T=70°C. The effect of temperature for each capping agent will be explained further in the next section.

Poly (Acrylic Acid) (PAA), is an example of biocompatible polymeric coatings used in CdS stabilization. Polymeric coatings such as PAA passivate the surface of the nanocrystals by the chemically adsorbed carboxylate groups. Remaining carboxylate groups provide water solubility and multiple attachment sites on polymers can provide surface stabilization and further functionalization simultaneously.

On the other hand, thiol (HS-) containing capping agents (such as mercaptoacetic acid, thioacetamide, cysteine) are attached to the surface by the thiol groups. Under some conditions, the thiol group can act as a sulfur source with slow release of sulfur for the case of CdS quantum dots. The remaining functional groups (such as -COOH) in the molecules can provide water solubility, colloidal stability and functionalization. Since thiolates bind to the surface cations, it is reasonable to keep Cd/S high. In this chapter, Cd/S mole ratio is fixed at 2.5 according to previous studies where the 2-MPA systems were investigated [75].

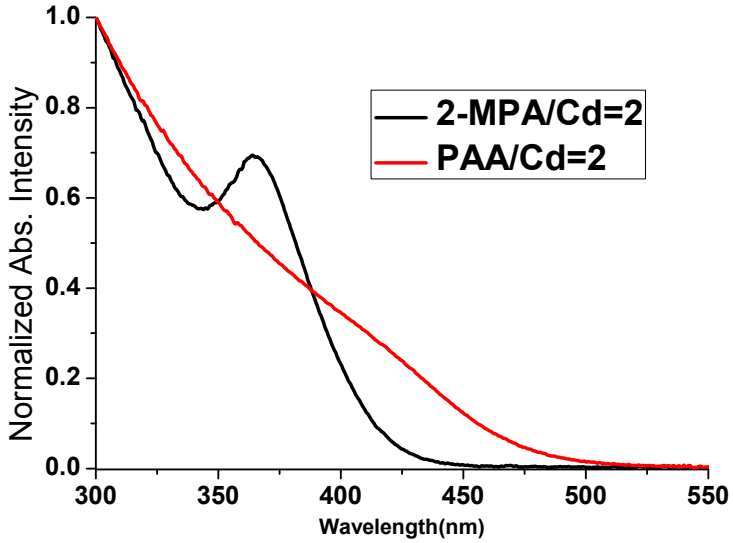


Figure 3.5 Normalized absorbance spectra

Figure 3.5 shows the normalized absorbance spectra of PAA-CdS and 2MPA-CdS quantum dots. The strong excitonic peak (absorption onset) around 360 nm observed for the 2MPA-CdS system indicates the highest distribution of average size of QDs. However, PAA-CdS system lacks this strong excitonic peak. This can be due to broad size distribution of nanocrystals or due to strong Coulomb screening.

The calibrated emission spectra (Figure 3.6) and quantum yield presented in Table 3.2 clearly shows that the fluorescence intensity for 2MPA-CdS is significantly larger than PAA-CdS, indicating that 2MPA provides a better surface coverage than PAA due to the higher affinity of $Cd^{2+}$ to thiol groups than to a carboxylate group. It is seen that both of the samples lack monodispersity according to large emission bandwidth (FWHM). As expected 2-MPA coating has larger quantum yield than a polymeric capping agent. Even though the calculated size from the absorbance spectrum is significantly different for each surfactant, there is not a dramatic difference in the PL maximum due to large size distribution.

Temperature dependence and properties of the capping agents are further discussed in the next section.

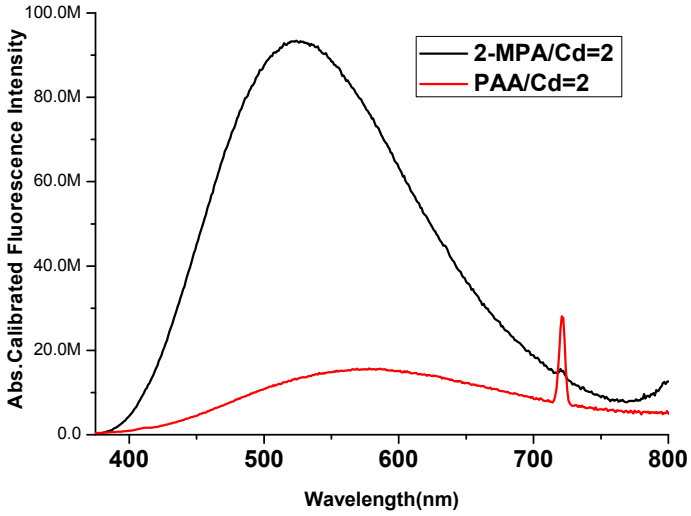


Figure 3.6 Absorption calibrated Fluorescence emission

Table 3.2 Properties of CdS QD as a function of capping agent

| Sample | Cd/S | Surfactant/Cd | pH | Temp | PL max(nm)[a] | FWHM (nm)[b] | Absorption Edge(nm)[c] | Size (nm) (diameter)[d] | Band Gap (eV)[e] | QY%[f] |
|---|---|---|---|---|---|---|---|---|---|---|
| C29 | 2.5 | PAA/Cd=2 | 7.25 | 70°C | 581 | 222 | 476 | 4.1 | 2.61 | 10 |
| C30 | 2.5 | 2-MPA/Cd=2 | 7.05 | 70°C | 524 | 176 | 417 | 2.8 | 2.98 | 38 |

a: PL Max, Maximum photoluminescence emission intensity, b: FWHM, Full width at half maximum were determined from the fluorescence spectra. c: Absorption Edge was determined from the absorption spectrum, d: Size was calculated from Brus Equation. e: Band gap energy was calculated from $E=hc/\lambda$. f: Quantum Yield was calculated with respect to Rhodamine B (QY=31% in water)

### 3.3.2 Effect of Temperature

In conventional methods, high quality quantum dots are provided by high-temperature syntheses. However for the reactions with ultrasound, the relationship between the temperature and ultrasound is rather different. It is important to remember that for the success of the reaction, cavitation must occur. Simply, cavitation is the formation, growth and collapse of the bubbles in an ultrasonic reaction. At high temperatures, under ultrasound, the bubble formation can be enhanced. However, the dissolved gases or the vapor pressure of the reaction medium can prevent the collapse these bubbles. This phenomenon is called the "cushioning effect". On the other hand, at low temperatures, effective collapse of the bubbles is enhanced, but then it becomes harder to form a bubble. Therefore, for ultrasonic reactions, there is not a simple temperature dependence. In ultrasonic reactions, the conditions are unique for every factor.

#### 3.3.2.1 Poly(Acrylic Acid) (PAA) as the surfactant

Polymeric coatings such as PAA can assure stabilization by multiple attachment sites. It is important to remember that the surface coverage provided by the polymer is limited to its chain length. Smaller chains can provide better coverage than longer chains since the coverage is obtained by the conformation of the polymer chain. The repulsion of the unattached carboxylate groups or the repulsion of neighboring chains can be observed for long chains.

The change in temperature does not significantly affect the absorption properties of the PAA-CdS nanocrystals. As mentioned before, absence of the strong absorption onset can be due to the large size distribution of particles or due to strong Coulomb screening (Figure 3.7).

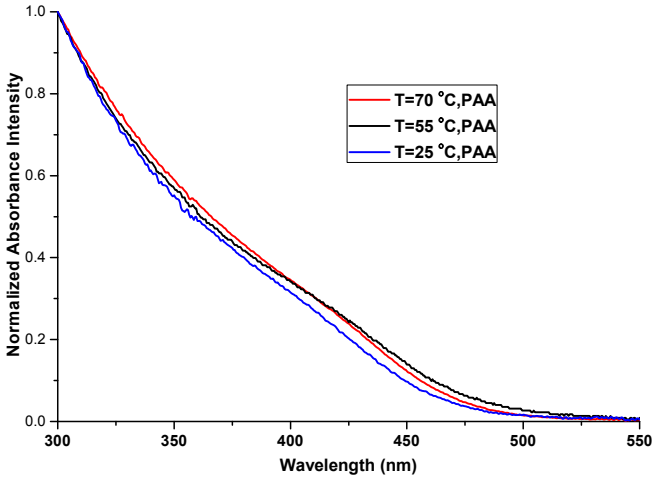


Figure 3.7 Normalized absorbance spectra of PAA-CdS

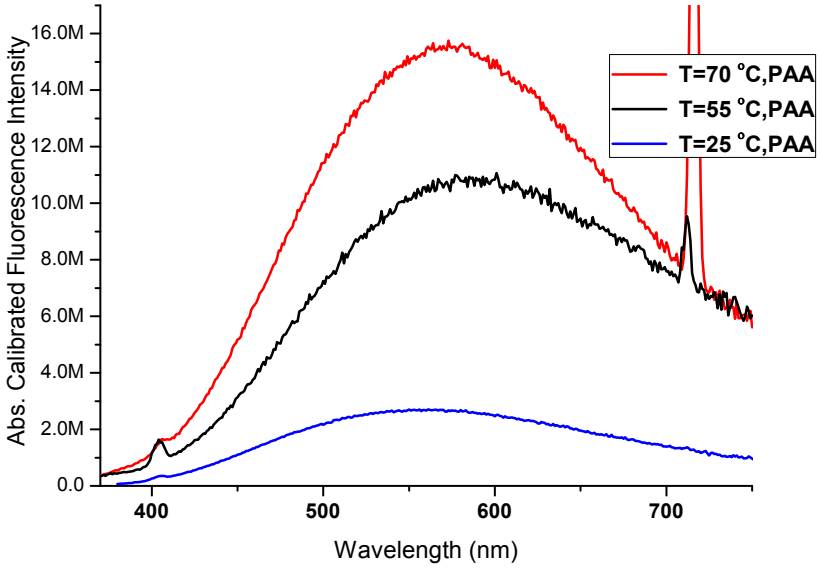


Figure 3.8 Absorption calibrated fluorescence emission of PAA-CdS

According to PL spectra (Figure 3.8), increasing temperature enhances the fluorescence intensity of the synthesized nanoparticles. Higher temperature can lead to better quality

crystals with fewer defects. High temperature can also enhance the movement of the polymer coating therefore leads to a better surface coverage which in turn eliminates the surface defects.

The lack of size tuning and narrow size distribution (Table 3.3) can be due to two reasons. The adsorption of the polymer on the surface of the nanocrystals can be restricted by insufficient coverage of the limited chain conformation. Also, the applied intense ultrasonic waves can prevent the efficient adsorption of the polymer.

The calculated quantum yields are found to be in good agreement with the CdS quantum dots synthesized with 5100g/mol PAA at pH 7.5 where the QY was reported to be 5-13% wrt to Rhodamine B dye [76]. This indicates that application of ultrasound to bulk CdO system can achieve almost the same performance with the quantum dots synthesized from Cd salt with PAA coating.

Table 3.3 Properties of PAA-CdS QD as a function temperature

| Sample | Cd/S | Surfactant/Cd | pH | Temp(°C) | PL max(nm) | FWHM (nm) | Absorption Edge(nm) | Size(nm) (Diameter) | Band Gap (eV) | QY% |
|---|---|---|---|---|---|---|---|---|---|---|
| C29 | 2.5 | PAA/Cd=2 | 7.25 | 70 | 581 | 222 | 476 | 4.1 | 2.61 | 10 |
| C50 | 2.5 | PAA/Cd=2 | 7.75 | 55 | 601 | 269 | 481 | 4.3 | 2.58 | 7 |
| C36 | 2.5 | PAA/Cd=2 | 7.40 | 25 | 565 | 253 | 467 | 3.8 | 2.66 | 11 |

#### 3.3.2.2 2-Mercaptopropionic Acid, 2-MPA as the surfactant

As most of the thiol containing organic molecules 2-MPA also forms a complex with $Cd^{2+}$. Interestingly, CdO also forms a complex with 2-MPA when pH is 7 and higher. The formation of this complex is observed by the disappearance of the brick-red colour of the CdO suspension. Formation of these complexes is important because the slow release of cadmium can be provided by the formed complex under ultrasound. This can contribute to

the size control of the nanoparticles by slower growth and nucleation. The pH's of the reactions are kept same for all of the reactions because the complex type may depend on the pH or the number of attached cadmium can be dependent on the pH.

The larger affinity of $Cd^{2+}$ to thiol groups than carboxylates and the small size of the organic molecules can provide more enhanced surface passivization than polymeric coatings. This is observed in the enhanced quantum yield of the 2MPA-CdS samples at any temperature (Table 3.4). According to FWHM, the size distribution is slightly narrower than PAA-CdS systems however large size distribution is still present.

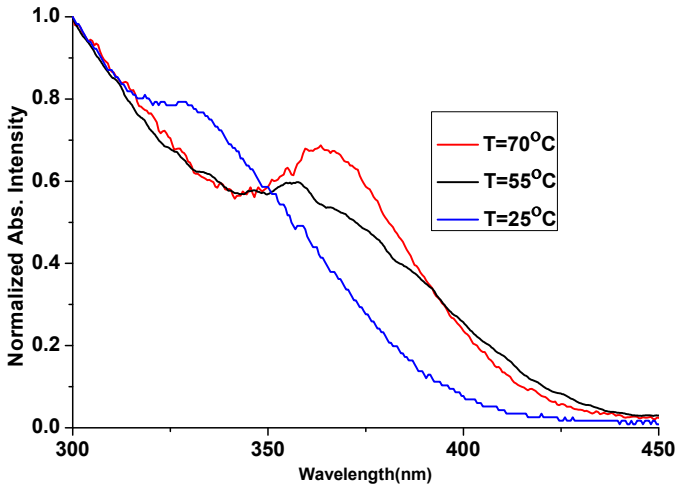


Figure 3.9 Normalized absorbance spectra of 2-MPA CdS

As expected, lower temperatures provides smaller size of nanoparticles due to slower release of precursors. Besides, the observed the slightly smaller quantum yield can be due to the lower crystallinity of the nanoparticles since higher crystallinity is achieved by higher temperatures.

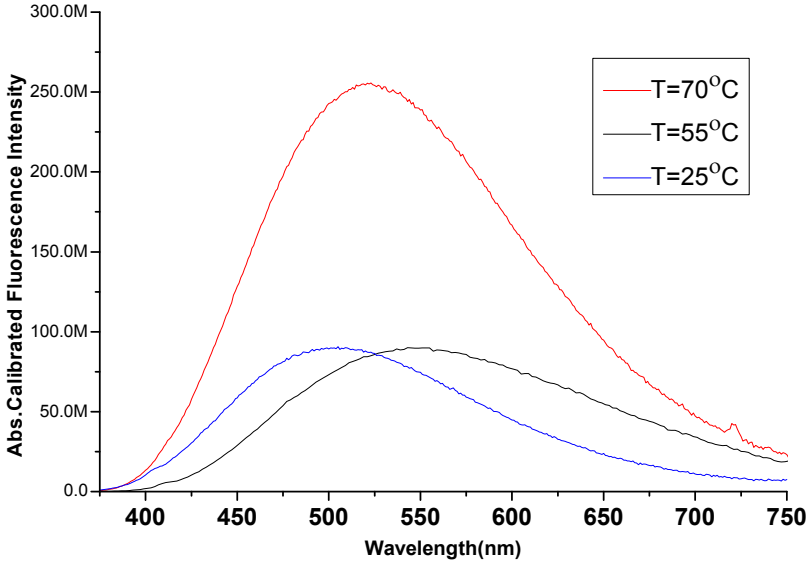


Figure 3.10 Absorption calibrated fluorescence emission of 2-MPA-CdS

Table 3.4 Properties of 2-MPA -CdS QD as a function temperature

| Sample | Cd/S | Surfactant/Cd | pH | Temp(°C) | PL max(nm) | FWHM (nm) | Absorption Edge(nm) | Size(nm) (Diameter) | Band Gap (eV) | QY% |
|---|---|---|---|---|---|---|---|---|---|---|
| C30 | 2.5 | 2-MPA/Cd=2 | 7.05 | 70 | 524 | 176 | 417 | 2.8 | 2.98 | 38 |
| C40 | 2.5 | 2-MPA/Cd=2 | 7.44 | 55 | 550 | 203 | 427 | 2.9 | 2.91 | 37 |
| C48 | 2.5 | 2-MPA/Cd=2 | 7.74 | 25 | 508 | 164 | 398 | 2.6 | 3.12 | 37 |

### 3.3.3 Surfactant /Cd ratio

Since it is found out that the 2-MPA-CdS systems are better luminescent than PAA-CdS systems, the relationship between the surfactant/Cd mole ratio and optical properties is investigated only for 2-MPA-CdS. Generally, the crystal size is expected to decrease with increased amount of surface capping agent. This may happen, if the full surface coverage was not obtained in the preceding case.

To investigate the coverage status of the 2-MPA-CdS system, surfactant/Cd mole ratio was increased to 5. This change did not show a significant difference on the size distribution or the position of the PL maximum indicating that the sufficient amount of coating was readily present when surfactant/Cd mole ratio was 2. It can be said that the size limit for the crystal growth is reached with sufficient capping agent and the excess coating is not effective on changing the size.

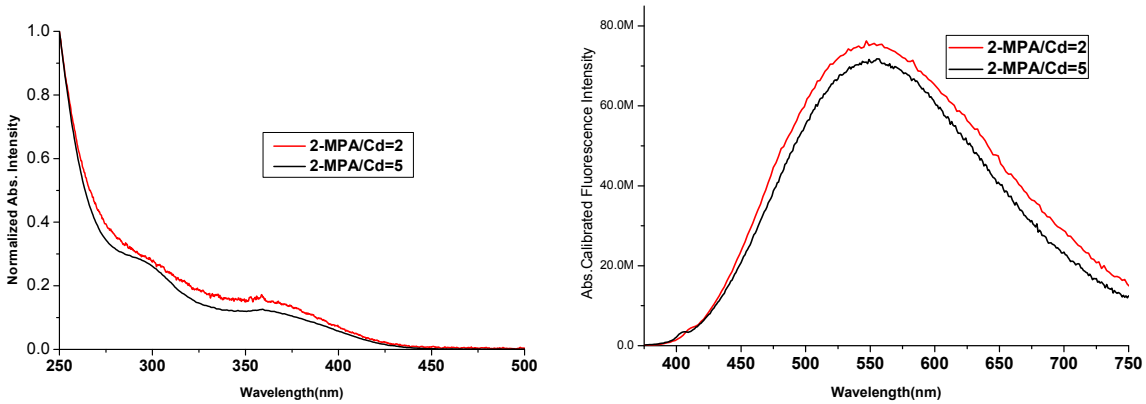


Figure 3.11 Normalized absorption spectra and absorption calibrated fluorescence emission of 2-MPA-CdS

Table 3.5 Properties of 2-MPA-CdS QD as a function of capping agent amount

| Sample | Cd/S | Surfactant/Cd | pH | Temp | PL max (nm) | FWHM (nm) | Absorption Edge(nm) | Size(nm) (Diameter) | Band Gap (eV) | QY% |
|---|---|---|---|---|---|---|---|---|---|---|
| C40 | 2.5 | 2-MPA/Cd=2 | 7.44 | 55 | 550 | 203 | 427 | 2.9 | 2.91 | 37 |
| C43 | 2.5 | 2-MPA/Cd=5 | 7.12 | 55 | 555 | 189 | 430 | 3.0 | 2.89 | 33 |

### 3.3.4 Effect of the Precursor

#### 3.3.4.1 Cadmium Source: Cd Salt vs CdO

The effect of formation of the CdO complex with 2-MPA and the cadmium release to the reaction can be compared by using cadmium salt as the $Cd^{2+}$ source. For this investigation, cadmium acetate dihydrate ($Cd(CH_3COO)_2.2H_2O$) was chosen not to introduce a different anion to the reaction mixture. In the case with cadmium acetate, there will be many nucleation sites in the reaction mixture and size of the synthesized quantum dots will be controlled only by the capping agent and the amount of available ions in the medium.

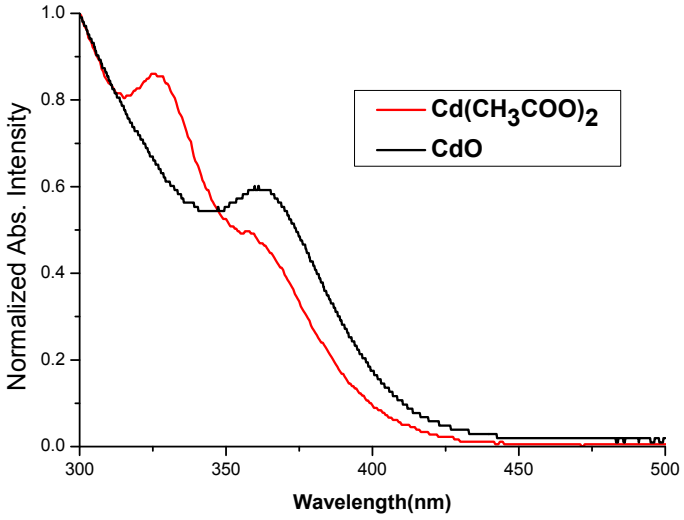


Figure 3.12 Normalized absorbance spectra of 2-MPA CdS of different precursors

At the same conditions, changing the cadmium precursor to a salt did not show a significant change in the size and the size distribution of the formed nanoparticles. The size and the size distribution is similar for the two samples according to the absorption edge, PL

max and emission bandwidth. However the second absorption onset at smaller wavelengths of the salt precursor suggests that there are two main sizes. Appearance of two absorption onset in the absorption spectrum may occur even if there is a tiny gap during the addition of the sulfur precursor. It is not specific to the salt precursor. On the other hand, the quantum yield of the sample synthesized from salt precursor has significantly higher quantum yield. The availability of many nucleation sites with the salt precursor indicates that the size limit is reached as soon as the sulfur precursor is introduced. Therefore, the size is not controlled by the applied ultrasound or the slow release of cadmium from the formed complex. The size can be controlled by the temperature or by the type of the capping agent or with the type of sulfur precursor which is explained in the next section. The dramatic quantum yield difference suggests that the growth rate of the CdS crystals is very large for the case of salt precursor. The spontaneous fast growth creates defect-free crystals. In the case of cadmium oxide precursor, for the growth of the crystals, first the formed complex should be broken by the applied sonication waves. After this step, the growth of the crystals is induced by the sonication. Therefore, the intense power should have created crystal defects compared to the case of salt precursor.

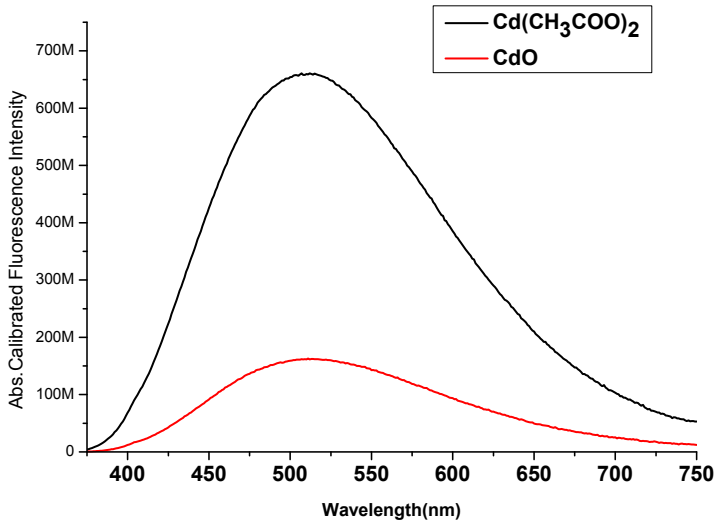


Figure 3.13 Absorption calibrated fluorescence emission of 2-MPA CdS of different precursors

Table 3.6 Properties of 2-MPA-CdS QD as a function of Cd precursor

| Sample | Sample | Cd/S | Surfactant/Cd | pH | Temp | PL max(nm) | FWHM (nm) | Abs Edge(nm) | Size(nm) (diameter) | Band Gap(eV) | QY% |
|---|---|---|---|---|---|---|---|---|---|---|---|
| C53 | Salt | 2.5 | 2-MPA/Cd=2 | 7.05 | 55°C | 505 | 174 | 402 | 2.6 | 3.09 | 75 |
| C56 | Oxide | 2.5 | 2-MPA/Cd=2 | 7.40 | 55°C | 514 | 167 | 408 | 2.7 | 3.04 | 38 |

#### 3.3.4.2 Sulfur source: $Na_2S$ vs Elemental Sulfur

As the source of sulfur for CdS quantum dots, $Na_2S$ is not the only option. In addition to salts, dangerous $H_2S$ gas or organosulfur compounds such as thiourea are used in literature. Also, it is shown that blue emitting CdS quantum dots can also be synthesized from elemental sulfur as the source of sulfur [77]. However, in all the reactions reported, the precursors are dissolved in an appropriate solvent (water, THF, liquid paraffin, etc.) [78].

In this thesis, elemental sulfur ($S_8$) was also investigated as the sulfur source. The main reason for using CdO in the reactions was to obtain narrower size distribution by the slow release of the cadmium. Just like CdO, elemental sulfur is also insoluble in water. Therefore, utilization of elemental sulfur can also provide slow release of sulfur under ultrasound. In the reactions, required amount of sulfur was used without dissolving. Application of ultrasonic waves has made it possible to synthesize smaller sizes of quantum dots compared to dots synthesized with $Na_2S$. The observed peak shift to smaller wavelengths in the absorption spectra of the samples (Figure 3.14) indicates that the crystals were smaller in size.

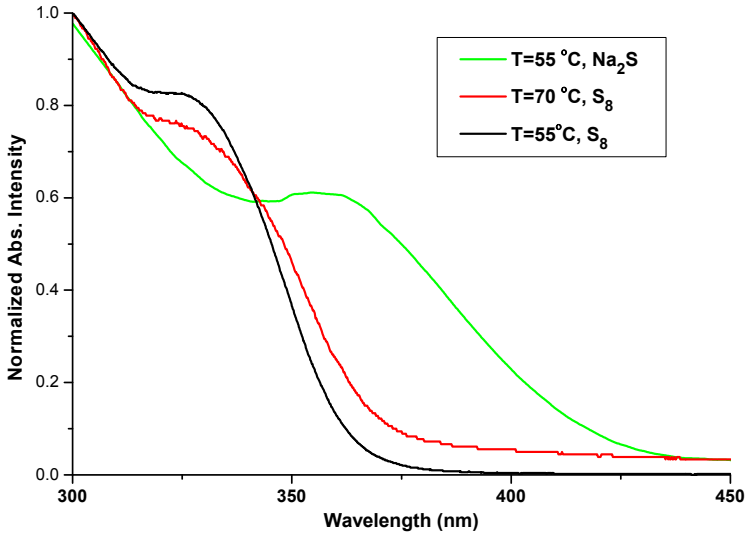


Figure 3.14 Normalized absorbance spectra of 2-MPA CdS of different sulfur precursors

The shift of the peak maximum to smaller wavelengths in the fluorescence spectra clearly shows that the synthesized nanoparticles were smaller in size and the size distribution was the narrowest according to FWHM, therefore blue emitting CdS nanoparticles were obtained. Also when excited under UV light, the samples glow in blue color. When sodium sulfide is dissolved in water, there are many nucleation sites present to be attached to available cadmium. The slow sulfur release during the reaction can cause small nucleation rates and control of the size.

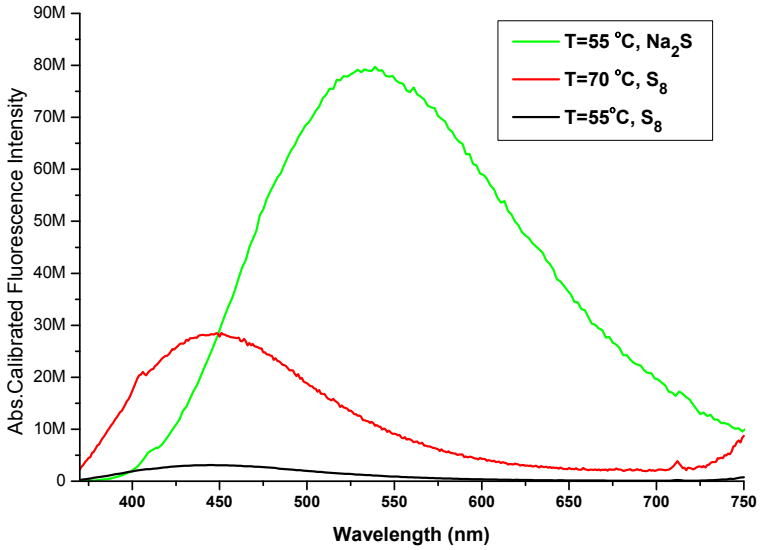


Figure 3.15 Absorption calibrated fluorescence emission of 2-MPA CdS of different sulfur precursors

Also, the fluorescence quantum yield (wrt Rhodamine B presented in Table 3.7) is found to be lower than the samples synthesized with $Na_2S$ as the sulfur source. Even though the reaction duration is extended for another 30 minutes than the conventional method, the reaction may not be complete at the end of 1 hour, because the reaction solution contains unreacted sulfur remaining on the surface. Elemental sulfur is not soluble in water and it tends to float on the surface. This property makes the incorporation in the reaction difficult because they tend to escape from the applied ultrasonic waves by staying on the surface. Thus, the reaction may not be complete due to slow release or the ineffective sonication.

Table 3.7 Properties of 2-MPA-CdS QD as a function of sulfur precursor

| Sample | S source | Cd/S | Surfactant/Cd | pH | Temp(°C) | PL max (nm) | FWHM (nm) | Absorption Edge(nm) | Size(nm) (diameter) | Band Gap (eV) | QY% |
|---|---|---|---|---|---|---|---|---|---|---|---|
| C40 | $Na_2S$ | 2.5 | 2-MPA/Cd=2 | 7.44 | 55 | 550 | 203 | 427 | 2.9 | 2.99 | 37 |
| C45 | $S_8$ | 2.5 | 2-MPA/Cd=2 | 7.25 | 70 | 448 | 127 | 368 | 2.3 | 3.37 | 10 |
| C44 | $S_8$ | 2.5 | 2-MPA/Cd=2 | 7.20 | 55 | 444 | 122 | 363 | 2.2 | 3.42 | 8 |

#### 3.3.4.3 2-MPA as the sulfur source

Hobson and colleagues [79] asserted that it is possible to produce quantum sized particles by the sonication of solutions of $Cd^{2+}$-thiol-sodium hexametaphosphate. The mechanism involves the formation of H· radical by the sonication of water. The attack of the H· radical to a thiol group in a molecule such as 2-MPA would lead to formation of $H_2S$. Formed $H_2S$ is further reacted with $Cd^{2+}$ to form nanosized CdS.

In this thesis, to determine whether the synthesized CdS is formed by the sulfur of the precursor ($Na_2S$) or by the sulfur of 2-MPA, reaction with only 2-MPA without any sulfur precursor was carried out at the same condition for the synthesis of CdS. At the end, when excited with 355nm, there was no significant fluorescence detected with the spectrophotometer, even though the sample was absorbing light in the UV region where a tiny absorption onset was present at 322nm. Therefore, very small crystals may have been formed but these particles are not large enough to be excited at 355nm. So, this reaction confirmed that the main sulfur source was the added $Na_2S$ or $S_8$ precursor.

## 3.4 Conclusions

In thesis for the first time; it is shown that the ultrasound can promote the synthesis of CdS quantum dots from bulk CdO in aqueous phase. The effects of temperature, capping agent, Cd/Surfactant mole ratio, the type of precursors on the optical properties of synthesized quantum dots were investigated. Fluorescence intensity and size distribution is linked to the performance of the capping agent and the crystallinity of the samples. As the capping agent, samples with 2-MPA had higher quantum yields and narrower FWHM than PAA at any temperature. T=70°C is found to be more convenient for better crystallinity and higher quantum yield. The narrowest emission bandwidth and smallest size was obtained with elemental sulfur precursor.

# Chapter 4

## CONCLUSIONS

This thesis was mainly focused on the development of unique synthesis methods by utilization of sonication. Greener, faster and simpler synthesis methods were investigated for two different kind of inorganic materials. In chapter 2, lanthanide doped upconverting $NaYF_4$ crystals were synthesized via sonication in aqueous phase when T< 80°C. Different reaction conditions were effective to produce desired phase of $NaYF_4$ crystals. β- $NaYF_4$ crystals were observed as microparticles and α- $NaYF_4$ crystals were observed as nanoparticles in SEM. Upconversion luminescence was observed for lower excitation powers for annealed crystals. Upon annealing, some α-$NaYF_4$ nanoparticles were transformed into much symmetrical and stable β-$NaYF_4$ phase or in some samples $YF_3$ impurity was observed. The precursor amounts and the surfactants such as, tri-sodium citrate, sodium acetate, citric acid, ethanol/water mixture was found to be effective for the shape and morphology control. Upconversion spectra of the $Yb^{3+}$(20%) , $Er^{3+}$(2%) or $Yb^{3+}$(20%) , $Tm^{3+}$(2%) co-doped , α- and β- $NaYF_4$ were investigated. Upconversion luminescence was also observed by the naked eye for the annealed samples. For the non-

annealed particles, the low upconversion efficiency can be explained by the high crystal defects facilitated by the intense ultrasonic waves.

In Chapter 3, for the first time CdS quantum dots are synthesized from undissolved bulk CdO precursor in aqueous phase while T< 80°C. The intense ultrasonic waves were used to facilitate the reaction. This method is a fast and a simpler synthesis route for the CdS production. As the capping agent, 2-MPA showed higher fluorescence intensity and narrower FWHM than PAA coated samples at any investigated temperature. Size distribution was found to be polydispersed as it is observed in aqueous synthesis methods of CdS quantum dots. T=70°C is found to be more proper for better crystallinity and higher quantum yield. The narrowest emission bandwidth and smallest size was obtained when elemental sulfur was utilized as the precursor.

# Appendix

## A.1 Determination of the Size of the CdS Quantum Dots by the Brus Equation

According to the Effective Mass Approximation (Eq. A-1) which was proposed by Brus [67], the energy of the observed band gap of the quantum dots changes with the size of the diameter (R) of the crystal. The difference between the band gap energy of the crystallite and the band gap energy of the bulk crystal is defined as $\Delta E = E_{crystallite} - E_g$.

$$\Delta E = \left(\frac{\hbar^2\pi^2}{2R^2}\right)\left(\frac{1}{m_e}+\frac{1}{m_h}\right) - 1.8\frac{e^2}{\varepsilon_{CdS} x 4\pi\varepsilon_o x R} \qquad \text{(Eq. A-1.1)}$$

For CdS crystal, the effective mass of the electron is $m_e = 0.3m_o$, and the effective mass of the hole is $m_h = 0.8m_o$ where the real free electron mass, $m_o = 9.10938188 \times 10^{-31}$kg
$\varepsilon_{CdS} = 5.7$ and $\varepsilon_o = 8.85410$ F/m

The first term on the right of Eq.A-1 is the quantum well approximation term. When the units are converted to electron volts, this term becomes 1.719 eV/ $R^2$. R is the diameter of the crystal in terms of nanometers.

The last term in the equation is derived from the coulomb interaction. When the units are converted to electron volts, the coulomb interaction term becomes $4.54x10^{-1}$ eV / R. Where R is the diameter of the crystal in terms of nanometers.

$E_{crystallite}$ is defined as the wavelength where the quantum dot crystals start to absorb light. This wavelength corresponds to the absorption edge in the absorption spectra (Figure A.1).

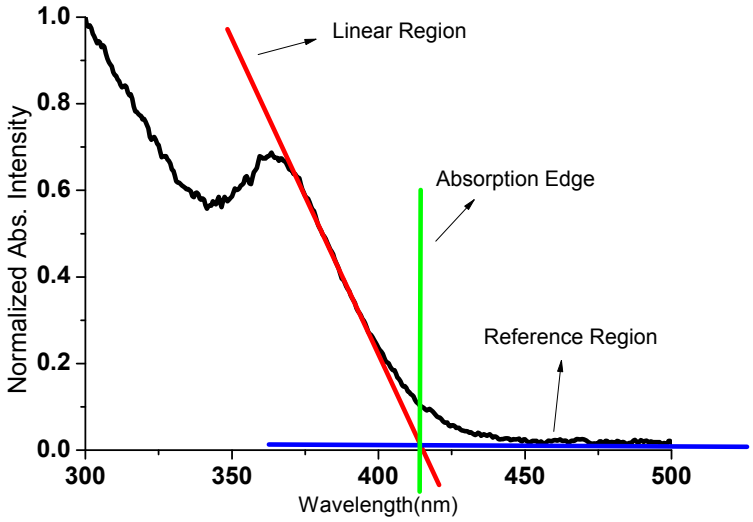


Figure A.1 Representation of the absorption spectra

$E_{crystallite}$= hc/λ, where the h is the Plank's constant, c is the speed of light and λ is the wavelength of the absorption edge. Therefore, in terms of electron volts,

$E_{crystallite}$= 1240.7 eV / λ, where the unit of λ is nm.

For CdS, $E_g$ = 2.42 eV

Therefore,

$\Delta E = E_{crystallite} - E_g$ = (1240.7 eV / λ) - 2.42 eV

When the units are converted to electron volts the Eq.A-1 is written as:

$$\frac{1240.7[eV]}{\lambda_{nm}} - 2.42[eV] = \frac{1.72[eV]}{(R_{nm})^2} - \frac{4.54 \times 10^{-1}[eV]}{R_{nm}} \qquad \text{Eq.A-1.2}$$

Then, the diameter of the quantum dot is calculated as $2xR_{nm}$.

By inserting the value of the absorption onset, the diameter of the quantum crystals can be determined.

**A.2 Quantum Yield Calculation**

Basically, quantum yield is the number of photons emitted per number of absorbed photons. For comparison, quantum yield should be reported according to a dye. Reference dye is selected according to its absorption and fluorescence wavelengths. For more accurate results, the reference dye should have the similar absorption and fluorescence wavelengths compared to the sample.

For the calculation of quantum yield by multiple measurements, several dilutions are prepared from the main solution. The maximum absorbance of the dilutions is kept under 0.75 in order to eliminate the concentration effects. When absorbance measurements are recorded, the fluorescence spectrum of each dilution is measured. All of the measuring procedure is also applied to the reference dye (Rhodamine B dye (quantum yield: QY= 31%) dissolved in DI water as a reference). Quantum yields are determined using the area under the emission curves. The areas under the emission curves are plotted against the absorbance values at the excitation wavelength. Then, a linear fit is applied to these points. The slope of this linear fit is used in the quantum yield calculation.

Quantum yield is calculated according to the following equation:

$$\Phi_x = \Phi_{ref} \left(\frac{m_x}{m_{ref}}\right)\left(\frac{n_x}{n_{ref}}\right)^2 \qquad \text{Eq.A-2.1}$$

Where,

Φ is the quantum yield,

m is the slope of the linear fits

n is the refractive index of the solvents used.

Subscripts “x” and “ref” refer to the sample and the reference dye solutions respectively.

## References


1. Thompson, L.H. and L.K. Doraiswamy, *Sonochemistry: Science and Engineering.* Industrial & Engineering Chemistry Research, 1999. **38**(4): p. 1215-1249.
2. Suslick, K.S., *Sonochemistry*, in *Kirk-Othmer Encyclopedia of Chemical Technology*2000, John Wiley & Sons, Inc.
3. Kenneth S. Suslick, G.J.P., *Application of ultrasound to materials chemistry.* Annu. Rev. Mater. Sci., 1999. **29**: p. 295-326.
4. Bang, J.H. and K.S. Suslick, *Applications of Ultrasound to the Synthesis of Nanostructured Materials.* Advanced Materials, 2010. **22**(10): p. 1039-1059.
5. Margulis, M.A., *Sonoluminescence and Sonochemical Reactions in Cavitation Fields. A Review.* Ultrasonics, 1985. **23**(4): p. 157-169.
6. Pankaj; Ashokkumar, M., *Theoretical and Experimental Sonochemistry Involving Inorganic Systems*2011: Springer. 404.
7. Adewuyi, Y.G., *Sonochemistry: Environmental Science and Engineering Applications.* Industrial & Engineering Chemistry Research 2001. **40**(22): p. 4681-4715
8. Capelo-Martínez, J.-L., *Ultrasound in Chemistry: Analytical Applications*2009: Wiley.
9. Ovsyankin, V.V., Feofilov,P.P. , Sov. Phys. JETP Lett., 1966. **4**: p. 317-318.
10. Auzel, F., C.R. Acad. Sci., 1966. **262**: p. 1016.
11. Auzel, F., C.R. Acad. Sci., 1966. **263B** p. 819.
12. Cheng, L., et al., *Highly-sensitive multiplexed in vivo imaging using pegylated upconversion nanoparticles.* Nano Research, 2010. **3**(10): p. 722-732.
13. He, X., K. Wang, and Z. Cheng, *In vivo near-infrared fluorescence imaging of cancer with nanoparticle-based probes.* Wiley Interdisciplinary Reviews: Nanomedicine and Nanobiotechnology, 2010. **2**(4): p. 349-366.
14. Li, Z. and Y. Zhang, *An efficient and user-friendly method for the synthesis of hexagonal-phase NaYF(4):Yb, Er/Tm nanocrystals with controllable shape and upconversion fluorescence.* Nanotechnology, 2008. **19**(34): p. 345606.
15. Mader, H.S., et al., *Upconverting luminescent nanoparticles for use in bioconjugation and bioimaging.* Current Opinion in Chemical Biology, 2010. **14**(5): p. 582-596.
16. Tian, Z., et al., *Autofluorescence-free in vivo multicolor imaging using upconversion fluoride nanocrystals.* Lasers in Medical Science, 2009. **25**(4): p. 479-484.

17. Wang, M., et al., *Immunolabeling and NIR-Excited Fluorescent Imaging of HeLa Cells by Using NaYF4:Yb,Er Upconversion Nanoparticles.* ACS Nano, 2009. **3**(6): p. 1580-1586.
18. Zhou, J., et al., *Fluorine-18-labeled Gd3+/Yb3+/Er3+ co-doped NaYF4 nanophosphors for multimodality PET/MR/UCL imaging.* Biomaterials, 2011. **32**(4): p. 1148-1156.
19. Cui, S., H. Chen, and Y. Gu, *Comparison of Two Strategies for the Synthesis of Upconverting Nanoparticles as Biological labels.* Journal of Physics: Conference Series, 2011. **277**: p. 012006.
20. Thrash, R.J. and L.F. Johnson, *Upconversion laser emission from Yb3+-sensitized Tm3+ in BaY2F8.* J. Opt. Soc. Am. B, 1994. **11**(5): p. 881-885.
21. Downing, E., et al., *A Three-Color, Solid-State, Three-Dimensional Display.* Science, 1996. **273**(5279): p. 1185-1189.
22. Chai, R., et al., *Preparation and characterization of upconversion luminescent NaYF4:Yb, Er (Tm)/PS bulk transparent nanocomposites through in situ polymerization.* Journal of Colloid and Interface Science, 2010. **345**(2): p. 262-268.
23. Cheng, Y.Y., et al., *Improving the light-harvesting of amorphous silicon solar cells with photochemical upconversion.* Energy & Environmental Science, 2012. **5**(5): p. 6953-6959.
24. Aarts, L., B.M. van der Ende, and A. Meijerink, *Downconversion for solar cells in NaYF[sub 4]:Er,Yb.* Journal of Applied Physics, 2009. **106**(2): p. 023522-6.
25. Mai, H.X., et al., *Highly Efficient Multicolor Up-Conversion Emissions and Their Mechanisms of Monodisperse NaYF4:Yb,Er Core and Core/Shell-Structured Nanocrystals.* Journal of Physical Chemistry C, 2007. **111**(37): p. 13721-13729.
26. Qian, H.-S. and Y. Zhang, *Synthesis of Hexagonal-Phase Core−Shell NaYF4Nanocrystals with Tunable Upconversion Fluorescence.* Langmuir, 2008. **24**(21): p. 12123-12125.
27. Qian, L.P., et al., *Critical shell thickness and emission enhancement of NaYF4:Yb,Er/NaYF4/silica core/shell/shell nanoparticles.* Journal of Materials Research, 2011. **24**(12): p. 3559-3568.
28. Yi, G.-S. and G.-M. Chow, *Water-Soluble NaYF4:Yb,Er(Tm)/NaYF4/Polymer Core/Shell/Shell Nanoparticles with Significant Enhancement of Upconversion Fluorescence.* Chemistry of Materials, 2007. **19**(3): p. 341-343.
29. Zhang, Q. and Q.-M. Zhang, *Synthesis and photoluminescent properties of α-NaYF4:Nd/α-NaYF4 core/shell nanostructure with enhanced near infrared (NIR) emission.* Materials Letters, 2009. **63**(3-4): p. 376-378.
30. Qian, L.P., et al., *Gold decorated NaYF4:Yb,Er/NaYF4/silica (core/shell/shell) upconversion nanoparticles for photothermal destruction of BE(2)-C neuroblastoma cells.* Journal of Nanoparticle Research, 2010. **13**(2): p. 499-510.

31. Schietinger, S., et al., *Plasmon-enhanced upconversion in single NaYF4:Yb3+/Er3+ codoped nanocrystals.* Nano Lett, 2010. **10**(1): p. 134-8.
32. Sudheendra, L., et al., *Plasmonic Enhanced Emissions from Cubic NaYF4:Yb:Er/Tm Nanophosphors.* Chemistry of Materials, 2011. **23**(11): p. 2987-2993.
33. Zhang, S.Z., et al., *Reversible luminescence switching of NaYF4:Yb,Er nanoparticles with controlled assembly of gold nanoparticles.* Chem Commun (Camb), 2009(18): p. 2547-9.
34. Shen, J., et al., *Superparamagnetic and upconversion emitting Fe3O4/NaYF4 : Yb,Er hetero-nanoparticles via a crosslinker anchoring strategy.* Chemical Communications, 2010. **46**(31): p. 5731-5733.
35. Chen, G., et al., *Intense Visible and Near-Infrared Upconversion Photoluminescence in Colloidal LiYF4:Er3+ Nanocrystals under Excitation at 1490 nm.* ACS Nano, 2011. **5**(6): p. 4981-4986.
36. Wang, L., et al., *Ultraviolet and violet upconversion fluorescence of europium (III) doped in YF3 nanocrystals.pdf.* Optics Letters, 2009. **34**(18): p. 2781.
37. Chen, G., et al., *Intense Visible and Near-Infrared Upconversion Photoluminescence in Colloidal LiYF4:Er3+Nanocrystals under Excitation at 1490 nm.* ACS Nano, 2011. **5**(6): p. 4981-4986.
38. Wang, G., et al., *Size-dependent upconversion luminescence in YF3:Yb3+/Tm3+ nanobundles.* Journal of Fluorine Chemistry, 2008. **129**(11): p. 1110-1113.
39. Wang, J., et al., *Lanthanide-doped LiYF4 nanoparticles: Synthesis and multicolor upconversion tuning.* Comptes Rendus Chimie, 2010. **13**(6-7): p. 731-736.
40. Wang, L., P. Li, and Y. Li, *Down- and Up-Conversion Luminescent Nanorods.* Advanced Materials, 2007. **19**(20): p. 3304-3307.
41. Yunxiang Wang, 王., 白. Yunfeng Bai, and 宋. Yinglin Song, *Multi-photon upconversion luminescence of Er3+-doped Y2O3 nanocrystals.* Chinese Optics Letters, 2009. **7**(6): p. 524-526.
42. Vetrone, F., V. Mahalingam, and J.A. Capobianco, *Near-Infrared-to-Blue Upconversion in Colloidal BaYF5:Tm3+, Yb3+Nanocrystals.* Chemistry of Materials, 2009. **21**(9): p. 1847-1851.
43. Wang, F. and X. Liu, *Recent advances in the chemistry of lanthanide-doped upconversion nanocrystals.* Chemical Society Reviews, 2009. **38**(4): p. 976.
44. Li, C., et al., *Highly Uniform and Monodisperse β-NaYF4:Ln3+(Ln = Eu, Tb, Yb/Er, and Yb/Tm) Hexagonal Microprism Crystals: Hydrothermal Synthesis and Luminescent Properties.* Inorganic Chemistry, 2007. **46**(16): p. 6329-6337.
45. Li, C., et al., *Different Microstructures of β-NaYF4Fabricated by Hydrothermal Process: Effects of pH Values and Fluoride Sources.* Chemistry of Materials, 2007. **19**(20): p. 4933-4942.

46. Shan, J., et al., *Synthesis of monodisperse hexagonal NaYF4:Yb, Ln (Ln = Er, Ho and Tm) upconversion nanocrystals in TOPO.* Nanotechnology, 2007. **18**(44): p. 445607.
47. Thompson, L.H. and L.K. Doraiswamy, *Sonochemistry: Science and Engineering.* Industrial & Engineering Chemistry Research, 1999. **38**(4): p. 1215-1249.
48. T.J. Mason, J.P.L., *Applied Sonochemistry: Uses of power ultrasound in Chemistry and Processing* 2002: Wiley-VCH.
49. M.D. Luque de Castro, F.P.C., *Analytical applications of ultrasonication*. Techniques and Instrumentation in Analytical Chemistry. Vol. Volume 26. 2007: Elsevier.
50. Cotton, S., *Lanthanide and Actinide Chemistry*2007: Wiley.
51. Wang, F., et al., *Simultaneous phase and size control of upconversion nanocrystals through lanthanide doping.* Nature, 2010. **463**(7284): p. 1061-1065.
52. Chen, D., et al., *Dopant-induced phase transition: a new strategy of synthesizing hexagonal upconversion NaYF4 at low temperature.* Chemical Communications, 2011. **47**(20): p. 5801.
53. Sun, Y., et al., *Controlled synthesis and morphology dependent upconversion luminescence of NaYF4:Yb, Er nanocrystals.* Nanotechnology, 2007. **18**(27): p. 275609.
54. Zhao, J., et al., *Controlled Synthesis, Formation Mechanism, and Great Enhancement of Red Upconversion Luminescence of NaYF4:Yb3+, Er3+Nanocrystals/Submicroplates at Low Doping Level.* The Journal of Physical Chemistry B, 2008. **112**(49): p. 15666-15672.
55. Chunxia Li, C.Z., Zhiyao Hou, Lili Wang , Zewei Quan, Hongzhou Lian, Jun Lin, *β-NaYF and β-NaYF :Eu Microstructures: Morphology Control and Tunable Luminescence Properties.* J. Phys. Chem. C, 2009. **113**(6).
56. Suyver, J.F., et al., *Upconversion spectroscopy and properties of NaYF4 doped with , and/or.* Journal of Luminescence, 2006. **117**(1): p. 1-12.
57. Shan, J., et al., *The Hidden Effects of Particle Shape and Criteria for Evaluating the Upconversion Luminescence of the Lanthanide Doped Nanophosphors.* The Journal of Physical Chemistry C, 2010. **114**(6): p. 2452-2461.
58. Xu, Z., et al., *Rare Earth Fluorides Nanowires/Nanorods Derived from Hydroxides: Hydrothermal Synthesis and Luminescence Properties.* Crystal Growth & Design, 2009. **9**(11): p. 4752-4758.
59. Tan, M.C., L. Al-Baroudi, and R.E. Riman, *Surfactant Effects on Efficiency Enhancement of Infrared-to-Visible Upconversion Emissions of NaYF4:Yb-Er.* ACS Applied Materials & Interfaces, 2011. **3**(10): p. 3910-3915.

60. Zhang, Z., et al., *Shape-controlled synthesis of Cu2O microparticles and their catalytic performances in the Rochow reaction.* Catalysis Science & Technology, 2012. **2**(6): p. 1207-1212.
61. Asryan, L.V. and R.A. Suris, *Theory Of Threshold Characteristics Of Quantum Dot Lasers: Effect Of Quantum Dot Parameter Dispersion.* International Journal of High Speed Electronics and Systems, 2002. **12**(01): p. 111-176.
62. Kaul, Z., et al., *Mortalin imaging in normal and cancer cells with quantum dot immuno-conjugates.* Cell Res, 2003. **13**(6): p. 503-507.
63. Giraud, G., et al., *Fluorescence lifetime imaging of quantum dot labeled DNA microarrays.* Int J Mol Sci, 2009. **10**(4): p. 1930-41.
64. Bruchez, M., et al., *Semiconductor Nanocrystals as Fluorescent Biological Labels.* Science, 1998. **281**(5385): p. 2013-2016.
65. Quimby, R.S., *Photonics and Lasers: an Introduction*2006: Wiley.
66. Ooba, H., *Synthesis of unique High Quality Fluorescence Quantum Dots for the Biochemical Measurements.* AIST TODAY, 2006. **6**(6): p. 26-27.
67. Brus, L., *Electron-electron and electron-hole interactions in smaller semiconductor crystallites: The size dependence of the lowest excited electronic state.* J. Chem. Phys., 1984. **80**(9).
68. Brus, L., *Electronic Wave Functions in Semiconductor Clusters: Experiment and Theory* J. Phys. Chem. , 1986. **90**: p. 2555-2560
69. Dybiec, M., *Spatially resolved photoluminescence of quantum dots,* in *Department of Electrical Engineering*2006, University of South Florida
70. Hui, L., et al., *Transfection of aqueous CdS quantum dots using polyethylenimine.* Nanotechnology, 2008. **19**(47): p. 475101.
71. Jiang, C., et al., *Synthesis of glutathione-capped CdS quantum dots and preliminary studies on protein detection and cell fluorescence image.* Luminescence, 2007. **22**(5): p. 430-437.
72. Winter, J.O., et al., *Variation of cadmium sulfide nanoparticle size and photoluminescence intensity with altered aqueous synthesis conditions.* Colloids and Surfaces A: Physicochemical and Engineering Aspects, 2005. **254**(1-3): p. 147-157.
73. Peng, Z.A.P.a.X., *Formation of High-Quality CdTe, CdSe, and CdS Nanocrystals Using CdO as Precursor.* J. Am. Chem. Soc, 2001. **123**: p. 183-184.
74. Ghows, N. and M.H. Entezari, *A novel method for the synthesis of CdS nanoparticles without surfactant.* Ultrason Sonochem, 2011. **18**(1): p. 269-275.
75. Havva Yagci Acar, R.K., Ersin Yurtsever,Can Ozen, Ingo Lieberwirth, *Emergence of 2MPA as an Effective Coating for Highly Stable and Luminescent Quantum Dots.* Journal of Physical Chemistry C, 2009. **113**: p. 10005–10012.

76. Serdar Celebi, A.K.E., Alphan Sennaroglu, Adnan Kurt, Havva Yagci Acar, *Synthesis and Characterization of Poly(acrylic acid) Stabilized Cadmium Sulfide Quantum Dots.* Journal of Physical Chemistry B, 2007. **111**: p. 12668-12675.
77. Yordanov, G.G., E. Adachi, and C.D. Dushkin, *Growth kinetics and characterization of fluorescent CdS nanocrystals synthesized with different sulfur precursors in paraffin hot-matrix.* Colloids and Surfaces A: Physicochemical and Engineering Aspects, 2006. **289**(1-3): p. 118-125.
78. de Azevedo, W.M. and F.D. Menezes, *A new and straightforward synthesis route for preparing Cds quantum Dots.* Journal of Luminescence, 2012. **132**(7): p. 1740-1743.
79. Hobson, R.A., P. Mulvaney, and F. Grieser, *Formation of Q-state CdS colloids using ultrasound.* Journal of the Chemical Society, Chemical Communications, 1994(7): p. 823-824.

# VITA

Cansu Yıldırım was born in İstanbul, Turkey on 28 March 1989. She was graduated from Terakki Foundation Private Şişli Terakki High School in 2006. She received her Bachelor of Science in Chemistry from Koç University in 2010. In the summer of 2010, she was accepted to M.Sc. program in Materials Science and Engineering in Koç University. She will start working as a Junior Research Assistant in Koç University Surface Science and Technology Center (KUYTAM) in October 2012.